Asia Pacific Research Initiative for Sustainable Energy Systems 2012 (APRISES12)

Office of Naval Research
Grant Award Number N00014-13-1-0463

Computational Fluid Dynamics (CFD) Applications at the School of Architecture, University of Hawaii: Generic CFD Workflow for Comfort Assessment

Task 7

Prepared For
Hawaii Natural Energy Institute

Prepared By
Sustainable Design & Consulting LLC, UH Environmental Research and Design Laboratory, UH Sea Grant College Program & HNEI

August 2015

HNEI
Hawai'i Natural Energy Institute
University of Hawai'i at Mānoa

Project Phase 1- 7.C

REPORT ON GENERIC CFD WORKFLOW FOR COMFORT ASSESSMENT

12.2

FINAL

August 10, 2015

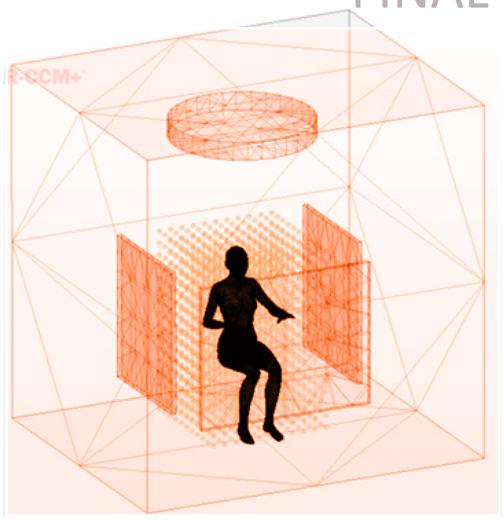

Prepared by:
Manfred J. Zapka, PhD, PE (Editor)
Tuan Tran, D.Arch
A. James Maskrey, MEP, MBA, Project Manager
Stephen Meder, D.Arch, Director
Eileen Peppard, M. Sc.

ERDL HNEI

Contract # N000-14-13-1-0463

Computational Fluid Dynamics (CFD) Applications at the School of Architecture, University of Hawaii

Project Phase 1 – 7.C

Task 7.C.3: Generic CFD Comfort Simulation Workflow (Phase 3)

Project Deliverable No. 12.2:

Report on Generic CFD Workflow for Comfort Assessment

FINAL

Prepared for Hawaii Natural Energy Institute

in support of

Contract #N000-14-13-1-0463

August 10, 2015

Prepared by:

Manfred J. Zapka, PhD, PE (Editor) [(1)]
Tuan Tran, D.Arch [(2)]
James Maskrey, MEP, MBA, Project Manager [(4)]
Stephen Meder, D.Arch, Director [(2)]
Eileen Peppard, M. Sc. [(3)]

(1) Sustainable Design & Consulting LLC, Honolulu, Hawaii
(2) Environmental Research and Design Laboratory (ERDL), School of Architecture, University of Hawaii
(3) University of Hawaii Sea Grant College Program
(4) Hawaii Natural Energy Institute Honolulu, Hawaii

ACKNOWLEDGEMENTS

The authors would like to thank the staff of the Environmental Design & Research Laboratory (ERDL) for their assistance in carrying out parts of this research study. Their support is gratefully acknowledged.

TABLE OF CONTENTS

ACRONYMS

3D	Three Dimensional
3D-CAD	Three Dimensional Computer Aided Design
CBE	Berkeley Center for the Built Environment.
CFD	Computational Fluid Dynamics
ERDL	Environmental Research and Design Laboratory
HNEI	Hawaii Natural Energy Institute
HVAC	Heating, Ventilating, and Air Conditioning
PMV	Predicted Mean Vote
PPD	Predicted Percent of Dissatisfied
RH	Relative Humidity
UHM	University of Hawaii at Manoa

UNITS:

°C	Degree Celsius
Clo	Clothing thermal insulation
BTU	British Thermal Unit
m	Meter
met	Metabolic Rate
m/s	Meter per second
Mph	Miles per Hour
Pa	Pascal
sqft	Square Feet
W	Watts

EXECUTIVE SUMMARY

The present report is sponsored by the Hawaii Natural Energy Institute (HNEI). The research program endeavors to develop advanced building modeling skills at the Environmental Design and Research Laboratory (ERDL) of the School of Architecture, University of Hawaii at Manoa.

The present report, Project Deliverable 12.1 (e.g. DRAFT), is part of Part 3 of the Computational Fluid Dynamics (CFD) research program. The objective of Part 3 of the research program is to investigate the use of CFD to predict occupant comfort in naturally ventilated spaces with comfort improving measures, and to provide validation of theoretical predictions with experimental studies.

The main objective of the research work presented in this report is the development of a generic CFD workflow that will be used in the remainder of Part 3 of the CFD research program to numerically predict or validate experimental comfort studies on the performance of "comfort islands". The experimental comfort study will be performed by the ERDL research team using a comfort test chamber, which was specifically built for this research program.

The concept of "comfort islands" - providing occupant comfort in otherwise non-conditioned spaces - was introduced by ERDL. Comfort islands combine established and innovative technologies to increase thermal comfort at the occupant level in warm climates, while leaving the space basically naturally ventilated. These comfort islands lower the operative temperature in the space directly adjacent to the occupant by providing actively cooled radiant surfaces. In addition, the comfort islands include ceiling fans to lower the perceived temperature for the occupants. The research hypothesis of this research project suggests that the use of comfort islands has significant energy reductions of up to 70% compared to full space cooling and ventilation, in order to provide comfort in naturally ventilated spaces also during those times when natural ventilation alone cannot provide relieve from hot internal temperatures. The present research endeavors to verify that the hypothesis of comfort islands is viable and provide experimental verification of certain heat transfer properties which are important for the overall thermal performance of radiant surfaces of comfort islands.

In this report a generic CFD comfort workflow is presented that was developed by the ERDL CFD research team to specifically validate and cross check experimental investigation on comfort islands. The CFD comfort simulation workflow uses an innovative approach of combining established comfort modeling with the numerical simulation of sensible convective and radiative heat loss. This combination integrates a proven comfort model, the analytical Predicted Mean Vote (PMV) model, with CFD based detailed determination of the flow field and thermal transfer properties of occupants. While the PMV

model relies on a uniform distribution and averaged values of flow field and thermal properties inside a space, the CFD simulation contributes a detailed modeling of sensible convective and radiative heat transfer close to the occupants. Since comfort islands achieve their performance gain through enhanced convective and radiative heat loss processes to cool occupants, a more detailed evaluation of convective and radiative heat transfer phenomena is of importance. The CFD comfort simulation workflow developed by the ERDL CFD research team will be used in the subsequent phases of the CFD research program.

The CFD comfort simulation workflow models sensible convective and radiative heat transfer occurrences to supplement latent and other heat transfer phenomena of the surrounding indoor environment and on the personal level of the occupant. The latent and other heat transfer phenomena as well as the resulting value for Predicted Percent of Dissatisfied (PPD) were provided by the PMV analytical model.

The ERDL CFD comfort simulation workflow was benchmarked against the common PMV analytical comfort assessment process and very good data consistency has been detected. For the benchmarking calculations, simplified boundary conditions such as a thermal steady-state and uniform distribution of temperature inside a generic test space have been employed in both the ERDL CFD model and the analytical PMV model. The uniform temperature distribution inside a sample space is a requirement for the PMV, and the ERDL CFD workflow could successfully recreate comfort predictions of occupant in the assumed thermal uniform internal environment. The ERDL experimental work will, however, introduce a non-uniform distribution of air and surface temperature inside the space by providing actively cooled surfaces. Under these conditions of non-uniformity, the ERDL CFD comfort simulation model will provide important insights in the performance of comfort islands.

SECTION 1 - OBJECTIVES OF THE INVESTIGATION

The CFD research program is divided into three parts. Two parts have been completed at this point: First, investigation of air movement outside and inside of buildings by means of numerical simulations, were measured with the use of Computational Fluid Dynamics (CFD). Second, the numerical predictions of air movement were then validated with measurements in the field. In general, good data consistency between the CFD simulations and actual tests were determined.

The objective of the remaining third part of the CFD research program is the investigation of occupant comfort by means of CFD and validating it with test measurements in a room at the University of Hawaii at Manoa (UHM) campus that was converted to a climate test chamber. The comfort investigation under the third part of the CFD research program focuses on determining the effects of so called “comfort islands” in spaces with elevated temperatures and humidity, which are not conditioned. In an effort to lower energy consumption, the use of natural ventilation as an alternative to fully conditioned space has been proposed. However, high temperatures and humidity conditions in naturally ventilated spaces, can negatively affect comfort to a point when normal operations are compromised.

During the summer months in 2014, the CFD research team identified high temperature and humidity indoor climatic conditions in a naturally ventilated office space on the UHM campus. For this research effort, which was outside the scope of the CFD research program, an ERDL team had identified and tested ventilation enhancing strategies to lower internal temperature and increase occupant comfort. It was found that while ventilation rates could be somewhat increased by lowering pressure losses through screened windows and doors, some form of localized cooling would have to be employed in order to increase occupant comfort to a point that would fall within a reasonable range.

Under the present CFD research program the effectiveness of localized comfort measures in an otherwise non-conditioned spaces is investigated. A combination of actively cooled cubicle walls and personal ceiling fans is being investigated which should provide occupants with more comfort.

The objective of this report of the CFD research program is the development of a generic CFD workflow to investigate feasibility of predicting comfort in a comfort chamber, e.g, test set-up, which has been installed at the UHM. The results of the CFD will be compared with the comfort tests in order to validate results.

The scope of the experimental tests will be mainly concerned with evaluating subjective thermal comfort experience of a selected sample group which is exposed to varying convective and radiative heat losses inside a climate test chamber.

The theoretical CFD results will be compared with actual experimental data obtained from the test set-up which has been built for Part 3 of this research program.

The main objectives of this investigation are as follows:

- Review appropriate procedures to describe thermal comfort provided in the literature and use this procedure both in the CFD simulations and in the experimental investigations of Part 3 of the research program.
- Determine the appropriate metrics that will be used in Part 3 of this research program to determine and quantify thermal comfort.
- Develop a procedure so that CFD results about thermal comfort can be compared with results obtained from subsequent thermal comfort experimental tests performed Part 3 of this research program.
- Develop CFD procedures to calculate sensitive convective and radiative heat transfer rates in the test set up. The CFD result will be compared to actual thermal measurements at the test set-up.
- Develop the CFD workflow procedures so that they can be readily applied in the subsequent phases of the CFD analysis of the thermal comfort tests in developing the test scenario matrix and plan for final comfort test in the test set-up.

SECTION 2 - GENERAL APPROACH

This section presents underlying assumptions and conclusions which were developed for this investigation. A condensed literature review was used to compare the conclusions of the CFD team to previous research.

2.1 Common Parameters used in the Simulation of Thermal Comfort

This section defines common parameters that are used in the thermal balance of humans, environmental thermal conditions and comfort assessments. The parameters are presented grouped in human physiology, human heat exchange with the environment and environmental thermal parameters. The presentation of pertinent parameters is related to

Human Physiology:

Body Temperature - Core (internal) temperature: Normal human body temperature measures differently depending in the location at which the measurement is made, the time of day, as well as the activity (metabolic) level of the person.

- Average core temperature: 37°C
- Maximum core temperature: 42° to 43°C
- Individual differences: 36° to 38°C
- Daily variations: ± 0.5 - 1.0°C
- Kept approx. constant within the limits of body's capacity to keep heat balance
- Shivering starts with the decrease of the core temperature
- Basal body temperature is the lowest body temperature attained during rest and in the absence of physical activities. Basal temperature is measured immediately after awakening and before any physical activity has been undertaken.

Body Temperature - Skin temperature:

- average skin temperature (AST): ≈ 33.2 °C ± 1 °C
- local skin temperature: 25 - 34 °C (refer to Figure 2.1.1 for a correlation between local skin temperature and ambient temperature)
- uniform at warm environment
- pain limit ≈ 45 °C
- Skin temperature
- temperature of extremities is critical factor for comfort in the cold

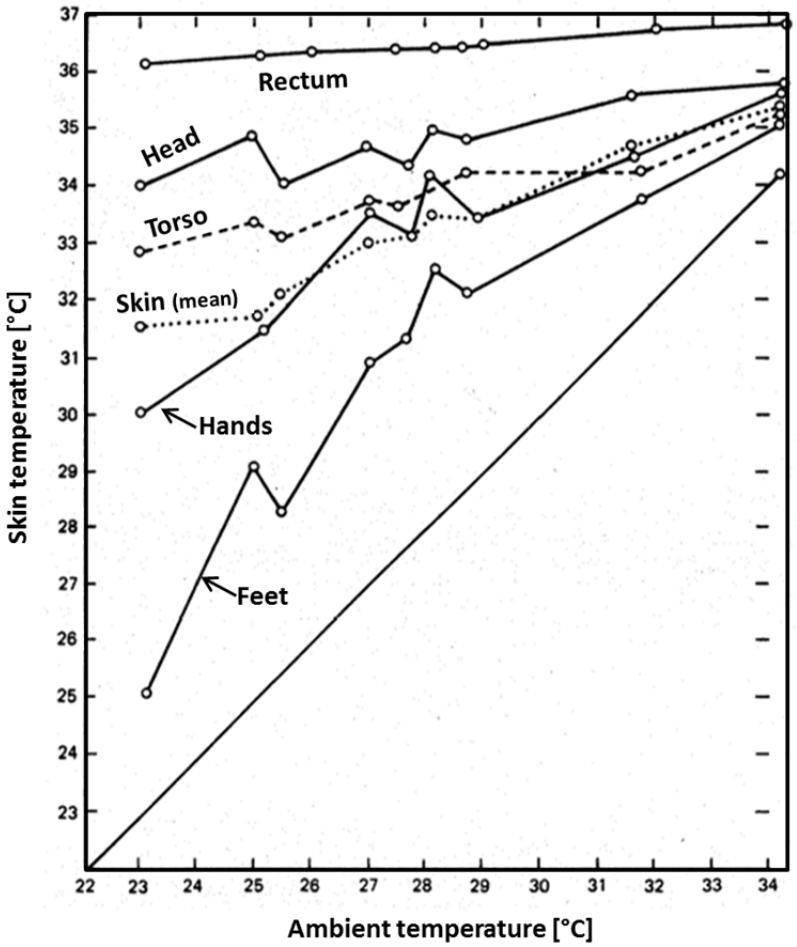

Figure 2.1.1: Local skin temperature in correlation with ambient temperature

Note: the figure shows that internal (core) temperature as measured in rectum remains relative constant under varying ambient temperatures while other body parts show a varity of temperature adjustments. Melikov (2010) modified

Body's Heat Balance:

- **Transport of heat:**
  - Conduction through tissues
  - Blood flow to the skin
  - Latent heat loss through respiration
- **Temperature control in the human body**
  - Hypothalamus
  - Thermal receptors (human temperature sensors)
  - Cold & warm receptors with static & dynamic discharge of thermal receptors
  - Response to mean temperature and rate of temperature change

Body's Heat Balance Regulation

In warm environment the heat balance is controlled through the following mechanisms:

- High skin temperature, with small temperature gradient between body core and skin surface as well as small heat exchange by conduction
- Vasodilation, with increased blood flow to skin surface and evaporation of sweat
- Controlled evaporation through hypothalamus, secretion of water from sweat glands that results in very effective cooling
- Uncontrolled continuous evaporation, water diffusion through the skin
- Water in exhalation (≈ 40 g/h)

Thermal Exchange with the Environment - Body's Heat Balance:

The following gives the basic heat balance equation for humans:

$$\mathbf{S = M \pm W \pm R \pm C \pm K - E - RES\ [W/m^2]}$$

For steady state S = 0 since the heat generated and absorbed by the body has to be equal to the heat rejected from the body. Note that certain parameters of the heat balance equation can be either positive or negative, describing heat gain or rejection.

The terms in the heat balance equation are as follows:

- S – rate of heat storage (e.g. change in heat in the body)
- M – rate of metabolic heat production
- W – rate of mechanical work accomplished
- R – rate of heat exchange by radiation
- C – rate of heat exchange by convection
- K – rate of heat exchange by conduction
- E – rate of heat exchange by evaporation
- RES – rate of heat exchange by respiration

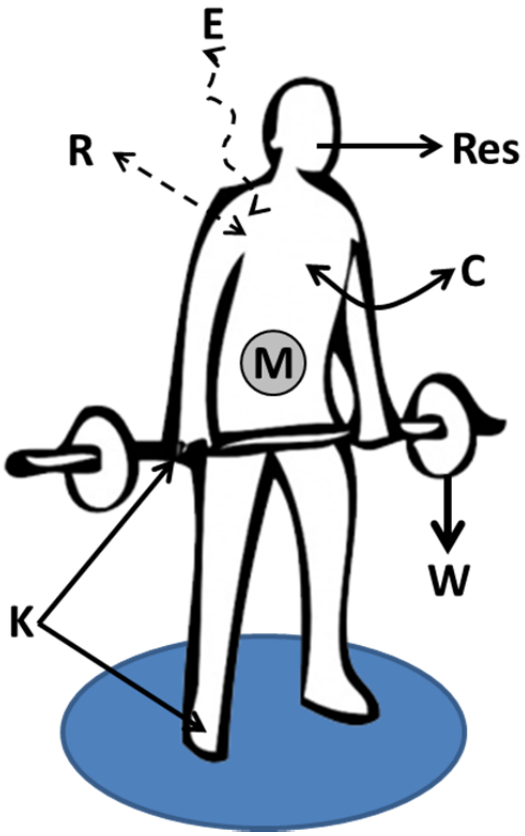

Figure 2.1.2: Terms used in Body's heat balance equation

$S = M \pm W \pm R \pm C \pm K - E - RES$ [W/m2]

S = rate of heat storage (e.g. change in heat in the body)

M =rate of metabolic heat production

W =rate of mechanical work accomplished

R = rate of heat exchange by radiation

C = rate of heat exchange by convection

K = rate of heat exchange by conduction

E = rate of heat exchange by evaporation

RES =rate of heat exchange by respiration

Thermal Exchange with the Environment - Body surface area

The rate of heat exchange has to be multiplied by the body surface. The correlation of body surface with typical mass and height of humans is given by the following equation

$A_D = 0.202 * M^{0.425} * L^{0.725}$

A_D – DuBois surface area [m2]; M – mass [kg]; L – height [m]

Average $A_D = 1.8\ m^2$ for a 1.73 m tall, 70 kg male

Terms of body's heat balance equation – Metabolic rate M

The metabolic rate, or human body heat or power production, is commonly expressed as the unit "Met". The metabolic rate of a relaxed seated person is unity, or one (1) Met, where

1 Met = 58 W/m2 (356 Btu/hr.)

With the average body surface of approximately 1.8 m2 the total metabolic heat can be calculated for a relaxed seated person as:

58 W/m2 x 1.8 m2 = 104 W (356 Btu/hr)

- Metabolic rate increases in proportion to exercise intensity
- Varies over wide range: 0.7 met - sleeping, ~8 met - wrestling
- Maximum capacity: 20 met
- Maximum rate for women is 30% lower than for man

Table 2.1.1: Typical metabolic rates for some common activities (source Engineering Toolbox www.engineeringtoolbox.com)

Activity	W/m^2	W[(1)]	Btu/hr[(1)]	Met
Reclining & Sleeping	46	83	282	0.8
Seated relaxed	58	104	356	1
Standing at rest	70	126	430	1.2
Sedentary activity (office, dwelling, school, laboratory)	70	126	430	1.2
Car driving	80	144	491	1.4
Graphic profession - Book Binder	85	153	522	1.5
Standing, light activity (shopping, laboratory, light industry)	93	167	571	1.6
Teaching	95	171	583	1.6
Domestic work -shaving, washing and dressing	100	180	614	1.7
Walking on the level, 2 km/h	110	198	675	1.9
Standing, medium activity (shop assistant, domestic work)	116	209	712	2
Building industry - Brick laying (Block of 15.3 kg)	125	225	768	2.2
Washing dishes standing	145	261	890	2.5
Domestic work - raking leaves on the lawn - washing by hand and ironing	170	306	1043	2.9
Golf, Softball	290	522	1780	5

Activity	W/m^2	W$^{(1)}$	Btu/hr$^{(1)}$	Met
Aerobic Dancing, Swimming	348	624	2137	6
Sports - Ice skating, 18 km/h	360	648	2210	6.2
Agriculture - digging with a spade (24 lifts/min.)	380	674	2333	6.5
Running 12 min/mile, Forestry - working with an axe	500	900	3070	8.5
Sports - Running in 15 km/h	550	990	3377	9.5
Gymnastics	319	574	1959	5.5
Note: (1) 1.8 m2 average body surface				

Terms of body's heat balance equation – Mechanical work W:

Expressed in body's mechanical efficiency: $\mu = W/M$

- $\mu > 0.05 – 0.1$ is unusual, typically μ is close to 0
- $\mu max = 0.20 – 0.24$ under optimal conditions (e.g. bicycle ergometer)
- For office work W<<M or 0
- W is approximated = 0 for design of HVAC – (results more conservative heat load)

Terms of body's heat balance equation - Respiration, RES:

Is typically small, 2 – 5 W/m^2; the heat loss due to respiration is approximated by the following equation

- $RES = C_{res} + E_{res}$
- $Cres = 0.0014\ M\ (34 – t_a)$
- $Eres = 0.0173\ M\ (5.87 – pa)$
- C_{res} - is sensible heat loss by convection
- E_{res} - is latent heat loss by evaporation of heat and water vapor from the respiratory tract
- p_a - is ambient water vapour pressure (in kPa)
- t_a - is ambient air temperature

Terms of body's heat balance equation - Evaporation, E:

Total evaporation is:

$$E = E_{rsw} + E_{dif}$$

With:

E_{dif} diffusion of water through the skin (approx. 10 W/m^2)

Er_{sw} evaporation of sweat from the skin surface by regulatory sweating: 0 – 400 W/m2, sweating limitations, large individual differences, acclimatization occurs

Terms used to describe evaporation and related phenomena:

- Skin wettedness, w, is the fraction of the skin covered with water to account for the total evaporation rate
- E_{max} occurs when the skin is completely wet (w=1)
- Skin wettedness caused by diffusion is 0.06
- Skin wettedness caused by regulatory sweating is w_{rsw}

Skin wettedness can be expressed as follows:

$w_{rsw} = E_{rsw}/E_{max}$

$E_{dif} = (1\text{-}wrsw)\ 0.06\ _{Emax}$

$w = 0.06 + 0.94\ E_{rsw}/E_{max}$ (weighted skin wittedness)

$E = w\ E_{max}$

Terms of body's heat balance equation - Convection, C:

Convective heat transfer rate is calculated by:

$$C = h_c\ (t_{skin} - t_a)\ [W/m^2]$$

With:

- t_a – air temperature [°C]
- t_{skin} – average skin surface temperature [°C]
- h_c – convective heat transfer coefficient [W/m2°C]; hc is function of air velocity past the skin, turbulence intensity and magnitude of temperature differences between skin and air.

Figure 2.1.3 depicts tabulated values for the convective heat transfer coefficient. Figure 2.1.4 shows that the convective heat transfer coefficient increases with the velocity past surfaces.

Equation	Limits	Condition
$h_c = 8.3V^{0.6}$ $h_c = 3.1$	$0.2 < V < 4.0$ $0 < V < 0.2$	Seated with moving air
$h_c = 2.7 + 8.7V^{0.67}$ $h_c = 5.1$	$0.15 < V < 1.5$ $0 < V < 0.15$	Reclining with moving air
$h_c = 8.6V^{0.53}$	$0.5 < V < 2.0$	Walking in still air
$h_c = 5.7(M - 0.8)^{0.39}$	$1.1 < M < 3.0$	Active in still air
$h_c = 6.5V^{0.39}$	$0.5 < V < 2.0$	Walking on treadmill in still air
$h_c = 14.8V^{0.69}$ $h_c = 4.0$	$0.15 < V < 1.5$ $0 < V < 0.15$	Standing person in moving air

Note: h_c in W/(m^2· K), V in m/s, and M in mets, where 1 met

Figure 2.1.3: Values for convective heat transfer coefficients

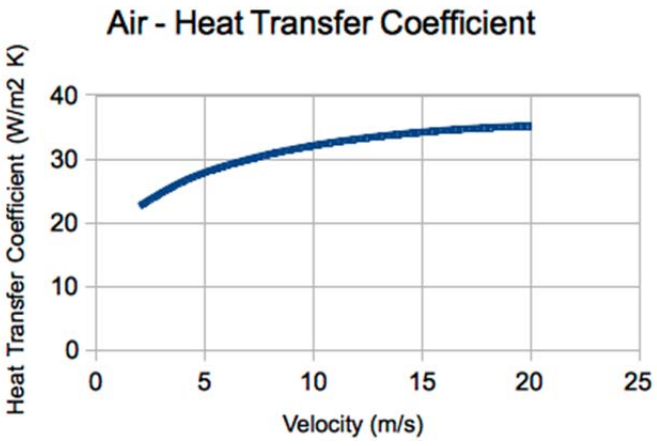

Figure 2.1.4: Convective heat transfer coefficient in air.

Note: For velocities from 2 to 20 m/sec the convective heat transfer coefficient can be approximated by the following empirical equation

$h_c = 10.45 - v + 10\ v^{1/2}$

where

v = the relative speed of the object through the air (m/s)
(source www.engineeringtoolbox.com)

Terms of body's heat balance equation - Radiation, R:

The radiative heat transfer to and from the human body can be approximated by the following equation:

$R = h_r (t_{cl} - t_r)$ [W/m^2]

With:

$h_r = 4 \varepsilon \sigma (A_r/A_D) [273.2 + (t_{cl}+t_r)/2]^3$ – with h_r – radiative heat transfer coefficient [W/(m^{2}K)]

t_r – mean radiant temperature [°C]

t_{cl} – average temperature of clothing surface [°C],

ε – average emissivity of clothing or body surface [-] (ε of skin is close to unity) Use the area weighted average emissivity for the clothing/body surface.

σ – Stefan-Boltzmann constant, 5.67x10^{-8}

A_r – effective radiation area of body, [m^2] Ar is 0.70 A_D for a sitting person and 0.73 A_D for a standing person.

For typical indoor temperature and ε close to unity h_r is nearly constant t 4.7 [W/(m^{2}K)

Thermal Exchange with the Environment - Clothing thermal insulation

$F_{cle} = (t_{cl} - t_o)/ (t_{sk} - t_o)$

F_{cle} – thermal efficiency of clothing [-]

The insulation of clothes are often measured in the unit "Clo", where

1 Clo = 0.155 m2K/W

- Clo = 0 - corresponds to a naked person
- Clo = 1 - corresponds to the insulating value of clothing needed to maintain a person in comfort sitting at rest in a room at 21 ℃ (70 ℉) with air movement of 0.1 m/s and humidity less than 50% - typically a person wearing a business suit

An overall insulation or Clo value can be calculated by simply taking the Clo value for each individual garment worn by the person, adding them together. The mean surface area of the human body is approximately 1.8 m2. Table 2.1 lists Clo values of different garments.

Table 2.1: Clo values for different clothing

Clothing		Insulation	
		Clo	m^2K/W
Nude body		0	0
Underwear - pants	Pantyhose	0.02	0.003
	Pantyhose	0.02	0.003
	Panties	0.03	0.005
	Briefs	0.04	0.006
Underwear - shirts	Bra	0.01	0.002
	Shirt sleeveless	0.06	0.009
	T-shirt	0.09	0.014
	Shirt with long sleeves	0.12	0.019
	Half-slip in nylon	0.14	0.022
Shirts	Tube top	0.06	0.009
	Short sleeve	0.09	0.029
	Light blouse with long sleeves	0.15	0.023
	Light shirt with long sleeves	0.20	0.031
	Normal with long sleeves	0.25	0.039
	Flannel shirt with long sleeves	0.30	0.047
	Long sleeves with turtleneck blouse	0.34	0.053
Trousers	Shorts	0.06	0.009
	Walking shorts	0.11	0.017
	Light trousers	0.20	0.031
	Normal trousers	0.25	0.039
	Flannel trousers	0.28	0.043
	Overalls	0.28	0.043
Sweaters	Sleeveless vest	0.12	0.019
	Thin sweater	0.20	0.031
	Long thin sleeves with turtleneck	0.26	0.040
	Thick sweater	0.35	0.054
	Long thick sleeves with turtleneck	0.37	0.057
Jacket	Vest	0.13	0.020
	Light summer jacket	0.25	0.039
	Smock	0.30	0.047
	Jacket	0.35	0.054
Sundries	Socks	0.02	0.003
	Thin soled shoes	0.02	0.003
	Quilted fleece slippers	0.03	0.005
	Thick soled shoes	0.04	0.006
	Thick ankle socks	0.05	0.008

Clothing		Insulation	
		Clo	m^2K/W
	Boots	0.05	0.008
	Thick long socks	0.10	0.016
Skirts, dresses	Light skirt 15 cm. above knee	0.10	0.016
	Light skirt 15 cm. below knee	0.18	0.028
	Heavy skirt knee-length	0.25	0.039
	Light dress sleeveless	0.25	0.039

2.2 Review of Existing Comfort Assessment Tools / Approaches

Thermal comfort is the condition of mind that expresses satisfaction with the thermal environment and is assessed by subjective evaluation. Thus, thermal comfort is based on personal experience and perception of the building occupant. Given the same environmental conditions, indoor as well as outdoor, people might respond differently in their experience of thermal comfort. Therefore, when using quantitative metrics, such as the level of being dissatisfied, people might describe thermal comfort levels of identical thermal conditions differently.

The thermal comfort experience can be related to the condition when thermal neutrality is maintained in the overall heat balance, e.g. heat loss and gain arte in dynamic equilibrium. Thermal neutrality is achieved when heat generated by human metabolism is allowed to dissipate in the presence of favorable heat barriers, thus maintaining thermal equilibrium with the surroundings. The main factors that affect thermal comfort perception are those that determine heat gain and loss, such as metabolic body function and heat gain from the environment, clothing insulation, air temperature, mean radiant temperature, air speed and relative humidity. Psychological parameters such as individual expectations can also affect thermal comfort.

There are prediction models that allow correlation of expected thermal comfort levels to objective, or quantifiable, thermal conditions to which people are subjected. Some of these models are based on statistical correlation some are on more detailed evaluation and comparisons to baseline conditions.

The following list presents the most widely used comfort assessment models. These comfort assessment models can be divided into two categories, environment based and physiological based comfort models.

Environment-based comfort model:

- Predicted Mean Vote (PMV): The comfort model Predicted Mean Vote (PMV), developed by Fanger, is the most representative thermal comfort model and is widely used internationally. PMV is an index ranging from -3 to +3. The index represents the predicted mean vote on a thermal sensation scale, of a large sample population exposed to a given environment. PMV is a function of air and mean radiant temperature (combined as the operative temperature), relative humidity, air flow velocity, closing resistance and metabolic rate. Typically a range of -0.5 to +0.5 is perceived as a range of satisfactory comfort. Fanger developed the PMV to estimate the comfort level of human subjects in different environmental conditions and at various activity levels. Fanger's comfort equation is a function of activity level, clothing resistance, air temperature, mean radiant temperature, air velocity and relative humidity.
- Predicted Percent Dissatisfied (PPD): The Predicted Percentage Dissatisfied (PPD) index is a quantitative measure of the thermal comfort of a group of people at a particular thermal environmental condition. Fanger developed the Predicted Percentage of Dissatisfied (PPD) index as a value that is a correlation with PMV. PPD is based on studies that surveyed subjects in a chamber where the indoor conditions could be precisely controlled. The correlation approach basically treats all occupants the same and disregards location and adaptation to the thermal environment. The determination assumes that indoor temperature do not change as the external conditions do. The PPD is based on the concept of a controlled indoor climate, rather than a climate that closely follows an external climate, to which humans can adjust. The PPD index is an important tool to predict or assess indoor thermal conditions. ASHRAE 55 uses the model and indicates that a satisfactory comfort can be attested to a building or internal space when at least 80% of the occupants are satisfied with thermal conditions.

Physiologically-based comfort model:

- Berkeley Comfort Model: The Berkeley comfort model was developed as a comfort model to account for non-stationary and non-uniform indoor thermal conditions and provide metrics with which comfort is quantified under such non-static conditions (CBE, 2014). The Fanger assumption is that buildings are currently designed to achieve comfort by creating static, uniform interior environments. In reality neither indoor environments nor building occupants are static and the indoor thermal environment experienced by an occupant in a building is often quite complex. Rather than the conventional PMV and PPD comfort indices, the Berkeley Comfort Model build on an advanced understanding of how occupants respond to thermal environments. By better understanding occupant comfort in buildings, building occupant health, satisfaction, and productivity is improved. The Berkeley Comfort Model, which was originally developed for the evaluation of human comfort in automobiles, is a sophisticated thermal

comfort model that uses local body parts and body overall to describe human thermal experiences. The model has been validated based on intensive human subject tests carried out at the Berkeley Center for the Built Environment.

2.3 Comparison between Environment-based and Physiology-based Comfort Models

Hepokoski et al (2013) compared the use of environment and physiologically based comfort models and demonstrated the differences in thermal comfort predictions between these two types of models. The authors pointed out that the accurate assessment of thermal comfort requires a comprehensive analysis of environmental effects which contribute to the heat transfer to and from the human body. The common comfort evaluation approach, such as the PMV/PDD approach, establishes a direct correlation of comfort to environmental conditions, which include operative temperature, relative humidity and air movement, and occupant specific parameters, such as clothing and metabolic rates. The alternative physiological based model explicitly correlates comfort to basic physiological response, such as skin and core temperature.

While the authors did not make recommendations about which model to use, they pointed out that environment-based models were developed under steady-state conditions and do not account for initial thermo-physiological state of the human body, or its transient response to rapidly changing thermal environments. Physiologically based comfort models, however, can describe the comfort experience in non-steady state thermal conditions. By discerning the main differences between and limitations of the two types of comfort models, the authors suggest preferred applications of the two comfort models. For the comparison the authors chose a thermal model of a representative transient cool-down scenario of a vehicle passenger compartment which provided the context from which the boundary conditions (surface temperatures, air temperatures, air velocities, solar load, etc.) and physiological response (skin and core temperature) could be obtained and subsequently applied to the comfort models.

To perform a comprehensive analysis of the environment affecting human thermal comfort, a full vehicle thermal model was constructed and simulated in a realistic natural environment including solar loading; radiation exchange with the sky and surroundings; and wind convection. The simulation consisted of two phases:

- In the first phase the unoccupied vehicle was subjected to a hot thermal soak while the vehicle was not operating and facing south for maximum solar gain. Concurrently, a series of human models (geometry representing a driver that was coupled to a human thermoregulatory model) were modeled at activity level between 1 and 7 MET for 30 minutes prior to entering the vehicle (i.e. the precondition activity).This was done to illustrate the differences between the environment-based metrics and the physiology based metrics.

- The second phase was a 15 minute transient cool down period in which the vehicle was operating and cooled by its AC systems. During the cool down period the driver's activity was fixed to 1.5 MET regardless of the prior activity level. During the transient cool-down state, heat balance inside the vehicle included cooling from the AC systems and warming from the environment and the heat output of the occupant. The convective heat transfer was modeled as internally internal stratified air. Convective heat transfer coefficients were used that were derived in earlier investigations. The metrics related to the environment based comfort model used a the human geometry as "boundary condition sensor" to calculate mean radiant temperature (MRT), the contribution of convection as well as other clothing properties, etc. These values were then used as input to determine environment based comfort.

The sensation and comfort metric scale for thermal sensation and comfort used in the investigation is depicted in Figure 2.3.1.

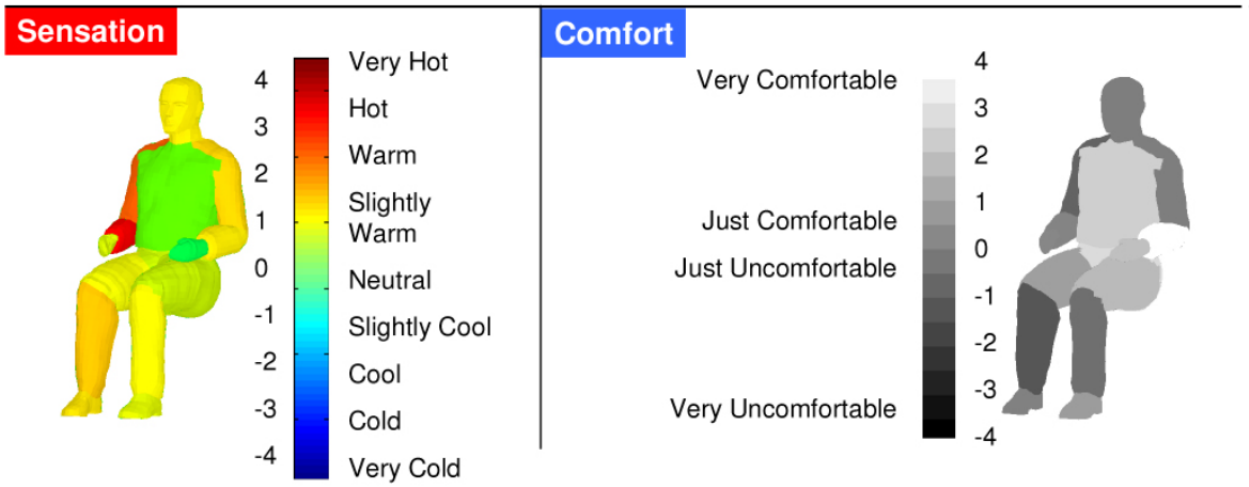

Figure 2.3.1: Sensation and comfort scales used in investigations, Hepokoski et al (2013)

The result of the investigation suggests that the activity level of the driver prior to entering a warm vehicle had a negligible effect on thermal sensation/comfort as predicted by the environment-based metrics. Figure 2.3.2 indicates the minor influence of the driver's activity levels prior to entering the vehicle for PMV. The slight differences depicted in Figure 2.3.3 can be attributed to the human heating effect of the driver. Figure 2.3.3 shows the same relationship between time and overall thermal sensation for the physiology based comfort model. As can be seen for the physiology model, there is a time correlation between overall thermal sensation and activity level prior of the driver entering the vehicle. Figure 2.3.3 suggest that the overall thermal sensation decreases more abrupt with lesser activity of the driver prior of entering the vehicle. Figure 2.3.3 also indicates that the driver's overall

thermal sensation approaches relatively small range after about 12 minutes. This is true for the different MET levels and for the PMV reference case.

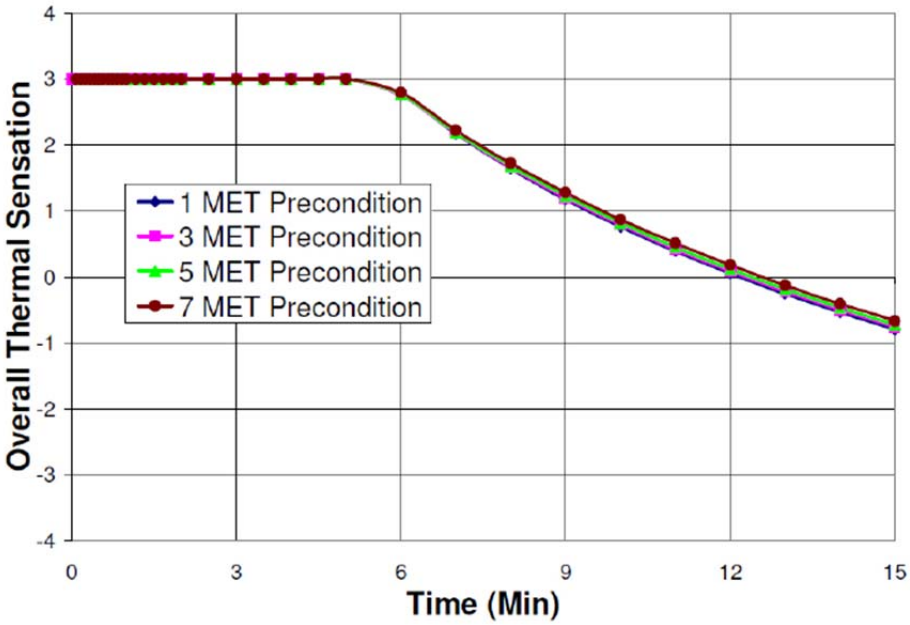

Figure 2.2.2: PMV for different pre-cool-down activities Hepokoski et al (2013)

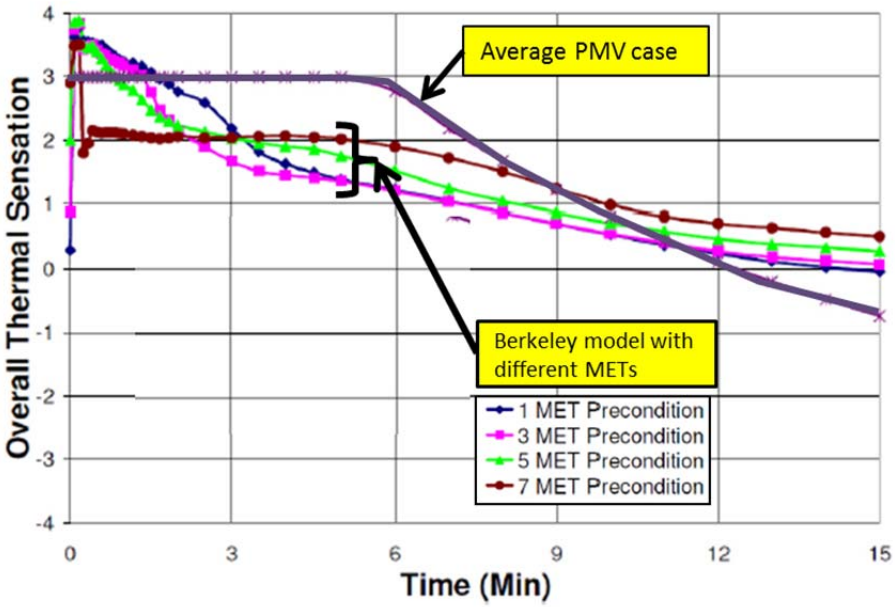

Figure 2.3.3: Overall Sensation (evaluated by Berkeley Comfort Model) for various pre-cool-down activities Hepokoski et al (2013)

In summary, results of the study suggest that PMV should be primarily used for the assessment of steady state thermal conditions. If comfort and thermal sensation is needed for non-steady state or transient thermal conditions the physiology based comfort model provide more detail description of the human comfort experience.

The present study will use the PMV comfort model as steady state conditions are assumed throughout the research. The follow up comfort tests will consider the need for steady state thermal experience for the test subjects. The team will therefore use an appropriate "thermal adjustment time" for test subjects to attain thermal equilibrium within the test chamber, before the tests start.

2.3 Experimental and CFD Approaches for Convective and Radiative Heat Loss

The main objective of part three of this CFD research program is the investigation of the effectiveness of providing localized comfort enhancing measures in other wise non conditioned spaces. Therefore the identification and quantification of convective and radiative heat transfer rates within the small confines of the chamber are of importance.

The rate of convective and radiative heat transfer can be determined by multiplying the convective and radiative heat transfer coefficients with pertinent temperature differential and constants, as described in Section 2.1 of this report. Fort this study a number of technical papers have been reviewed which describe the determination of convective and radiative heat transfer coefficients. For this determination analytical elaboration, experimental investigation or numerical simulations (e.g. CFD) were used by different authors. The following describes two of the reviewed papers for experimental determination of relevant heat transfer coefficients through experimental investigation Masayuki (2002) and and numerical simulation (Sorensen, 2003), which are discussed in the following as representative approaches.

Masayuki (2002) evaluated convective heat transfer coefficients for each part of on seated and standing manikin using an infrared-imaging radiometer. Clothed and nude manikins were compared and the author reports that convective heat transfer coefficients for the clothed manikin were larger than for the nude manikin. Differences were found to be as large as 100 to 200% for some individual parts, and for the overall body the difference was 30 to 50%. While there are numerous previous studies on local convective heat transfer in calm and air flow conditions the author pointed out that there was a need for direct measurements of convective heat transfer and local clothing insulation of manikins in different positions, especially for airflow between 0.2 and 5 m/s.

The test procedure included determining convective heat transfer coefficients and clothing insulation for each body part and merging the local values to whole body values through an area weighted procedure. The authors used the following calculation procedures:

- Direct measurements of clothing insulation, where the difference between the skin temperature and the average clothing surface was used and use in conjunction with the dry heat loss of each clothed body segment to arrive at the clothing insulation.

- Estimation of convective heat transfer coefficients for clothed body parts, was based on the assumption of a uniform surrounding temperature field of air and walls. Therefore the total dry heat transfer between the clothing and the surrounding environment for each part of the manikin can be described as the sum of convective and radiative heat transfer. The convective part of the total heat transfer coefficient is obtained by subtracting the radiative transfer coefficient from the total dry heat coefficient for each body part. The author points out that, strictly speaking, this calculation can only be applied to non-permeable clothing, in which there is no convection bypassing or permeating the clothing insulation layer. Therefore, the convective heat transfer coefficient and clothing insulation calculated through this procedure includes some effect of het loss through air penetration.

- Estimation of radiative heat transfer coefficients for clothed body parts: The authors pointed out that, strictly speaking, the object to object radiative heat transfer for each body parts has to include radiative heat exchange between different body parts. However, with such small temperature differences, this can be neglected. Therefore, using the equation for radiative heat transfer in Section 2.1 of this report, assuming that the mean radiant temperature equals ambient air, and using values for emissivity, clothing temperature and effective radiation areas factor, the radiative heat transfer coefficient for each clothed body part can be calculated.

The author reported values for each body parts and the aggregate whole body. As an illustration of the results, Figure 2.3.1 shows the convective heat transfer coefficients for each body part and Figure 2.3.2 for the whole body, calculated using an area weighted procedure. It should be noted that the authors report that the convective heat transfer coefficient is larger for the clothed than for the nude manikin.

Figure 2.3.3 shows a comparison between results for whole body convective heat transfer coefficients reported in previous studies. The results point out that convective heat transfer coefficients for the sitting and standing manikin positions do not deviate significantly.

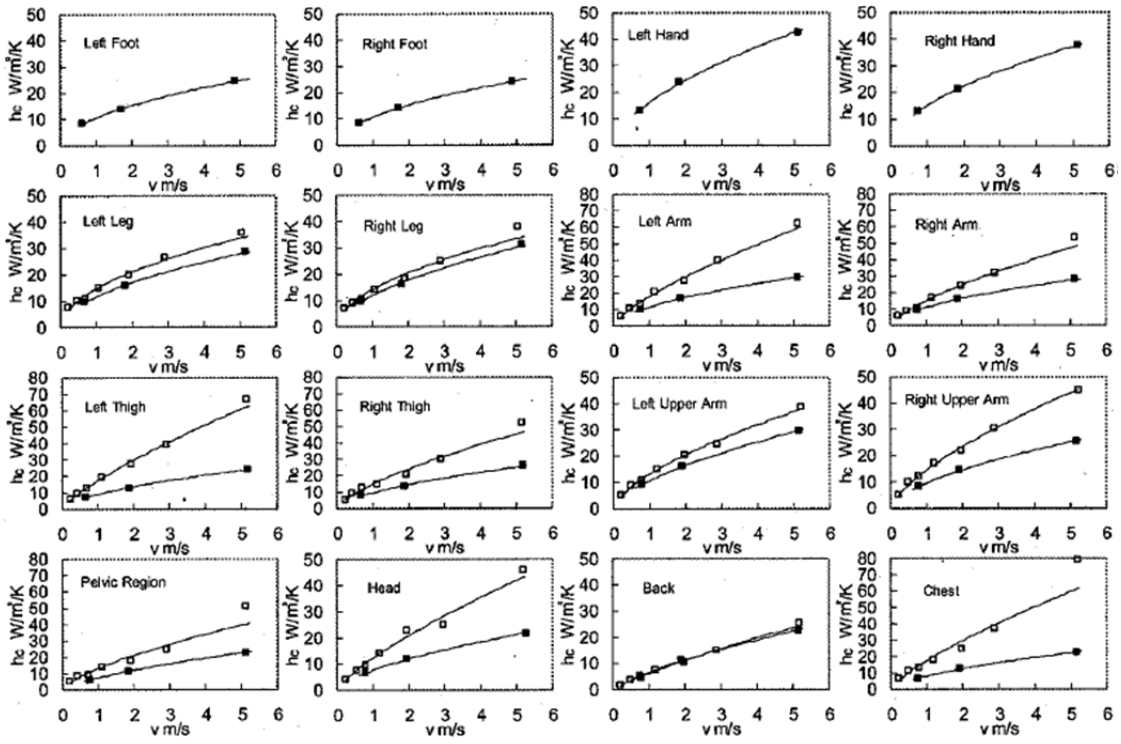

Figure 3(a) Convective heat transfer coefficients for each part of a sitting manikin when the manikin faces upwind (Open square means the results from clothed manikin and solid square means those from nude manikin)

Figure 2.3.1: Convective heat transfer coefficients for different body part so the manikin, reported by Masayuki (2002)

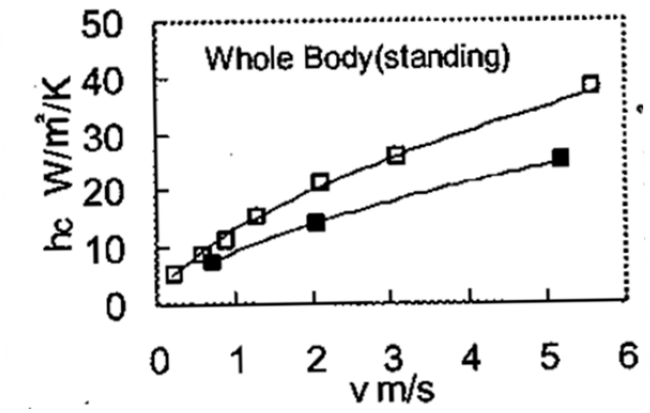

Figure 2.3.2: Convective heat transfer coefficients for whole body, , reported by Masayuki (2002)

(Open and solid squares depict clothed and nude manikin)

Note: convective heat transfer coefficient for clothed manikin is significantly larger than for nude manikin

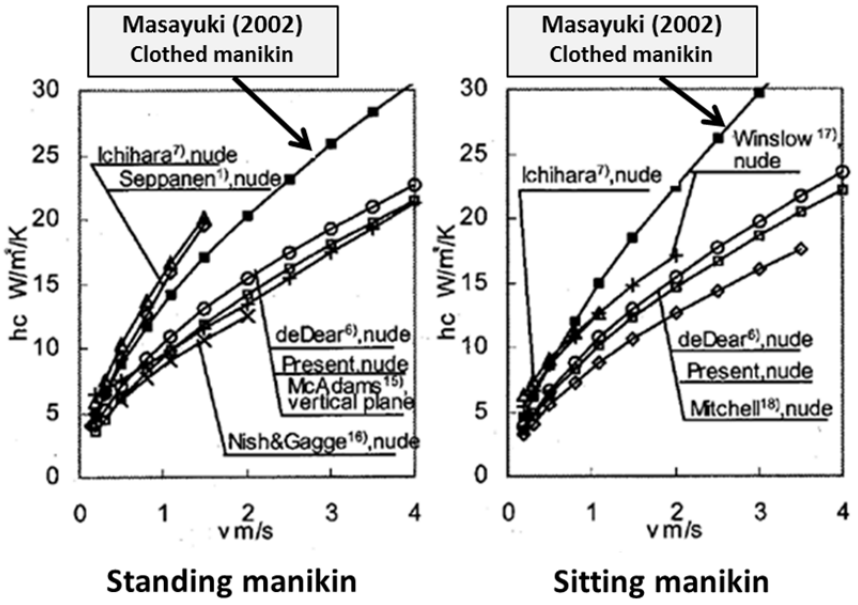

Figure 2.3.3: Comparison of whole body convective heat transfer coefficients reported by different authors , reported by Masayuki (2002) modified

Sorensen (2002) presents results of an investigation of convective and radiative heat transfer that was conducted using CFD simulations. The author points out differences between experimental investigations using human subjects and manikins and numerical simulations (CFD). He suggested that CFD may be used as an effective alternative of deriving heat transfer rates alternative to experimental investigations of manikins and human subjects. This especially applies to obtain detailed information about the flow field and distributions of temperature and concentrations inside a room and particularly in the close vicinity of a person. While the author cites other investigations of using CVFD models in comparable investigations he pointed out the fact that his investigation was the first to employ detailed geometries of the 3D-model of a person.

The CFD investigations used the same geometry of a manikin that was used during earlier investigations which was obtained through laser scanning of the manikin. The geometry of the CFD test object (e.g. person) included detailed information as depicted in Figures 2.3.4. Figure 2.3.5 shows the computational grid used in the CFD simulations.

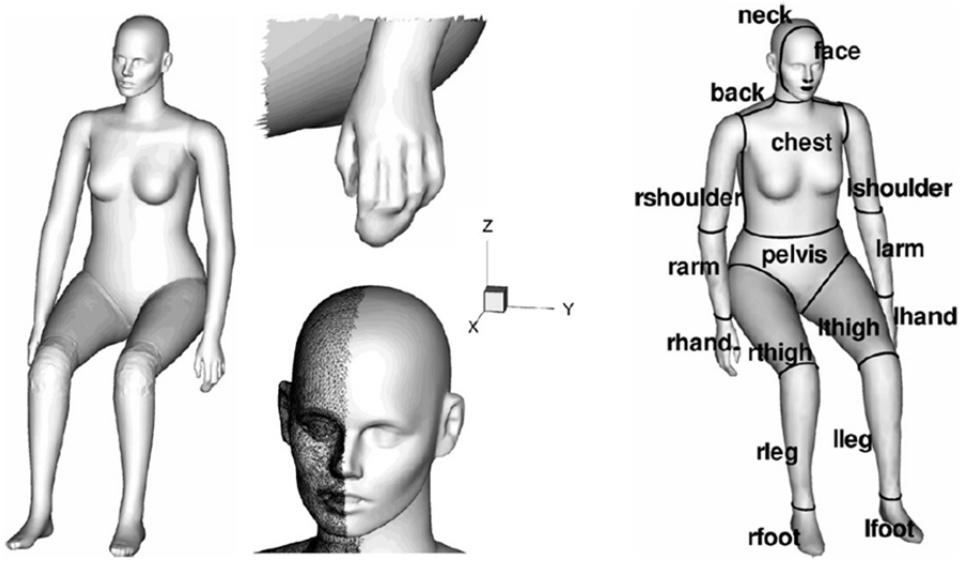

Figure 2.3.4: Geometry of the CFD person used in the investigation (Sorensen, 2002); the geometry of the CFD object is the same as the real world manikin used in previous experiments

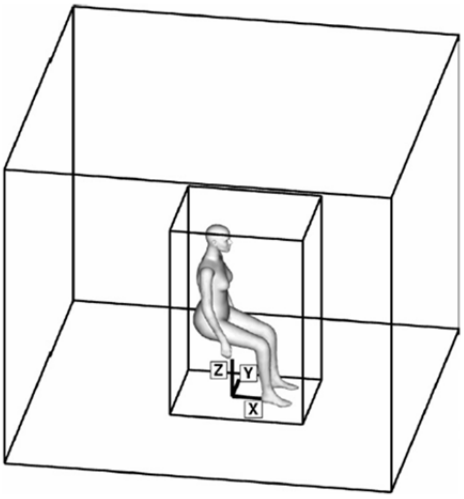

Computational domain with two regions of different resolution and cell types, the inner region round the person has a higher mesh resolution

Detail of the computational grid; there is a high mesh resolution close to areas of special interest such as the face; full grid had slightly more than one million cells.

Figure 2.3.5: Computational domain and mesh (Sorensen, 2002)

The CFD simulation was carried out using steady state Reynolds averaged Navier–Stokes (RANS) equations and with a low Reynolds number k–ϵ turbulence model. The CFD simulation used a surface-to-surface radiation approach in which surfaces of the calculation domain are subdivided into adjoining patches and beams are emitted and traced through the fluid until another patch is reached. This created radiation-dependent pair of patches with beams between two such patches determining the view factor between the patches. The radiative heat exchange between two patches was thus a function of the view factor between the two patches as well as the emissivity and average temperature of each of the two patches. This numerical approach resulted in a detailed depiction of radiative heat transfer between objects which cannot be readily attained by experimental test.

Figure 2.3.6 depicts the calculated radiative heat transfer coefficients. The CFD simulation allows high resolution post processing and a contour map of radiative heat transfer coefficients can be derived as shown in Figure 2.3.6. As can be seen in the figure, the sides of the body and the inner sides of the arms have smaller radiative heat transfer coefficients than the front, back and outer sides of the arms because of the proximity between the arms and the body.

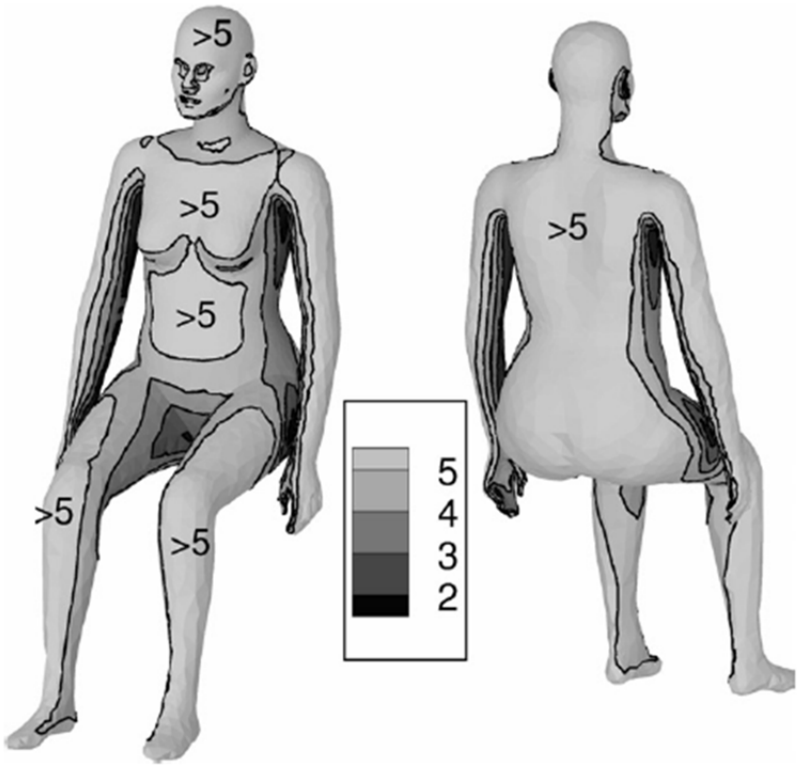

Figure 2.3.6: Distribution of radiative heat transfer coefficient [W/(m^2 K)] (Sorensen, 2002)

The average values of the radiative heat transfer coefficient for all body parts were calculated using the same emissivity of 0.95, the surrounding wall temperature of 19 ◦C and the skin temperature of 31 ◦C. The whole-body values are based on area-averaging of the individual body segment-values. Figure 2.3.7 shows the results of radiative heat transfer coefficients for body segments and the area-averaged whole body reported by the author. The results were fairly consistent between CFD simulations and previous experiments using the same manikin geometry and deviated only 7%, for the whole body.

Radiative heat transfer coefficients for different body segments[a]

Body segment	Calculations [W/(m^2 K)]	Experiments [W/(m^2 K)]	Deviation (%)
Foot	5.36	4.2	24
Leg	5.12	5.4	−5
Thigh	4.61	4.6	0
Hand	4.12	3.9	5
Arm	4.30	5.2	−21
Shoulder	4.63	4.8	−4
Pelvis	5.01	4.8	4
Head	5.22	3.9	25
Chest	4.73	3.4	28
Back	5.07	4.6	9
Whole body	4.83	4.5	7

Figure 2.3.7: Results of radiative heat transfer coefficients for different body segments and the averaged whole body (Sorensen, 2002)

The CFD simulation also investigated convective heat transfer coefficients. The type of convection was limited to the buoyance induced free (natural) convection between a warmer body into the colder surrounding air. For the experiments, the heat flux of the thermal manikin varied for each segment of the manikin to obtain the specific temperature differential with the surrounding air, and the heat flux for each segment was logged. By measuring the total heat flux, both radiative and convective heat losses from ten bodies were measured. All surface boundaries had fixed temperatures in the CFD simulations. Radiation between body segments and outer surfaces was decoupled from the flow field and temperature distribution of the domain. Therefore the complexity of non-linearity introduced by radiation was avoided.

The buoyance induced flow field and temperature distribution around the CFD manikin are depicted in Figure 2.3.8. Figure 2.3.9 depicts the distribution of convective heat transfer coefficient on the CFD manikin. The figure illustrates the complexity of the calculated distribution of the natural convection heat transfer coefficient around the computational manikin. Locally, values below one are found inside the recirculating zones at the upper part of the head and shoulders, whereas values above ten are found at the tip of the Angers and at the lower side of the ears and nose.

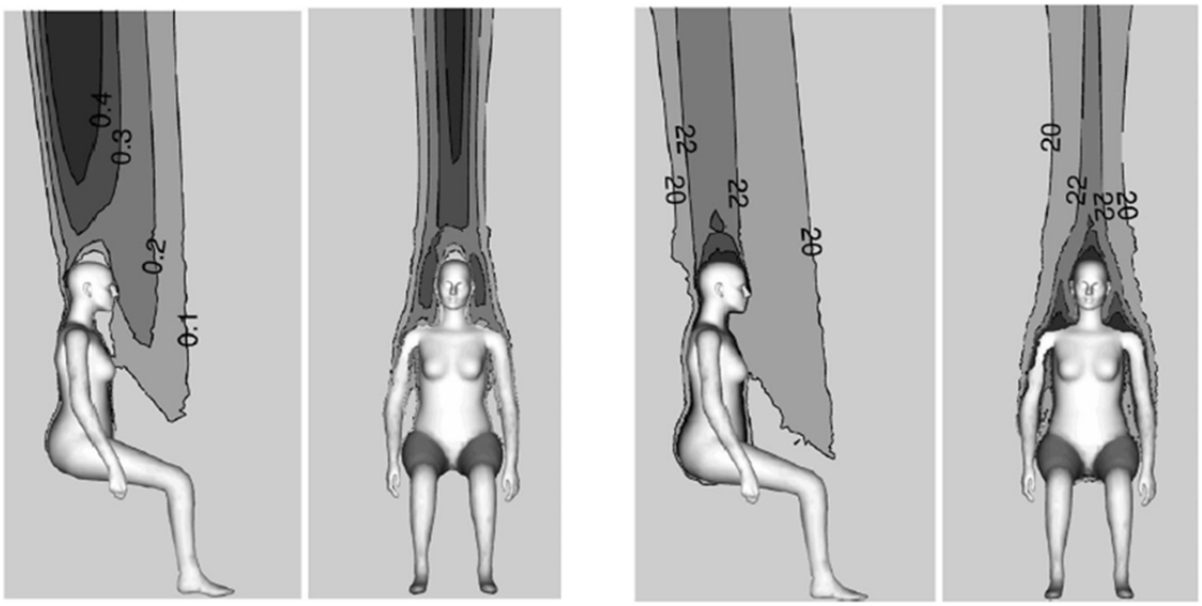

Distributions of vertical velocity (m=s) (top) Distributions of and temperature (◦C)

Figure 2.3.8: Distribution of vertical velocities and temperature around the CFD manikin (Sorensen, 2002)

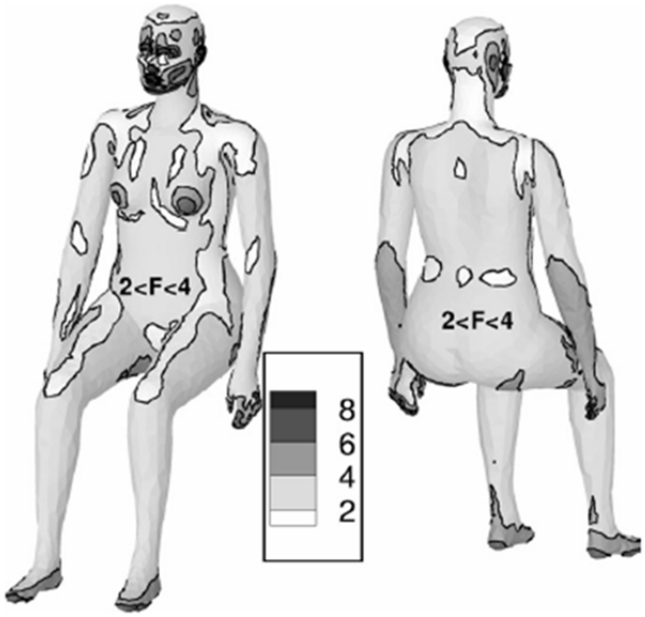

Figure 2.3.9: Calculated convection heat transfer coefficient [W=(m2 K)] of CFD manikin (Sorensen, 2002)

Figure 2.3.10 shows the resulting overall heat flux [W/m2] and the derived convective heat transfer coefficients for body segments and the area-averaged whole body. The results suggest that the area-averages whole body natural convective and radiative heat loss from the body represents around 40% and 60% of the total heat loss, respectively.

Segment	Total heat flux			Conv. coeff.
	CFD (W/m^2)	Experiments (W/m^2)	Deviation (%)	CFD [$W/(m^2\ K)$]
Foot	113.0	101.7	11	4.66 (4.64)
Leg	92.0	116.7	−21	3.04 (3.03)
Thigh	87.8	98.8	−11	3.18 (3.19)
Hand	97.0	101.2	−4	4.50 (4.49)
Arm	91.5	99.1	−8	3.82 (3.76)
Shoulder	82.7	85.9	−4	2.71 (2.70)
Pelvis	88.1	90.5	−3	2.80 (2.82)
Head	99.8	104.0	1	3.62 (3.59)
Chest	80.2	78.5	2	2.38 (2.44)
Back	82.4	76.9	7	2.23 (2.23)
Whole body	89.67	88.26	2	3.13 (3.13)

2.3.10: Total heat flux and calculated convective heat transfer coefficients from each body segment; the whole-body values are based on area-averaging of the individual segment-values.(Sorensen, 2002)

SECTION 3 - METHODOLOGY

This section presents the methodology of determining comfort levels using CFD analysis. Validation of the CFD simulation will be done by measuring main thermal environmental parameters in the test set-up under steady state conditions. Measurements that determine local thermal heat transfer and related comfort experience are beyond the scope of the present comfort tests.

3.1 Selection of the Model to Asses Comfort

The main objective of the present comfort investigation is the effectiveness of using radiant surfaces such as cubicle walls to lower the operative temperature without conditioning of the entire space as well as providing enhanced air movement through a ceiling fan for supplemental cooling.

Therefore the main objective of CFD simulation is to develop an approach, e.g. a CFD workflow, to quantify the contribution of convection and radiation of the test set-up condition through modeling and simulation of the test-set-up geometry and thermal performance.

The CFD analysis will be used to determine representative convective and radiative heat transfer rates through simulation of actual flow fields inside the test-set up and thermal radiation between bodies inside the test set-up. Having determined representative convective and radiative heat transfer coefficients these value will be imported into a PMV comfort model

3.2 Linking CFD analysis to PMV model

For the quantitative assessment of the PMV thermal comfort model six parameters have to be quantified. These parameters are that those describing the thermal conditions of the surrounding environment and those describing the thermal conditions of the human:

- Environmental variables are T_a (°C) – air temperature, T_r (°C) – mean radiant temperature, *Vel* (m/s) – air velocity and RH (%) - relative humidity.
- Human thermal conditions are *M* - rate of metabolic heat production and *W* (W/m2) - rate of mechanical work accomplished (both in units of met (1 met – 58.2 W/m2);Clo (1clo = 0.155 m2-K/W) - clothing thermal insulation). These aresubsequently referred to as “personal thermal parameters”.

Figure 3.2.1 depicts the simplified process diagram of how the present investigation uses the two types of thermal parameters in the PMV model. Environmental conditions will be derived from CFD investigations with input assumption which will be subsequently validated with measurements in the field. Personal thermal variables will be evaluated directly from the specifics of the human test subject.

Personal variables include the assessment of the person's activity level, such mechanical work done and heat energy generated by metabolic body function, and the type of clothing the person is wearing, which impedes the heat exchange with the surrounding environment.

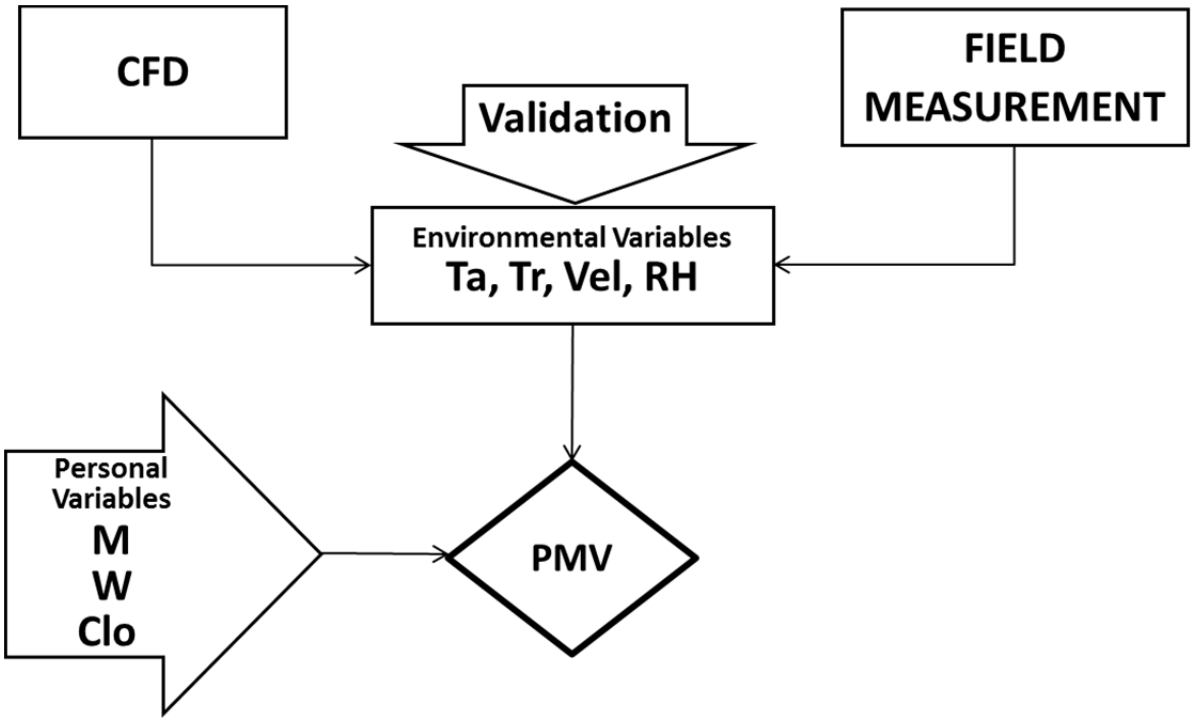

Figure 3.2.1: The overall workflow of linking CFD analysis to PMV model

The PMV index, introduced by Fanger (1970), correlates to the ASHRAE thermal sensation scale. The PMV index describes and quantifies the thermal imbalance between actual heat loss from a body to environment and the amount of internal heat production for optimal thermal comfort at a specific activity. The PMV index and PDD (Predicted Percent Dissatisfied) equations are calculated as follows:

$$PMV = TS * L$$

$$PPD = 100 - 95\exp[-(0.03353\ PMV^4 + 0.2179\ PMV^2)]$$

where $TS = 0.303\exp(-0.036M) + 0.028$; and $L = (M - W) - (C + R + E_{dif} + E_{rsw} + E_{res} + C_{res})$

where *TS* is the so-called thermal sensation transfer coefficient and *L* is thermal load on the body, which in turn is the difference between internal heat production and heat loss to the actual environment. The body heat loss to the actual environment consists of sensible heat and latent heat which is derived from the following components:

- Heat loss by convection (sensible heat)

$$C = f_{cl} h_c (t_{cl} - t_a) \qquad (W/m2)$$

- Heat loss by radiation (sensible heat)

$$R = f_{cl} h_r (t_{cl} - \overline{t_r}) \qquad (W/m2)$$

- Evaporative heat loss from natural diffusion of water through skin (latent heat)

$$E_{dif} = 3.05[5.75 - 0.007(M - W) - p_a] \qquad (W/m2)$$

- Evaporative heat loss from sweating (latent heat)

$$E_{rsw} = 0.42(M - W - 58.15) \qquad (W/m2)$$

- Evaporative heat loss from respiration (latent heat)

$$C_{res} = 0.0014M(34 - t_a) \qquad (W/m2)$$

- Convective heat loss from respiration (latent heat)

$$E_{res} = 0.0173(5.87 - p_a) \qquad (W/m2)$$

Where f_{cl} is the clothing factor, *Icl* is clothing insulation and estimated as:

$$f_{cl} = \begin{cases} 1.0 + 0.2I_{cl} & I_{cl} < 0.5\ clo \\ 1.05 + 0.1I_{cl} & I_{cl} < 0.5\ clo \end{cases}$$

h_c is the convective heat transfer coefficient. For natural convection, $h_c = 2.38(t_{cl} - t_a)^{0.25}$ or $h_c = 12.1\sqrt{V}$ for forced convection having average air velocity of *V* (m/s). t_{cl} is cloth temperature, t_a is the air temperature, $\overline{t_r}$ is the mean radiant temperature, p_a is the water vapor pressure of the air.

Within the scope of this study, all latent heat loss components will be calculated through the PMV analytical approach using the above formulas, while sensible heat loss components (convection and radiation) will be calculated using CFD simulation. By using CFD to calculate sensible convective and radiative heat loss components accuracy of the PMV predictions will increase, because of the higher accuracy in predicting the flow field characteristics around the body. CFD simulations will precisely evaluate flow field and heat transfer variables in the vicinity of the body, including air temperature, mean radiant temperature, air velocity and, depending on these average, convective and radiative heat transfer coefficients.

The CFD models require skin and cloth temperatures as inputs for boundary conditions of the virtual manikin. For these investigations these parameters are calculated as follows:

$$t_{sk} = 35.7 - 0.0275\,(M - W) \qquad (°C)$$

$$t_{cl} = 35.7 - 0.028(M - W) - R_{cl}\left\{39.6 \times 10^{-9} f_{cl}\left[(t_{cl} + 273)^4 - (\bar{t}_r + 273)^4\right] + f_{cl} h_c (t_{cl} - t_a)\right\} \qquad (°C)$$

Skin and cloth temperatures are calculated iteratively with Microsoft Excel using a Visual Basic process called the PMV analytical approach. Results are tabulated in a spreadsheet shown in Figure 3.2.2. In order to increase calculation accuracy, the air temperature, mean radiant temperature and average air velocity were assessed in an initial CFD simulation. The skin and cloth temperatures obtained through the PMV analytical approach were used as the boundary condition inputs for updating the final CFD models.

Input		
Clothing	{clo}	0.57
Skin area	{m2}	1.8
Metabolic rate	{met}	1
External work	{met}	0
Air temperature	{C}	27
Mean radiant temperature	{C}	27
Relative air velocity	{m/s}	0
Relative humidity	{%}	60

Clothing thermal resistance (Rcl)	{m2.K/W}	0.08835
Clothing area factor (fcl)	n/a	1.107
Convective heat transfer coefficient (hc)	{W/m2.K}	3.33
Radiative heat transfer coefficient (hr)	{W/m2.K}	4.37
Total heat transfer coefficient of skin	{W/m2.K}	7.71
Total heat transfer coefficient of clothing	{W/m2.K}	6.96
Skin temperature	{C}	34.1
Clothing temperature	{C}	31.2
Vapor pressure of air	{kPa}	2.177

Metabolism	{W/m2}	{W}
Metabolic heat generation	58.2	104.7
Total Heat Generation	**58.2**	**104.7**

Skin	{W/m2}	{W}
Heat loss by convection (C)	14.3	25.7
Heat loss by radiation (R)	18.7	33.7
Heat loss from vapor difussion through skin (Edif)	9.6	17.3
Heat loss from sweating (Ersw)	0.0	0.0
Respiration	{W/m2}	{W}
Evaporative heat loss from respiration (Eres)	3.7	6.7
Convective heat loss from respiration (Cres)	0.5	1.0
Total Heat Loss	**46.8**	**84.3**

Heat Load	**11.3**
PMV	**0.7**
PPD (%)	**17**

Figure 3.2.2: A snapshot of the spreadsheet in Excel showing the calculation of PMV and PPD model. Skin temperature and cloth temperature are used as inputs for manikin's surface boundary conditions for CFD models.

A process diagram showing the developed CFD comfort workflow for linking PMV and CFD approach is depicted in Figure 3.2.2. The sequential steps are explained in the following:

Step 1: An initial CFD simulation run is carried out to predict mean air temperature and mean air velocity close to the body, and mean radiant temperature from objects with direct line of sight to the body.

Step 2: The analytical procedure of the PMCV model is carried out using the personal thermal parameters are used, including M metabolic rate (refer to Appendix F), W mechanical work (assumed as 0 w/m2 for sedentary activity), skin area (assumed as an average 1.8m^2), Clo clothing thermal insulation depending on clothing ensembles worn be the test objects (refer to Appendix G) as well as environmental parameters obtained from the initial CFD simulation run.

Step 3: The skin temperature and clothing temperature considered for the test subject are used as boundary condition inputs for the manikin's surface of the final CFD simulation run.

Step 4: Based on the results of three process steps four latent heat loss components, calculated from the PMV analytical calculation in Step 2, and two sensible heat loss components, convection C and Radiation R from CFD simulation in Step 3, are used to determine the PMV index.

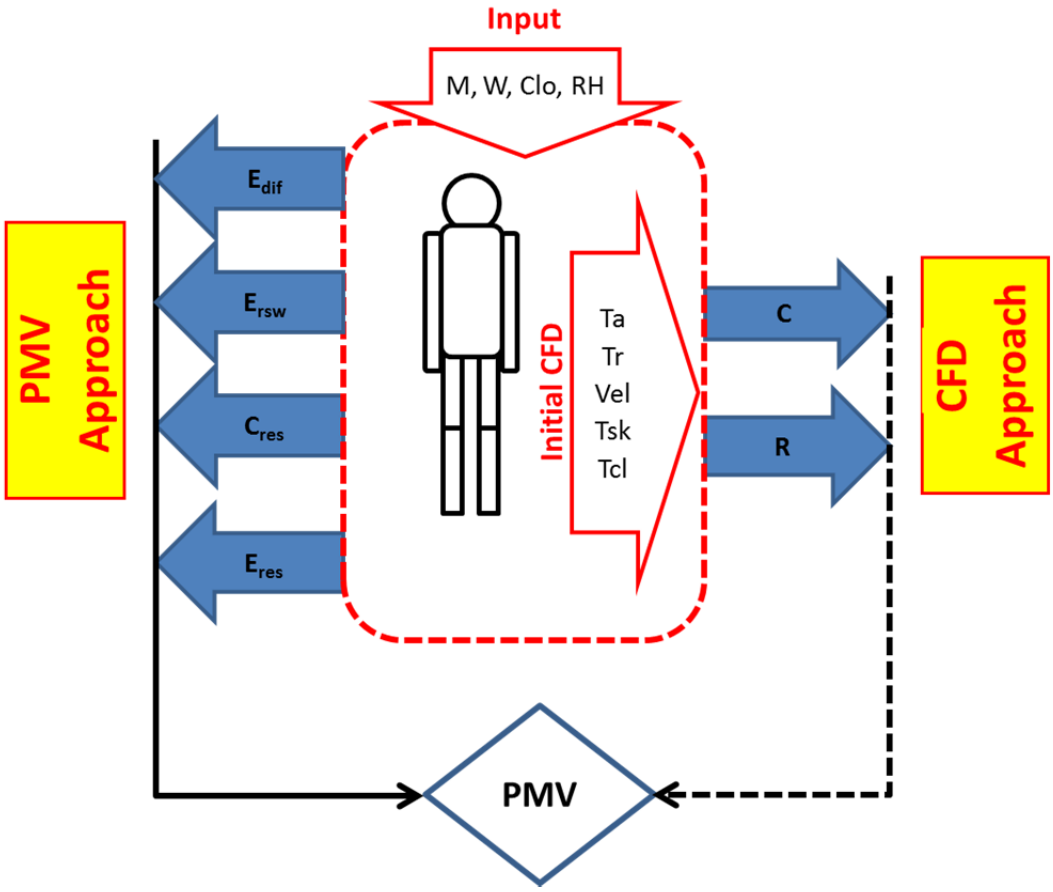

Figure 3.2.3: Workflow of linking PMV and CFD approach

3.3. Overview of CFD Workflow of Convective and Radiative Heat Transfer

This section describes the process developed for these investigations of modeling the convective and radiative heat transfer processes in a space that resembles the geometry of the test set-up which will be used for validation of numerical values. The geometry used for developing the generic CFD comfort workflow includes one seated manikin, three cooling panels surrounding the manikin and one ceiling fan directly above the seated manikin. The geometry is shown in Figure 3.3.1.

The generic CFD comfort work is depicted in Figure 3.3.1 and consists of three main process steps:

1. 3D-CAD modeling of the geometry of the computational domain
2. Creating the computational grid (meshing)
3. Solving the equations of the flow field and heat transfer rates, including definition of boundary conditions, defining the solver, solution convergence and monitoring.

The results from CFD simulation will allow predicting convective and radiative heat transfer of a body working within a “comfort island”, which is defined as the space with the cooling panel system around the occupant and ceiling fan induced air movement ventilation. The goal of the “comfort island” is the improvement of comfort without the need to condition a larger space which would include multiple comfort islands.

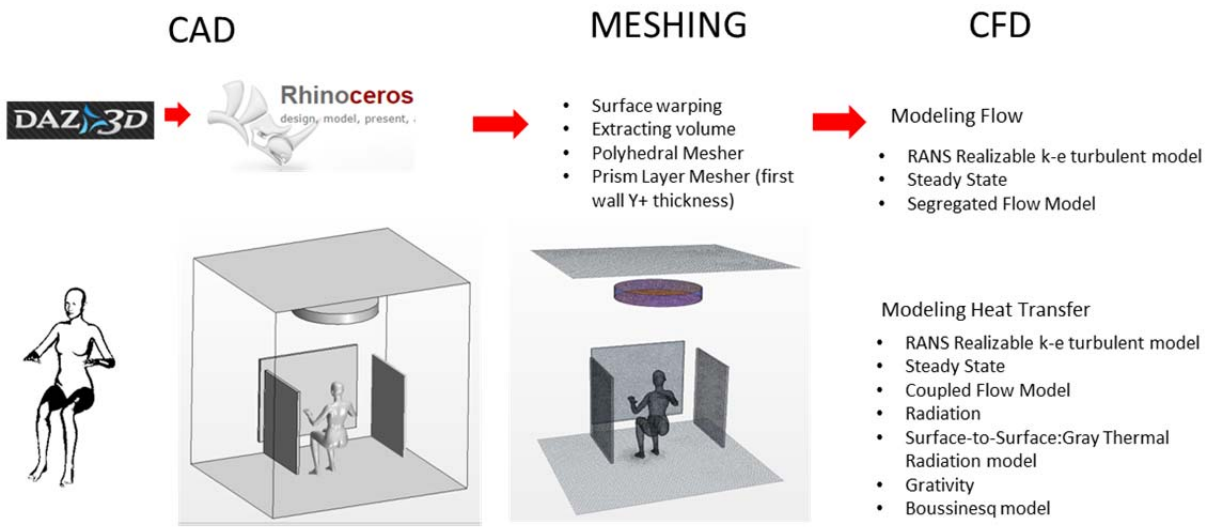

Figure 3.3.1: Sequential workflow steps of CFD modeling and assessing flow field and thermal transfer characteristics of a typical “comfort island” workspace.

3.4 Detailed Description of Steps in the Generic CFD Comfort Simulation Workflow

This section provides a more detailed description of steps in the generic workflow.

Creating the 3D geometry – the 3D-CAD model:

For the development of the generic workflow a small workspace of 2.5m x 3.0m x 3.m (LxWxH) were modeled in Rhino3d modeling software. The workspace included the geometry of a manikin, three vertically oriented panels and one cylinder that represented a ceiling fan. The 3D-manikin was modeled in the DAZ3d software and then imported into Rhino3d, where it was repositioned within the 3D office model before being exported to the CFD software STAR-CCM+, where it was refined with the surface wrapping mesher function for subsequent for surface and volume meshing. Figure 3.4.1 shows the geometry used for these investigations.

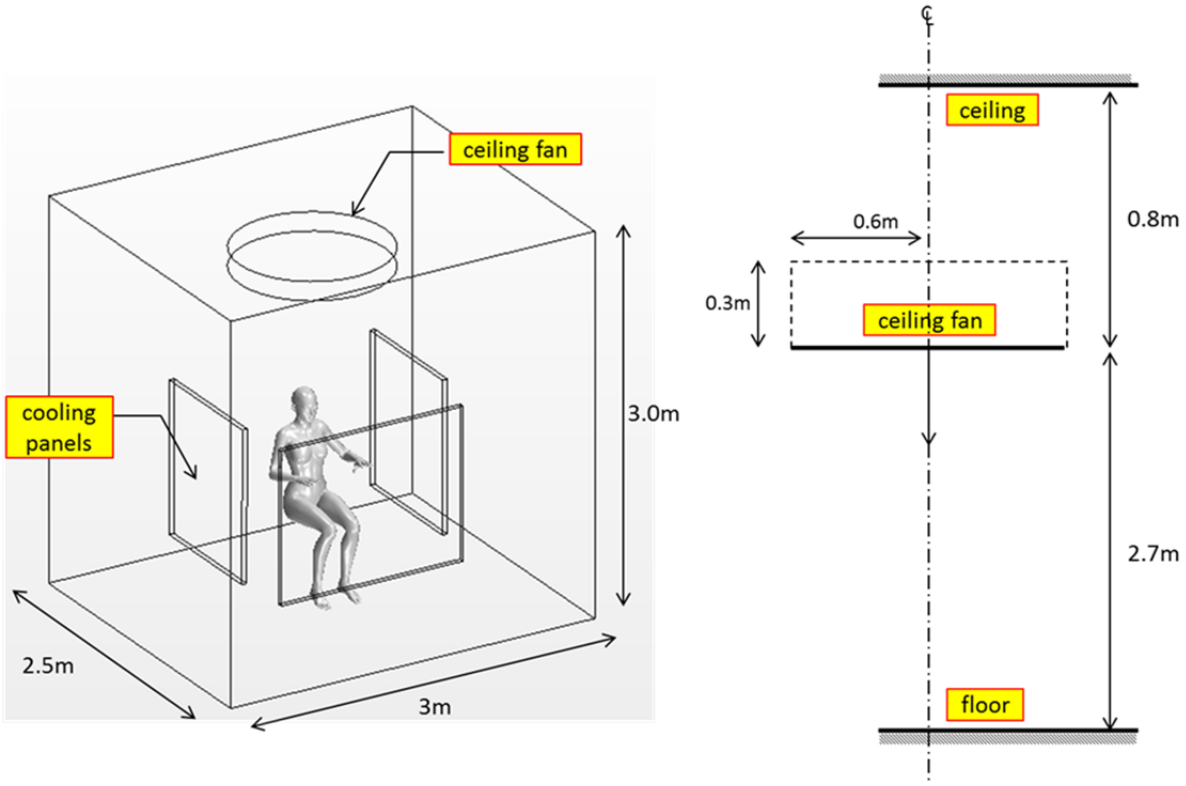

Figure 3.4.1: A 3D-CAD model of the office with a manikin, a ceiling fan and three cooling panels.

Creating the Computational Grid – Meshing:

A parts-based meshing approach was deployed for this study, since it offered advances over the region-based meshing in terms for flexibility in modifying the model and grid and thus allowing reuse of the meshing process if any part was to be updated or replaced.

The 3D manikin model after being imported from Rhino3d into STAR-CCM+ was split into different parts called heat, torso, etc. (see Figure 3.4.2, upper expanded function tabs at the left). The surface wrapping mesher function was then used to create a new and error-free surface wrapping around the manikin's body surfaces. The internal air volume was created by using "Extract Volume" feature. The automated Mesher function was used to create surface mesh and volume meshing for the CFD model. Surface Wrapping Mesher, Extract Volume Mesher, Automated Mesher were activated in the Operations node shown in Figure 3.4.2.

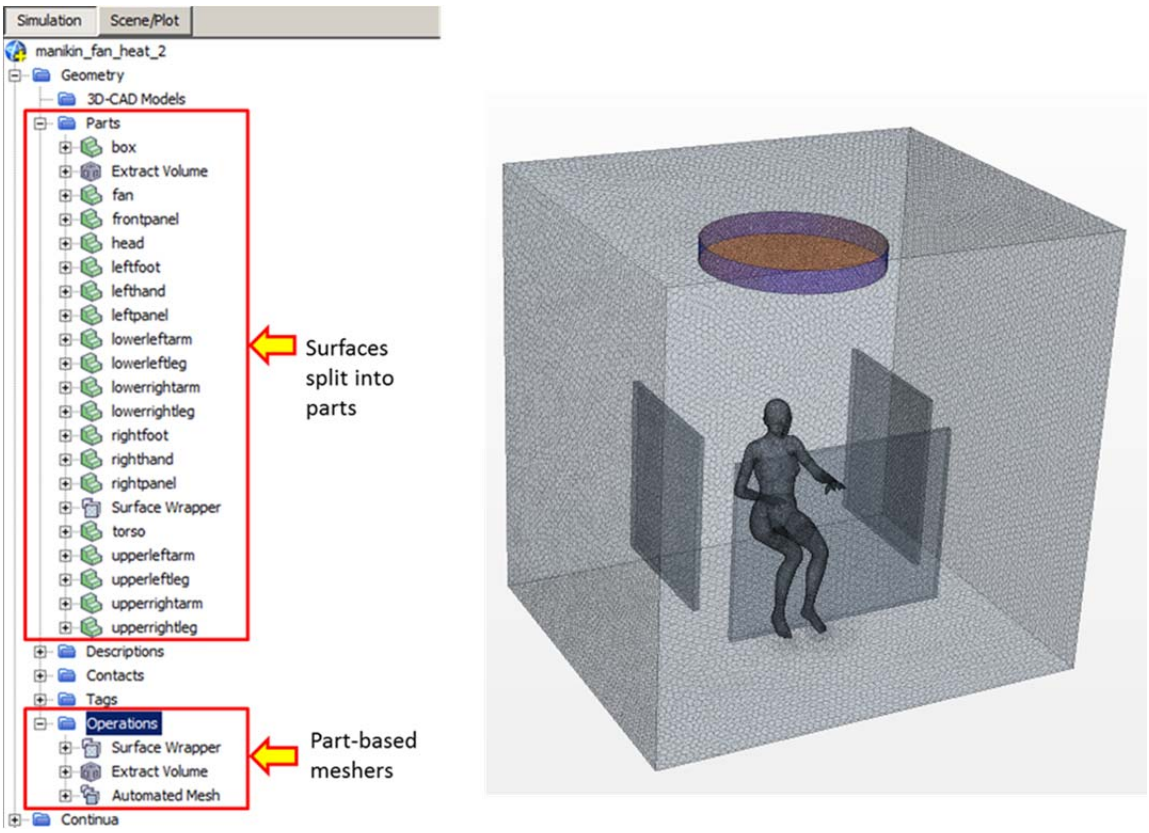

Figure 3.4.2: Meshing settings in STAR-CCM+, showing surface splitting for part-based meshing, meshers being used and the final surface meshing of the cfd model.

Volume meshing was carried out by using the Polyhedral Mesher function to spatially discretize the computational domain into polyhedral grids. Figure 3.4.3 shows the final computational grid.

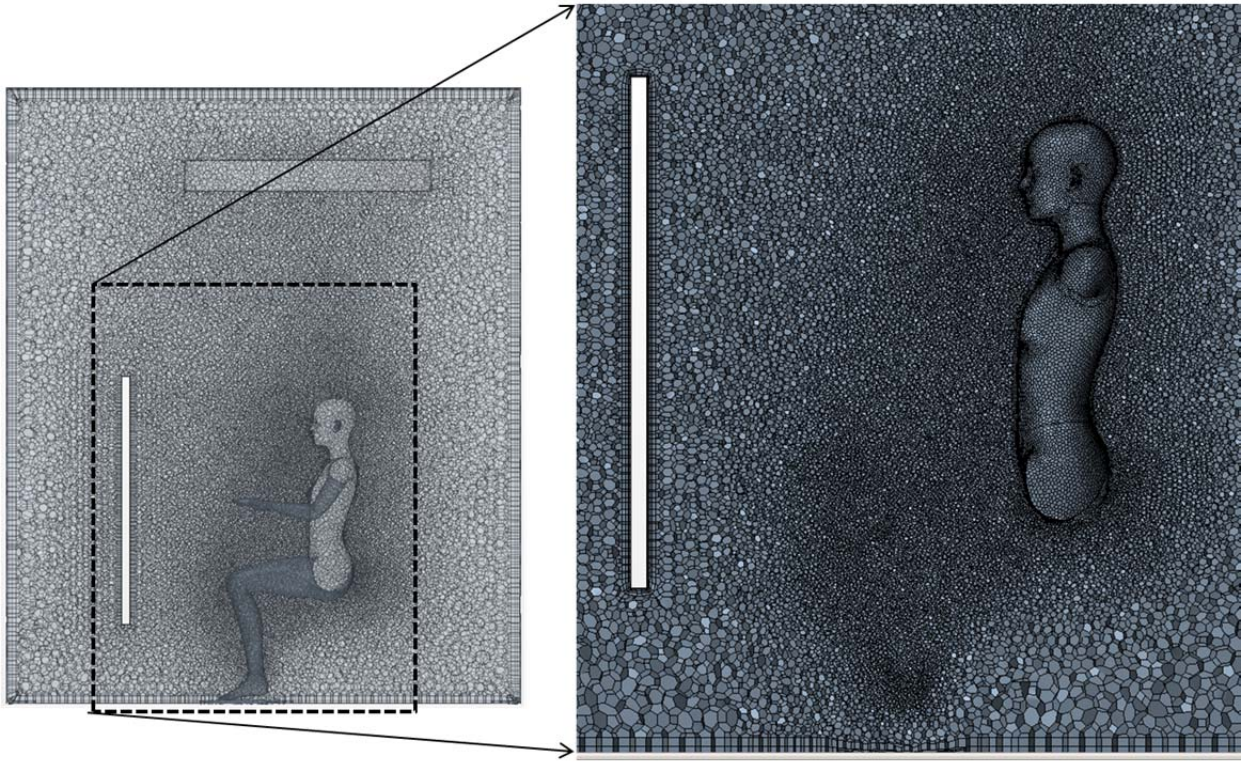

Figure 3.4.3: Final volume meshing of the CFD model using STAR-CCM+ polyhedral mesher, showing finest resolution at the area of interest

The area around the manikin was refined so that a higher cell density in order to achieve a better convergence and accuracy. For properly solving the airflow within near wall region (the laminar sublayer region), fine meshing with four-layer prism layer meshing was used and sized so that the dimensionless near-wall distance y+ is smaller than 12 (recommended by STAR-CCM+, STAR-CCM+ User Guide 10.02). A scalar plot showed the y+ spectrum of the model lying within 0 and 12. Two small areas on the floor were clipped from the plot for having y+ greater than 12. However, these areas are not within the area of interest and these areas will not significant affect the result of the solution (see Figure 3.4.4). A finer resolution can be applied to further reduce the y+ however requiring more computational resources.

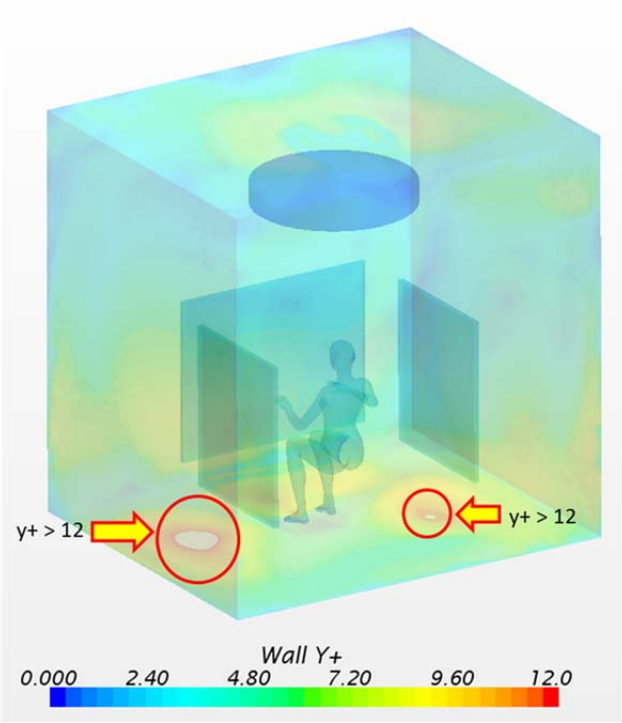

Figure 3.4.4: A plot of dimensionless wall distance y+

Boundary conditions:

For ease of measurement, all wall surface and cooling panels were set at constant temperature during the development of the generic workflow. This assumption assumed a steady state after reaching thermal equilibrium. This assumption reduced complexity and calculation time and was thought sufficient for the development of the generic workflow.

Consequently the surface temperatures of ceiling, floor, all walls and cooling panels were all set 27°C. The manikin's surface temperatures are determined from analytical approach taking account for metabolic rate, clothing thermal insulation, air temperature, mean radiant temperature and average air velocity.

The flow field induced by the ceiling fan was determined by assigning a velocity inlet function to the bottom of the cylinder which represented the outlet of the ceiling fan rotor. In the first round of CFD simulations the spatial distribution of velocities in the ceiling fan's plane was as interpolated from a discrete velocity values obtained for a generic ceiling fan. In a following refinement of input variables a velocity profile was obtained that closely resembled the ceiling fan that would be used in the subsequent comfort tests. The measurements of the velocity profile of the preliminary ceiling fan

configuration in the test set up are shown in Appendix D. The top plane of the cylinder representing the ceiling fan was assigned as pressure outlet with 0 Pa for solving the fluid's momentum equations.

Figure 3.4.5 shows all boundary conditions used in the CFD simulation of the simplified workspace used in the development of generic workflow.

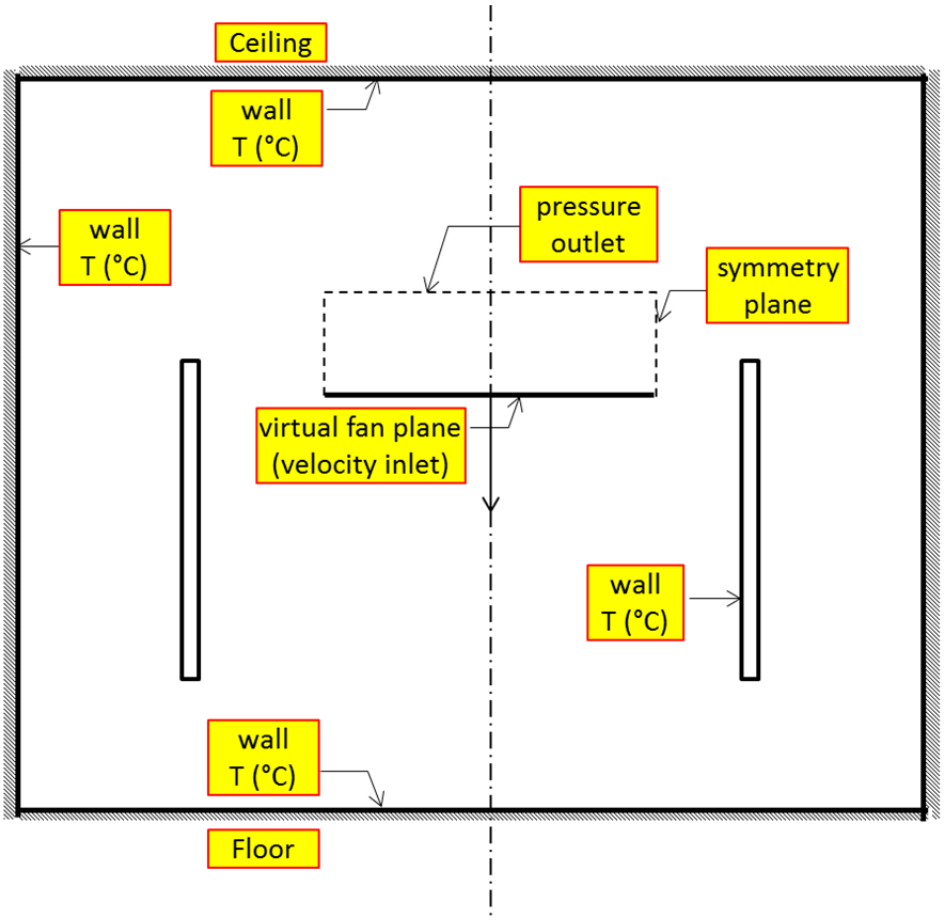

Figure 3.4.5: Boundary condition types of the CFD model

Solver settings:

Reynolds-Average Navier-Stokes (RANS) turbulence modeling with the Realizable *k-ε* turbulence model was selected. Only steady-state model was used for two reasons. One, the steady state assumption in the CFD simulation significantly reduces the require computational resources which will allow the CFD team to carry out a significant number of simulations scenarios for the validation with the subsequent tests in the comfort test chamber. Two, the subsequent test of real world performance of the comfort

island will be conducted in steady state, using time averages of environmental variables and personal responses of test subjects.

A coupled flow and energy model were assigned to the model for solving natural convection problems or low-velocity forced convection. For natural convection problem, Gravity and Boussinesq model were used.

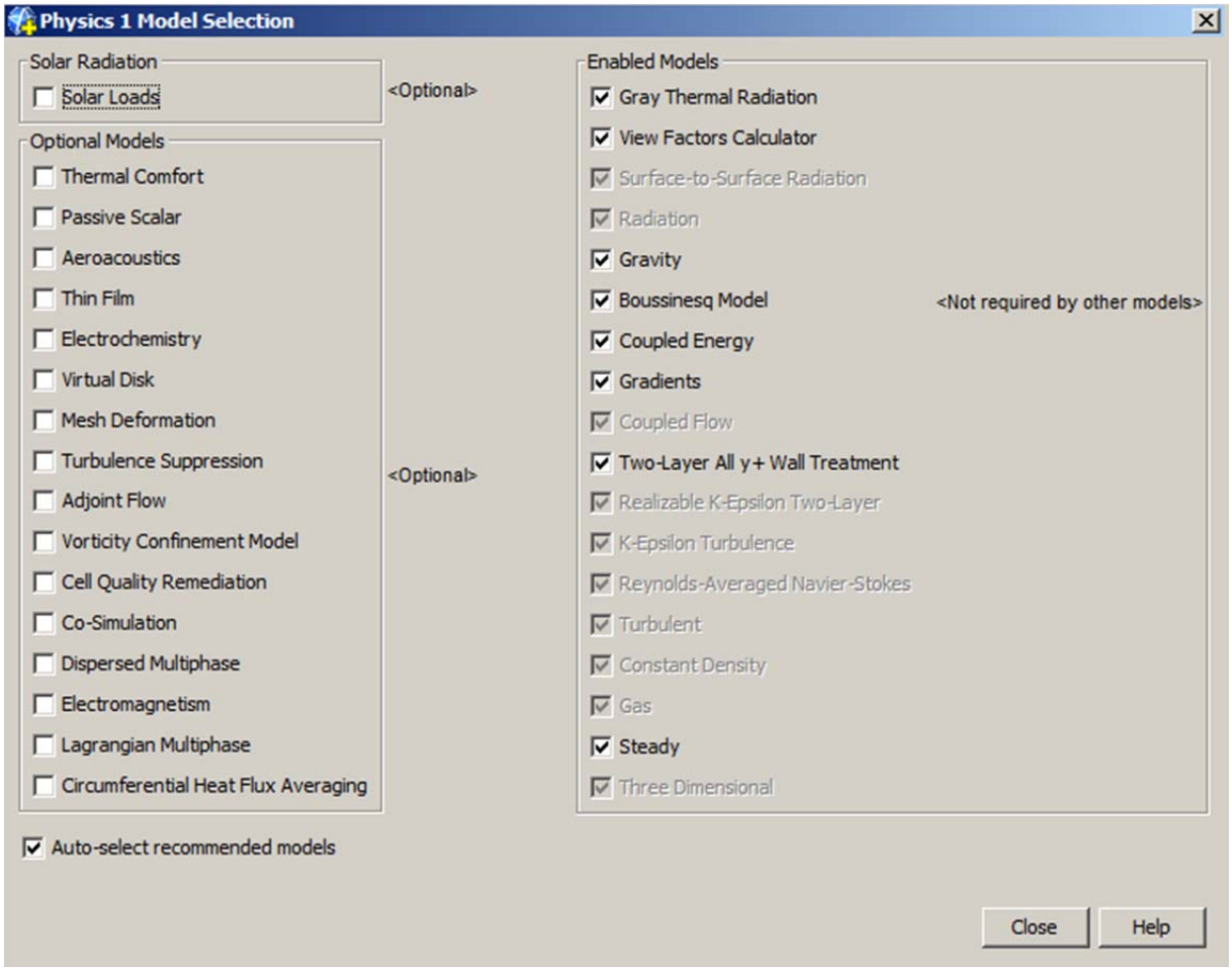

Figure 3.4.6: *Solver settings chosen for solving convective and radiative heat transfer model in STAR-CCM+.*

Radiative heat transfer was solved by using a radiative transfer and radiation spectrum model. The radiative transfer model used spatial discretization and solid angle to solve the Radiative Transfer Equation (RTE) function in STAR-CCM+. For this investigation, the Surface-to-Surface (S2S) the radiative heat transfer function and Gray Thermal Radiation (GTR) as the radiation spectrum models were selected. Figure 3.4.6 shows a screen plot of the solver setting in STAR-CCM+

Surface-to-Surface model was selected to omit non-participating media scatter, this means that the radiative energy that is emitted or absorbed by the air volume that fills the space between the surfaces. In the S2S radiative transfer model, the amount of radiation a surface receives and emits only relies on the radiation properties and the thermal boundary conditions of the surfaces, including emissivity, reflectivity, transmissivity and radiation temperature.

The radiation spectrum selected in these investigations was the Gray Thermal Radiation (GTR) model. The GRT can be used in typical problem solving as a good approximation of more complicated frequency dependent thermal radiation properties. GTR approximates the full thermal wavelength domain as a single spectrum, thus radiation properties of the media and surround surfaces were based on the same wavelengths. The GRT approximation is based on the fact that the emissivity values of the surfaces of the computational domain boundaries body can be considered as constant around the peak emission wavelength.

Convergence criteria and solution monitoring

Several convergence criteria were used in these CFD simulations. One of the convergence criteria was residuals computed during iterative process to determine the RMS errors of the main parameters solutions, such as continuity, momentum, kinetic turbulence energy (e), turbulence dissipation rate (k). The convergence criteria for these parameters were set at a 10e-4 (See Figure 3.4.7). Most useful, mean intuitive convergence indicators were the solution characteristics of heat flux, average velocity, mean radiant temperature, particular within the area of interest. Figure 3.4.8 illustrates the convergence of the heat flux for the manikin as an example.

In order obtain the average wind velocity and the mean air temperature around the body from the CFD model simulation, a 3D array of 1887 virtual probes around the manikin was used to extract data from simulation results (Figure 3.4.9). The virtual probes determine flow field data at particular points in the computational domain. A report of the mean air velocity and air temperature was plotted per iteration for checking solution convergence (Figure 3.4.10).

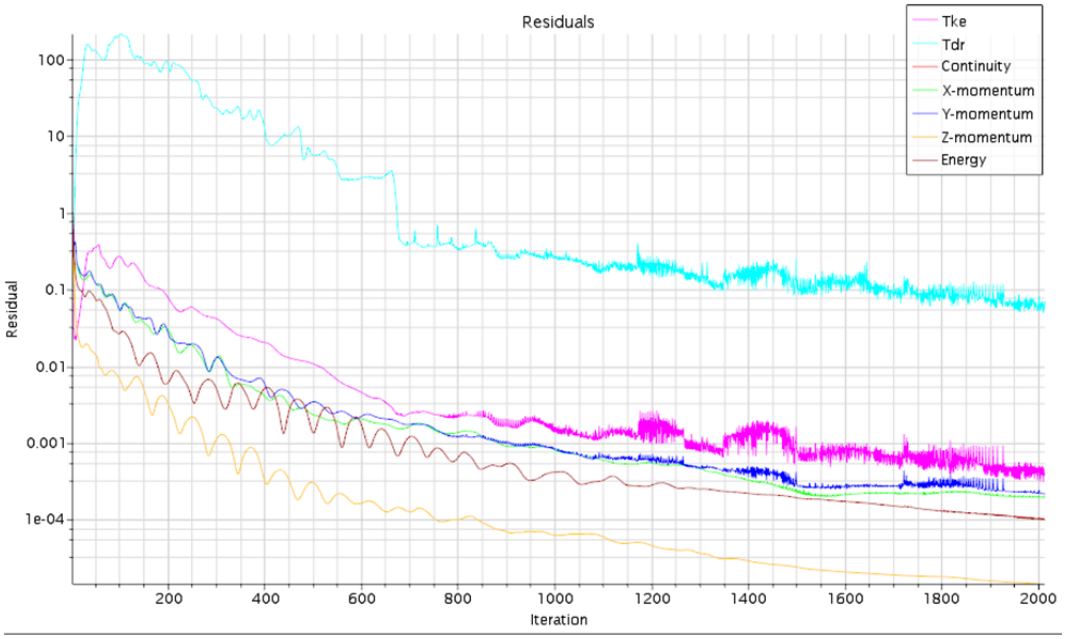

Figure 3.4.7: *A plot of residuals of continuity, momentum, kinetic turbulence energy, turbulence dissipation rate for checking solution convergence.*

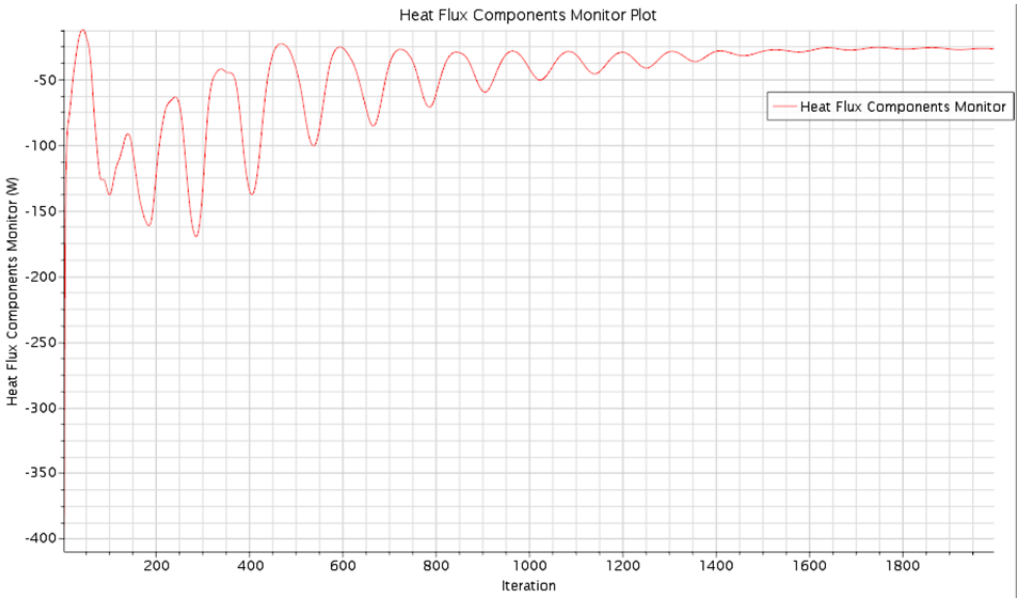

Figure 3.4.8*: A plot showing the total heat flux (convective heat flux and radiative heat flux) of the manikin per iteration for checking solution convergence.*

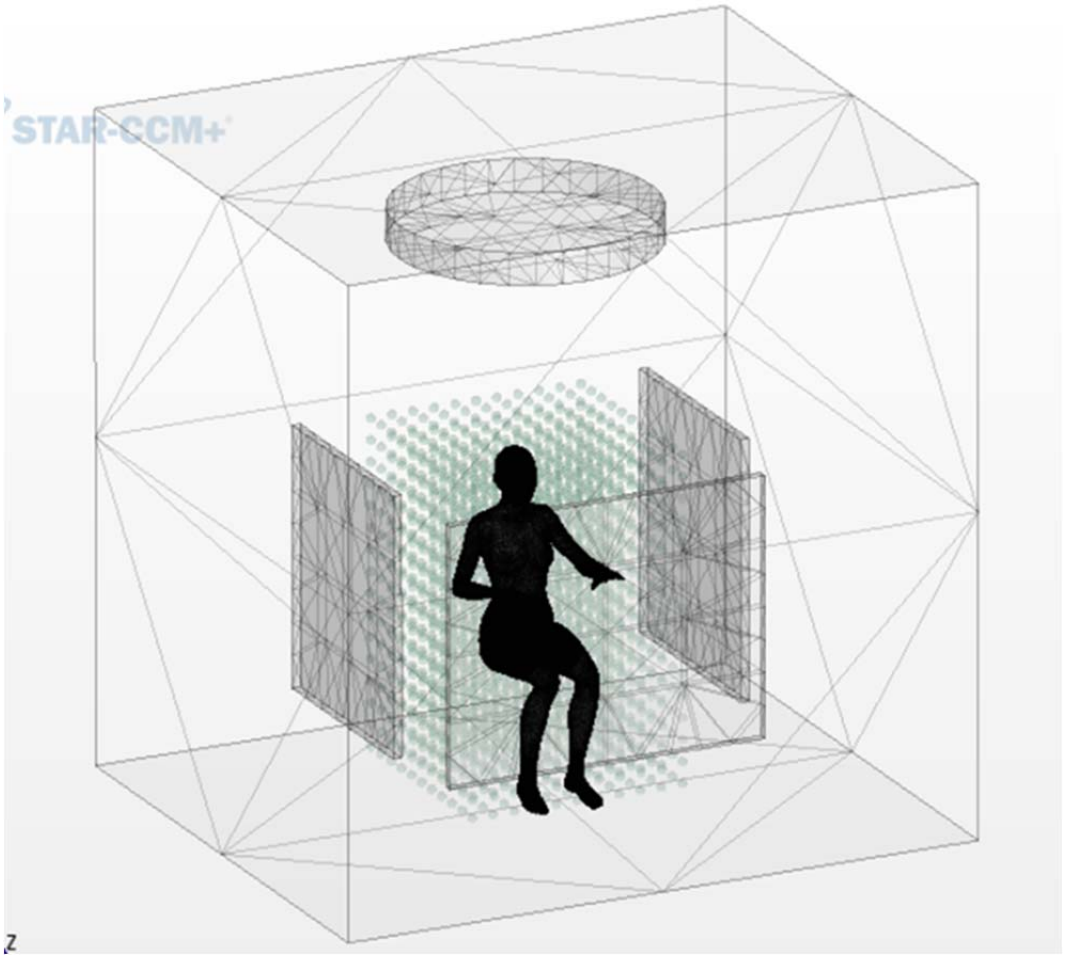

Figure 3.4.9*: 1887 probes located around the* manikin *to extract the flow field data from the simulation results to determine mean air velocity.*

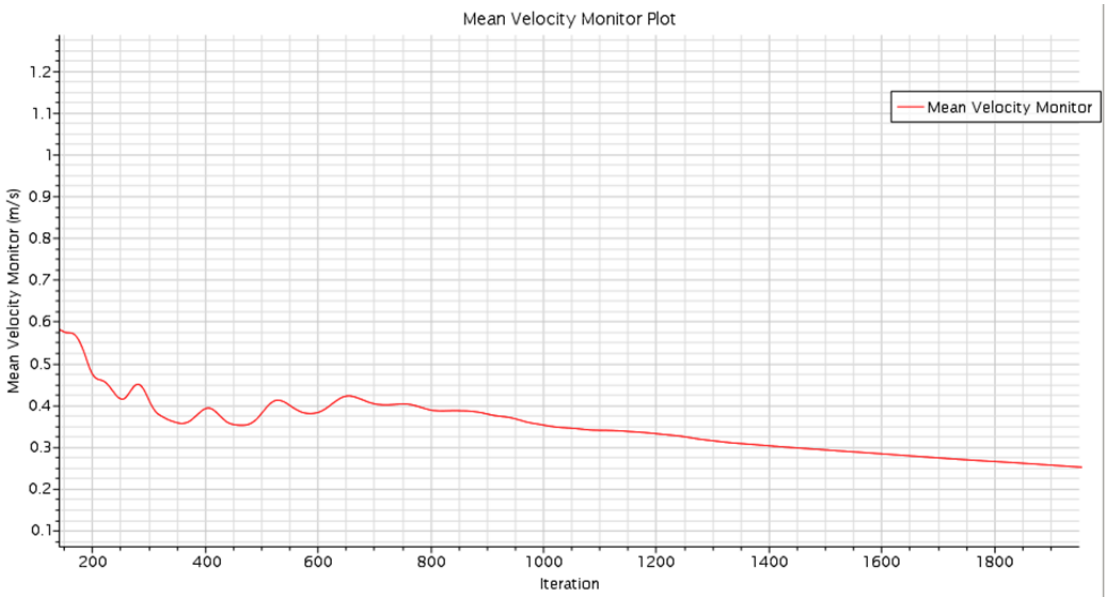

Figure 3.4.10 *A plot showing mean air velocity per iteration for checking solution convergence.*

SECTION 4 - PRESENTATION OF RESULTS

This section presents the qualitative (Section 4.1) and quantitative (Section 4.2) results of the investigations. The results show that the proposed generic workflow will be a suitable and effective approach to generate CFD based predictions of comfort related properties in geometries of the comfort test chamber.

As shown in this section, the developed work flow resulted in appropriate accuracy of solutions, good convergence performance, and most of all a streamlined process that will allow the CFD research tam to carry out a significant number of CFD simulations for various scenarios to be tested in the comfort chamber.

4.1 Qualitative Results

The visualization of CFD solutions of two scenarios (ceiling fan off and ceiling fan on) is presented hereafter to illustrate flow field conditions within the generic workspace space, including contour maps of velocity and air temperature at vertical section plane and the horizontal section plane located one meter above the floor plane. Figures 4.1.1 through 4.1.4 show representative temperature and velocity contour maps.

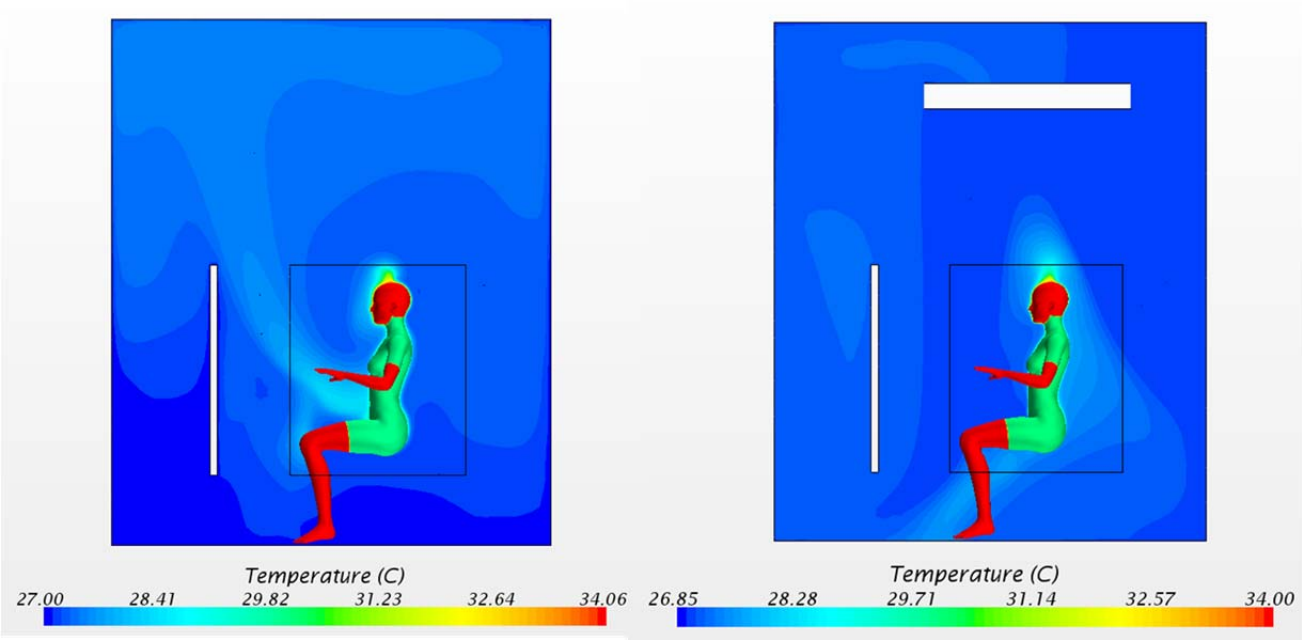

Figure 4.1.1: Temperature contour map at vertical cross section plane when ceiling fan is off (left) and on (right)

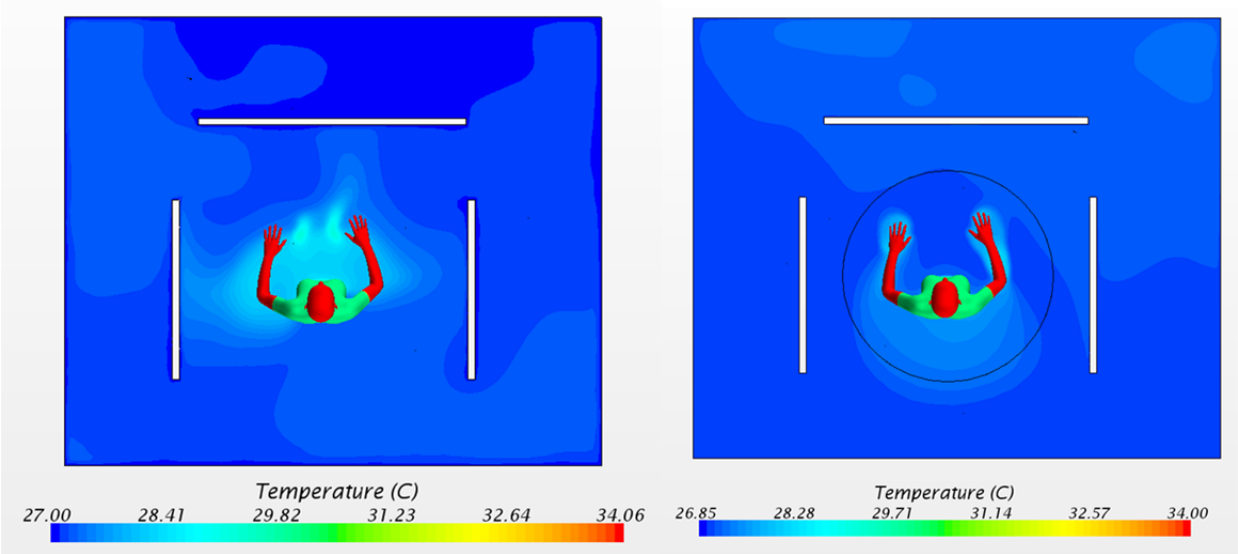

Figure 4.1.2: Temperature contour map at horizontal section plane at 1m above the floor plane when ceiling fan is off (left) and on (right)

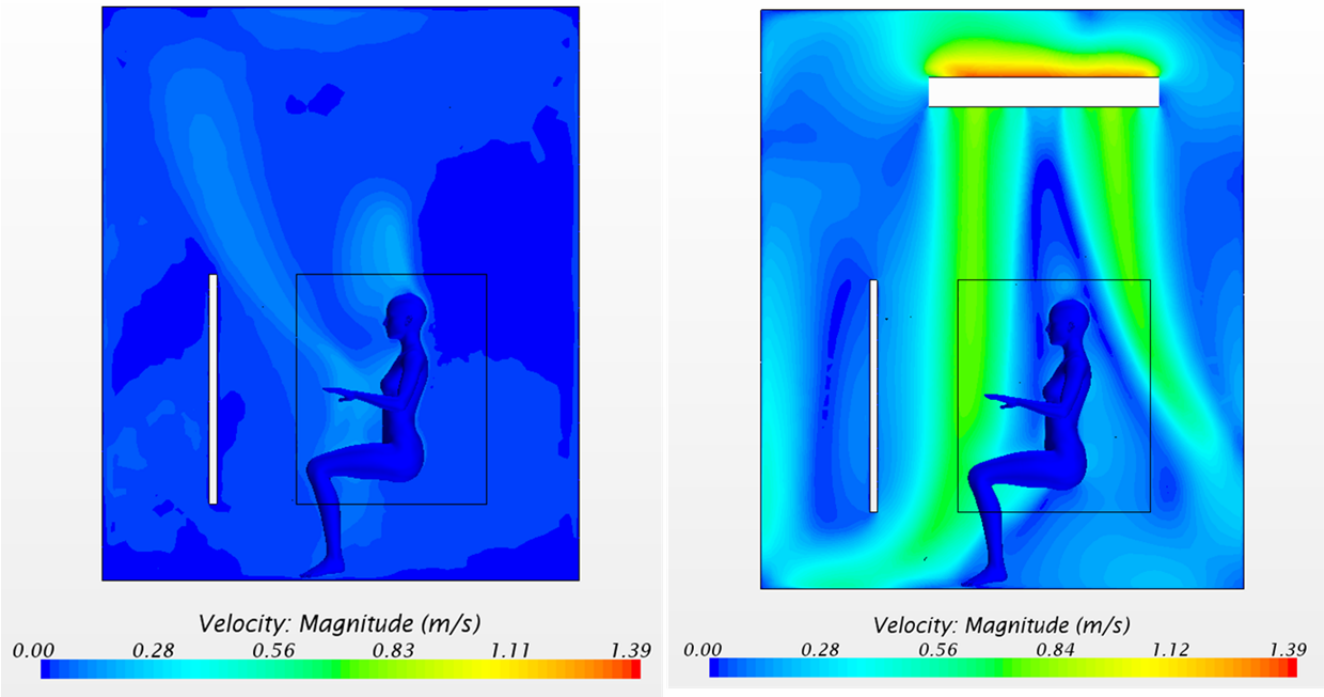

Figure 4.1.3: Air velocity contour map at vertical cross section plane when ceiling fan is off (left) and on (right)

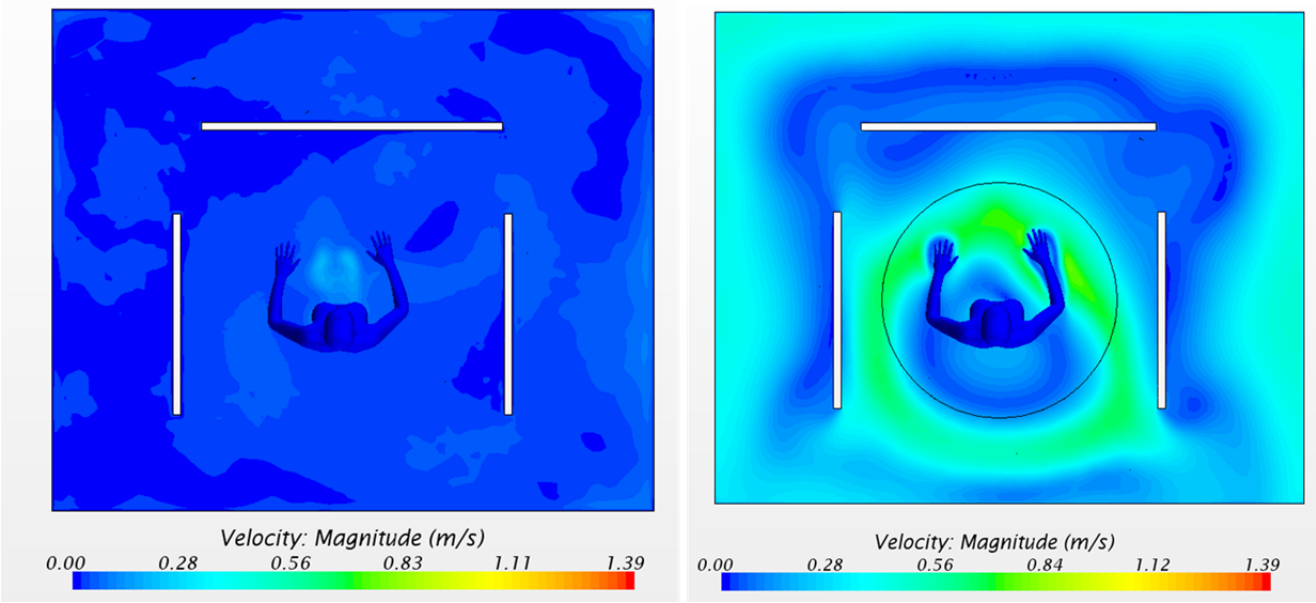

Figure 4.1.4 : Air velocity contour map at horizontal section plane at 1m above the floor plane when ceiling fan is off (left) and on (right)

4.2. Quantitative Results

Determining sensible convective and radiative heat loss:

The CFD results provided a quantitative analysis to extract the convective heat transfer and radiative heat transfer under two test scenarios of ceiling fan on and off. The convective heat transfer is the convective heat loss C and radiative heat transfer is the radiative heat loss R of a body into the environment. These convective heat transfer and radiative heat transfer obtained from CFD approach was compared to those calculated from the PMV analytical approach and are presented in the Figure 4.2.1.

The sensible convective and radiative heat losses calculated in the CFD solution were compared sensible heat loss obtained by PMV analytical approach. It should be stressed that the CFD model used simplified wall boundary conditions with constant temperature distribution. Therefore the CFD and the PMV analytical approaches were both using similar thermal conditions for the sensible convective and radiative heat. Latent heat losses were not modelled in CFD and those were taken from the PMV analytical approach.

	Scenario 1		Scenario 2	
	Convective heat transfer C (w)	**Radiative heat transfer R (w)**	**Convective heat transfer C (w)**	**Radiative heat transfer R (w)**
CFD approach	25.82	32.33	49.87	28.97
PMV analytical approach	25.70	33.70	43.06	28.33
Discrepancy	*0.46%*	*-4.07%*	*15.81%*	*2.27%*

Figure 4.2.1: Comparison of convective heat transfer and radiative heat transfer between two approaches: CFD vs. PMV analytical approach: Scenario 1 ceiling fan ON, Scenario 2 ceiling fan OFF

Determining the PMV index and PPD:

According to Fanger's thermal balance equation, thermal neutrality is achieved when the total heat generation equals to total heat loss, consisting of sensible heat loss (convection and radiation) and latent heat loss (see illustration in Figure 4.2.2). Thermal imbalance will cause thermal stress which is mathematically approximated by using Fanger's PMV equation. Using sensible heat loss obtained from CFD solution and total latent heat loss obtained from the PMV analytical approach allows calculation of the PMV indexes and PPD of the office spaces under two test scenarios (Figure 4.2.3).

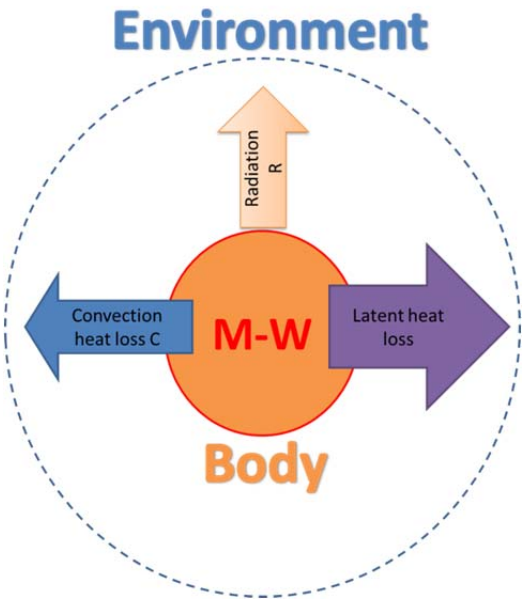

Figure 4.2.2: Thermal neutrality is achieved when heat generation from human metabolism (M-W) equals all sensible heat loss (convection and radiation) and latent heat loss.

	Scenario 1										
	Sensible heat loss (w)		Latent heat loss (w)				Total heat loss (w)	Total heat generation (w)	Heat load (w/m2)	PMV	PPD (%)
	C	R	Edif	Ersw	Eres	Cres					
CFD approach	25.82	32.33	17.27	0.00	6.69	0.98	83.09	104.67	11.99	*0.78*	*18*
PMV analytical approach	25.70	33.70					84.34	104.67	11.29	*0.74*	*16*
	Scenario 2										
CFD approach	49.87	28.97	17.27	0.00	6.69	0.98	103.79	104.67	0.49	*0.03*	*5*
PMV analytical approach	43.06	28.33					96.34	104.67	4.63	*0.30*	*7*

Figure 4.2.3: Comparison of PMV and PPD using two different approaches: CFD vs. PMV analytical approach

SECTION 5 - CONCLUSIONS AND RECOMMENDATIONS

This report summarizes a significant work effort by the ERDL CFD research team to develop a generic CFD comfort simulation work flow, which can numerically predict and/or validate the performance of comfort enhancing measures pertaining to the comfort island concept, which is investigated in this third phase of the HNEI-ERDL CFD research program.

The man objective of this work task was successfully met with the development and testing of a CFD simulation process which uses reasonable simplification of the computational process to arrive at a workflow that is effective using of ERDL's computational resources but yet produces good results that can be validated with the ERDL test set up.

The CFD team makes the following observations, conclusions and recommendations:

- A review of existing CFD approaches to model comfort levels in small spaces was conducted. The review suggested that many numerical prediction applications were concerned with predicting the comfort level in automobiles. In fact much of the CFD comfort simulation applications and other comfort investigations were developed specifically for the automobile as well as the aerospace industry.

- Several specific CFD comfort simulation "wizards" were reviewed and found that they were created for specific applications and were not appropriate for the present investigations due to flexibility in the application. The CFD team therefore decided to develop a generic CFD comfort simulation approach based on a combination of the common PMV comfort model, addingcomponents that would provide an increase in CFD analytic accuracy. The commonly used PMV analytical model is based on steady state and uniform (or averaged) thermal condition of the surrounding environment.

- Other previous CFD comfort simulation approaches reviewed by the CFD research team considered the contribution to overall comfort experience by local comfort, such as thermal sensation of different body parts. The local heat losses modelled in these investigations were then subsequently validated by direct measurements at the human test subject of instrumented manikins. The consideration of local thermal sensation is closely related to physiological comfort levels which offer new approaches to asses comfort.

- While the CFD comfort simulation model developed by the ERDL CFD team can also distinguish and quantify local heat transfer phenomena, these local heat fluxes are averaged to determine a whole body average heat loss. The experimental approach of the ERDL test set-up is based on using average and steady state determination of the whole body thermal environmental and

personal (of the test subject) properties. While creating a whole body averaged thermal losses and an average description of the flow field is a simplification of the potential numerical comfort prediction and a somewhat reduction in accuracy, this approach is used to complement the specific test procedure in the ERDL comfort chamber. The available ERDL instrumentation precludes the measurement of different body parts of the human test subject or an instrumented manikin and I used instead averaged environmental parameters.

- Using the developed CFD comfort simulation approach specifically to determine sensible convective and radiative heat loss is unique for the investigation of the effectiveness of the "comfort island" approach, which has been developed by the ERDL research team. The comfort island approach is based in increasing convective heat loss through ceiling fans and radiative heat loss through actively cooled panels, which are placed in close proximity to the human occupant. The use of comfort islands precludes the thermal conditioning and dehumidification of the space that would contain "comfort islands". The avoidance of space-wide conditioning can save significant amounts of energy and building equipment and is therefore cost attractive for future sustainable building designs. In addition, the convective and radiative heat losses represent the main portions of overall heat loss.

- The generic CFD comfort simulation presented in this report will be used in a subsequent CFD simulations to determine heat loss and flow filed characteristics of the final test set-up of the ERDL confer chamber. During the development of the generic CFD comfort simulation work flow the test set-up in the ERDL comfort chamber was still under development and therefore the CFD team has to finalize certain aspects of the workflow once the experimental test set-up is operational and measurement data can be obtained. The CFD team is confident that the developed CFD comfort workflow is flexible enough to allow subsequent modifications if the finalized ERDL comfort chamber calls for specific changes in boundary conditions.

- Lastly, the CFD team benchmarked the workflow against a PMV analytical model and concluded good consistency of simulations results, where simulations were based on simplified boundary conditions and averaged environmental properties which are typical for the PMV approach. These simplifications included uniform distributed temperatures of air and surfaces. In the experimental tests of the ERDL comfort chamber, air and surfaces temperatures will be non-uniform and the CFD team expects that the developed CFD comfort simulation workflow will provide more accurate results than obtained by using space wide averages.

- As a view on future research work by ERDL, the CFD comfort simulation approach will be available when local comfort measures will be included in the numerical as well as the experimental assessment of occupant comfort levels. In this future research work instrumented

manikins could be used to validate numerical predictions performance in determining effectiveness of comfort island performance.

LITERATURE

Arens, E., et al (2005) "Partial- and whole-body thermal sensation and comfort, Part I: Uniform environmental conditions", Parts 1 through 3, Center for the Built Environment, UC Berkeley

ASHRAE (2005) "Fundamentals handbook", American Society of Heating, Refrigeration and Air-Conditioning Engineers (ASHRAE), Atlanta,

Center for the Built Environment (CBE) (2014) "Advanced Human Thermal Comfort Model; A tool for predicting human comfort resulting from HVAC, building and facade design decisions." Center for the Built Environment, http://www.cbe.berkeley.edu/research/briefs-thermmodel.htm accessed 6/30, 2015

Huang, Li (2014) "Applicability of whole-body heat balance models for evaluating thermal sensation under non-uniform air movement in warm environments", Building and Environment, www.elsevier.com/locate/buildenv, accessed, April 2015

Karadag, Refet (2008) "New approach relevant to total heat transfer coefficient including the effect of radiation and convection at the ceiling in a cooled ceiling room", Applied Thermal Engineering, www.elsevier.com/locate/apthermeng, April 2015

Kurazumia, Y., et al (2008) "Radiative and convective heat transfer coefficients of the human body in natural convection", Building and Environment 43 (2008) 2142–2153

Kim, J.-H., et al (2013) "Is the PMV Index an Indicator of Human Thermal Comfort Sensation?", International Journal of Smart Home, Vol. 7, No. 1, January, 2013

Li, C. and Ito, M (2014) "Numerical and experimental estimation of convective heat transfer coefficient of human body under strong forced convective flow", Journal of Wind Engineering and Industrial Aerodynamics, www.elsevier.com/locate/jweia, accessed, April 2015

Mark Hepokoski et al. (2013) "A Comparison of Physiology-Based Metrics to Environment-Based Metrics for Evaluating Thermal Comfort", SAE International Technical paper provided by the author.

Masayuki,O. (2002) "Convective heat transfer coefficients and clothing insulations for parts of the clothed human body under airflow conditions", Center for the Built Environment, University of California Berkeley

Melikov, A.K. (2010) "Human Physiology and Body's Heat Balance", International Centre for Indoor Environment and Energy Department of Civil Engineering, Technical University of Denmark

Oliveira, V. (2014) "Analysis of natural and forced convection heat losses from a thermal manikin: Comparative assessment of the static and dynamic postures", Journal of Wind Engineering and Industrial Aerodynamics, www.elsevier.com/locate/jweia, accessed, April 2015

Sorensen, D. and Viogt, L. (2003) "Modelling flow and heat transfer around a seated human body by computational fluid dynamics", Building and Environment 38 (2003) 753 – 762

Zhang H.(2003) "Human thermal sensation and comfort in transient and non-uniform thermal environments", Center for the Built Environment (CBE), University of California at Berkeley

APPENDICES

There are six appendices attached to this report:

APPENDIX A - SOLVER SETTINGS CONVECTIVE & RADIATIVE HEAT TRANSFER SIMULATIONS

APPENDIX B - CFD SIMULATIONS FOR CEILING FAN ON/OFF

APPENDIX C - RESULTS OF PMV ANALYTICAL CALCULATION OF TWO TEST SCENARIOS

APPENDIX D - SIMULATING THE CEILING FAN

APPENDIX E - LINKING THE FAN VELOCITY PROFILE INTO CFD BOUNDARY CONDITION

APPENDIX F - TYPICAL METABOLIC HEAT RATES

APPENDIX G - TYPICAL CLOTHING THERMAL INSULATION

APPENDIX A
SOLVER SETTINGS FOR CONVECTIVE AND RADIATIVE HEAT TRANSFER SIMULATIONS

The following settings should be used for convective and radiative heat transfer simulation in the study: Reynolds-Average Navier-Stokes (RANS) turbulence modeling with the Realizable *k-ε* turbulence model, steady-state model, Coupled Flow, Coupled Energy model, Gravity, Boussinesq and Radiation model with Surface-to-Surface (S2S) model) using Grey Thermal Radiation model. These models should be appeared under the Continua>Physics 1> Model as follows:

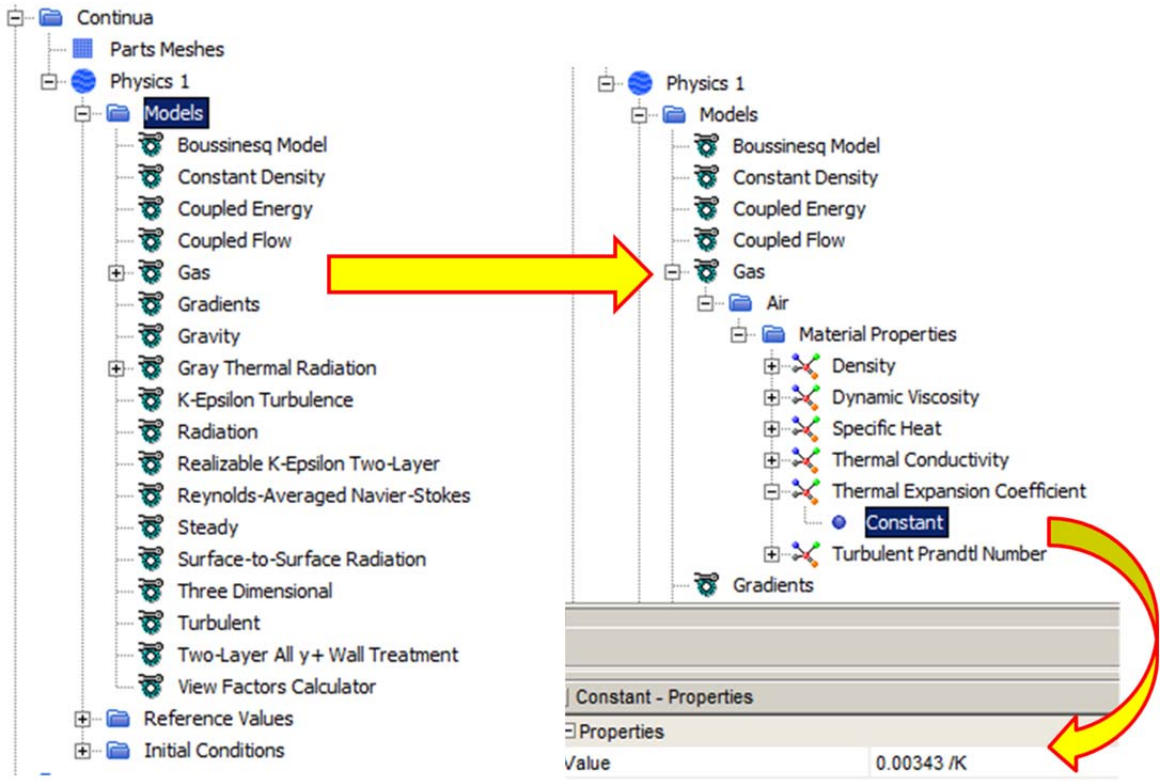

Figure A-1: All solver models are specified in the Physics section of the model and where to specify air properties for the CFD model.

Air properties such as air density, dynamic viscosity, specific heat, thermal conductivity, thermal expansion coefficient are specified at standard conditions, e.g. with the air properties at 20°C, as follows:

Temperature - t - (^oC)	Density - ρ - (kg/m^3)	Specific Heat - c_p - ($kJ/(kg\ K)$)	Thermal Conductivity - k - ($W/(m\ K)$)	Kinematic Viscosity - ν - $x\ 10^{-6}\ (m^2/s)$	Expansion Coefficient - b - $x\ 10^{-3}\ (1/K)$	Prandtl's Number - P_r -
-150	2.793	1.026	0.0116	3.08	8.21	0.76
-100	1.980	1.009	0.0160	5.95	5.82	0.74
-50	1.534	1.005	0.0204	9.55	4.51	0.725
0	1.293	1.005	0.0243	13.30	3.67	0.715
20	1.205	1.005	0.0257	15.11	3.43	0.713
40	1.127	1.005	0.0271	16.97	3.20	0.711
60	1.067	1.009	0.0285	18.90	3.00	0.709

Figure A-2: Density, specific heat, thermal conductivity, kinematic viscosity, expansion coefficient and Prandtl's number for air at temperatures ranging -150 °C to 400°C . Source: www.Engineering ToolBox.com

APPENDIX B

PRESENTATIONS OF CFD SIMULATION RUNS OF TWO TEST SCENARIOS

Scenario 1: Ceiling fan **NOT OPERATING** inside generic work space

Scenario 2: Ceiling **OPERATING** inside generic work space

Presentation of selected results for Scenario 1: Ceiling fan **NOT OPERATING** inside generic work space

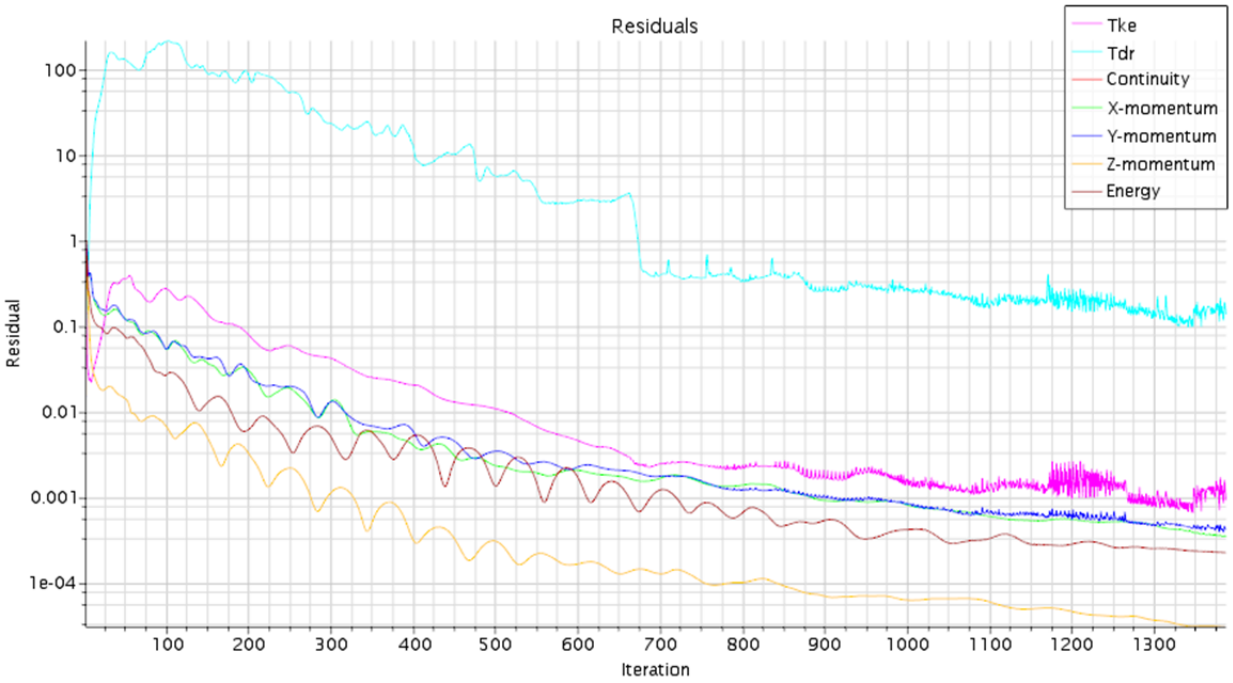

Figure B- 1: **Scenario 1 -** Solution convergence monitor of RMS residuals

Presentation of selected results for Scenario 1: Ceiling fan **NOT OPERATING** inside generic work space

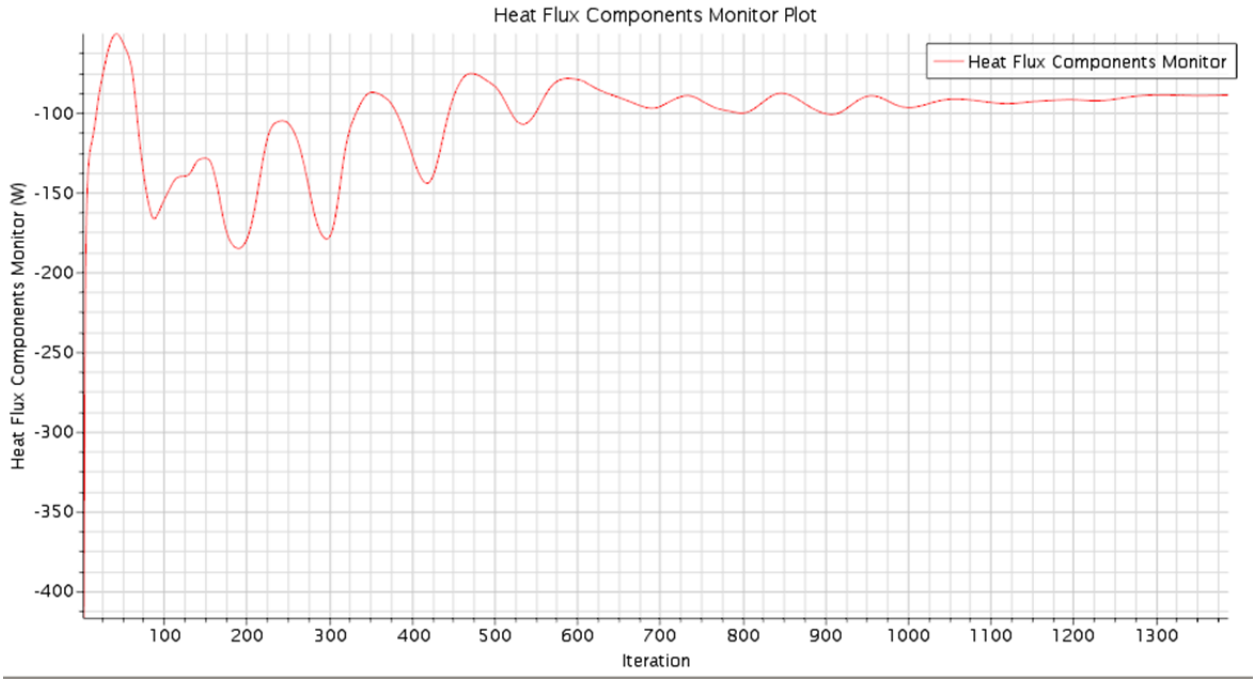

Figure B- 2: **Scenario 1 -** Solution convergence monitor of total heat flux (convective and radiative hat flux)

Presentation of selected results for Scenario 1: Ceiling fan **NOT OPERATING** inside generic work space

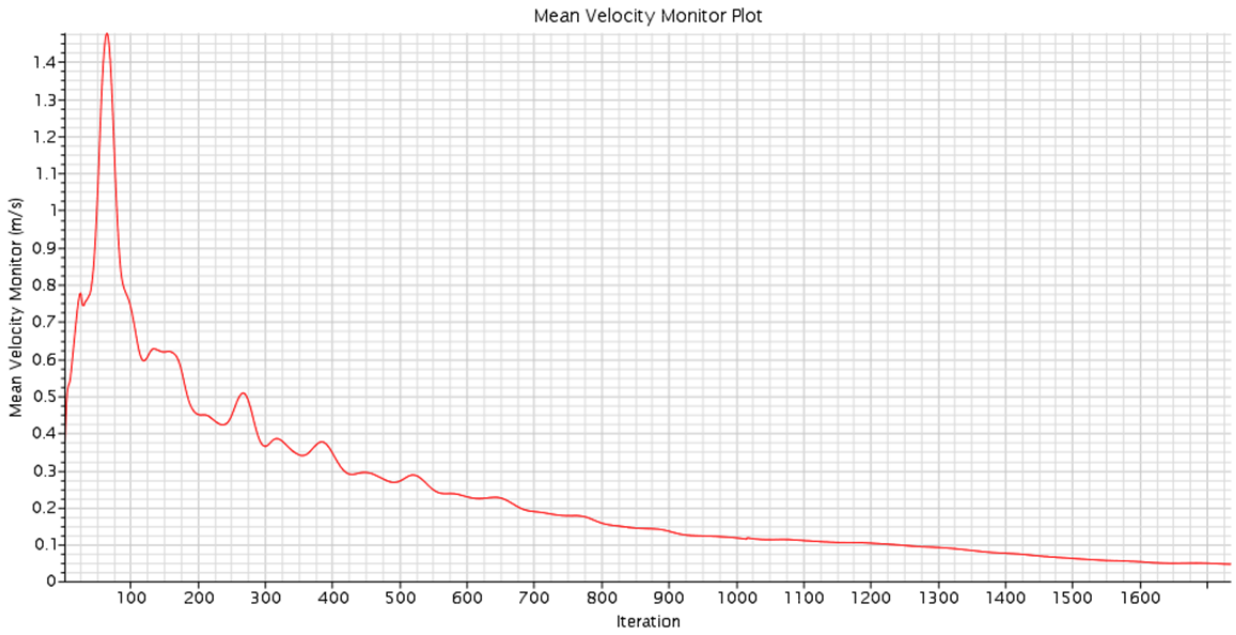

Figure B- 3: **Scenario 1 -** Solution convergence monitor of mean air velocity. Solution converged when mean air velocity reached 0.05m/s

Presentation of selected results for Scenario 1: Ceiling fan **NOT OPERATING** inside generic work space

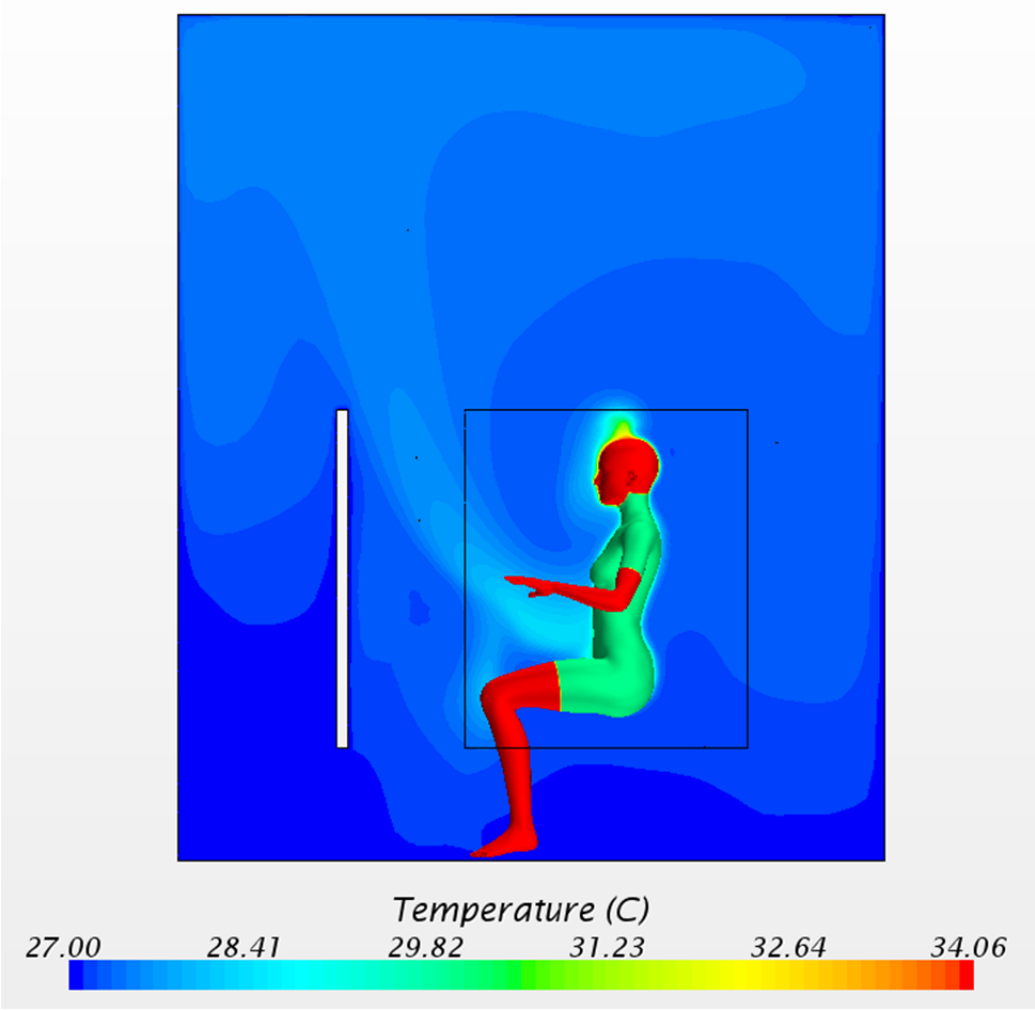

Figure B- 4: **Scenario 1 -** Temperature contour map on the longitudinal section plane

Presentation of selected results for Scenario 1: Ceiling fan **NOT OPERATING** inside generic work space

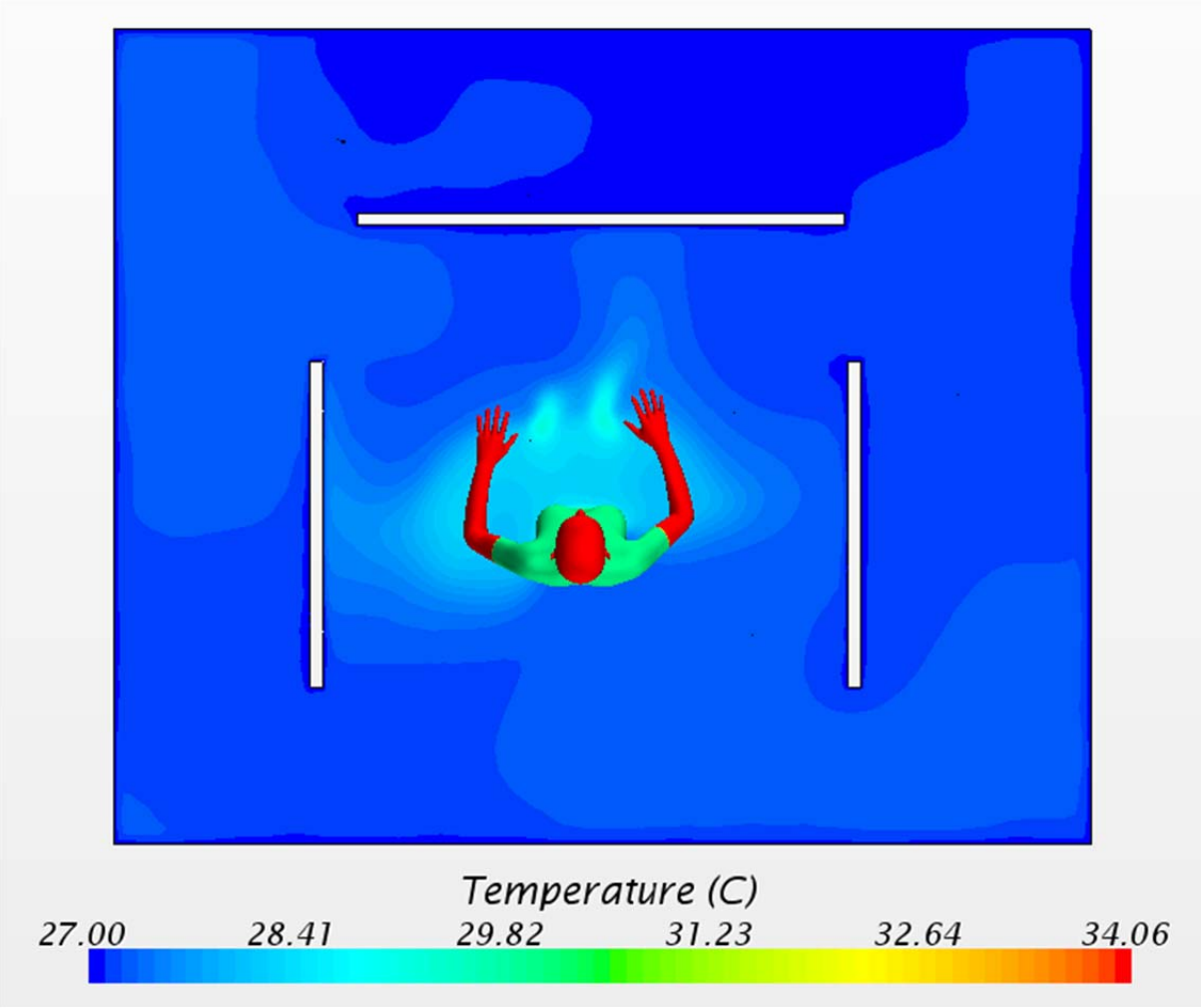

Figure B- 5: **Scenario 1 -** Temperature contour map on the horizontal section plane at 1.0m above the floor level.

Presentation of selected results for Scenario 1: Ceiling fan **NOT OPERATING** inside generic work space

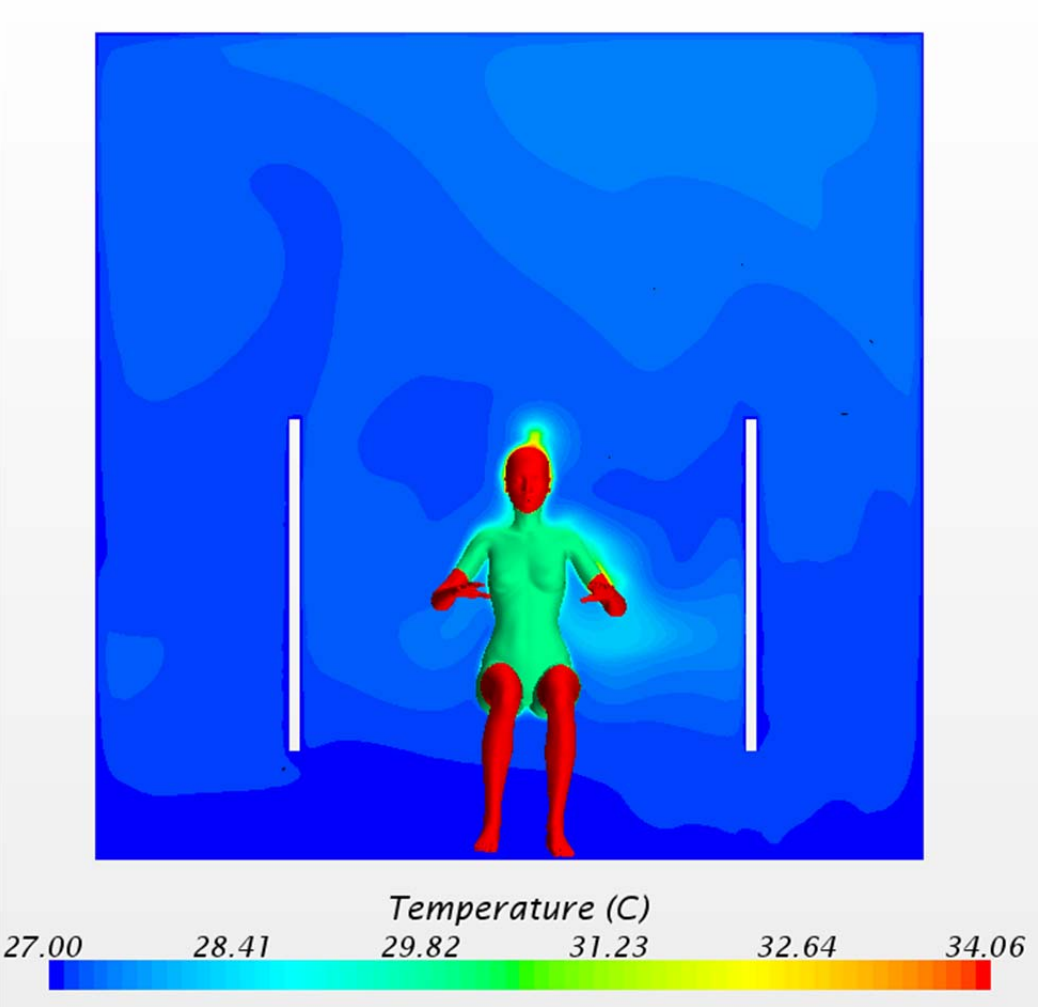

Figure B- 6: **Scenario 1 -** Temperature contour map on the transverse section plane

Presentation of selected results for Scenario 1: Ceiling fan **NOT OPERATING** inside generic work space

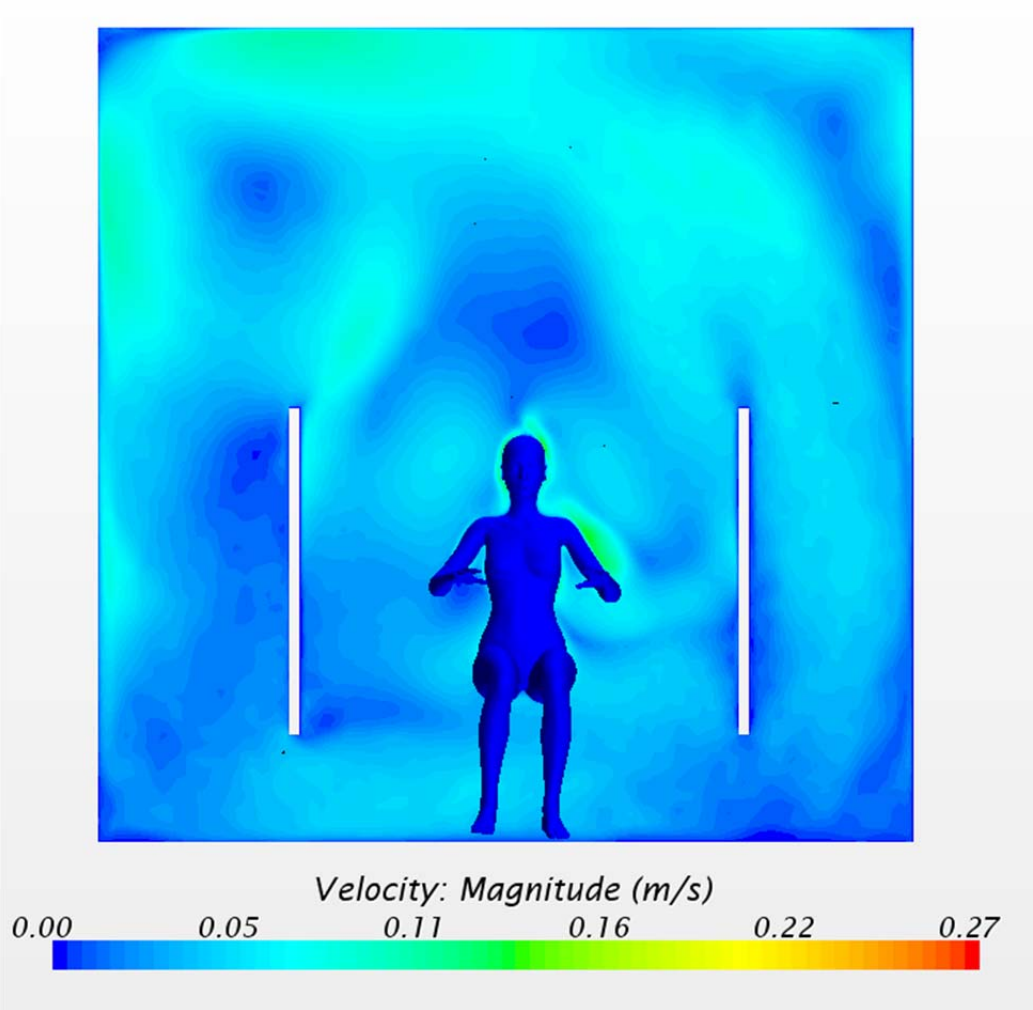

Figure B- 7: **Scenario 1 -** Velocity contour map on the transverse section plane

Presentation of selected results for Scenario 1: Ceiling fan **NOT OPERATING** inside generic work space

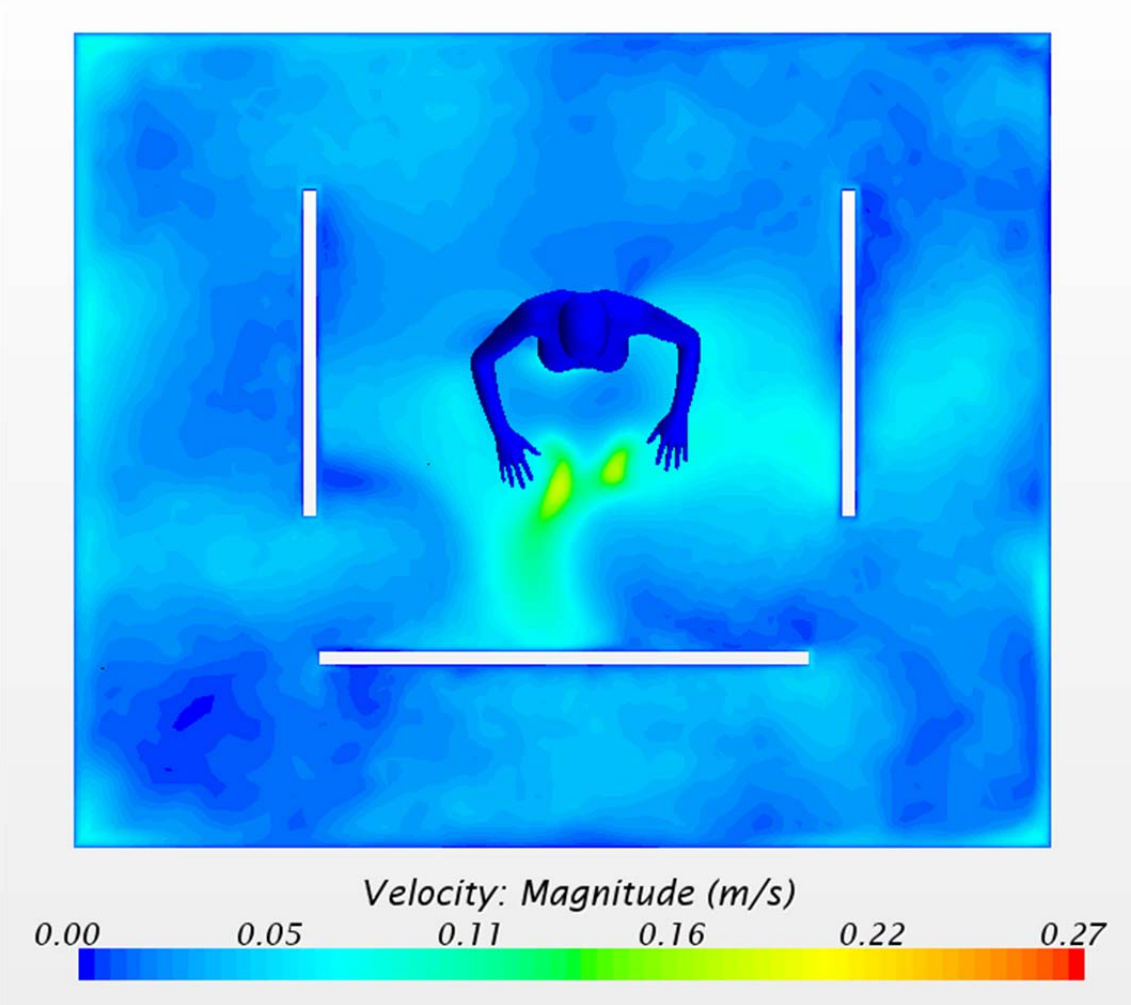

Figure B- 8: **Scenario 1 -** Velocity contour map on the horizontal section plane, at 1.0m above the floor level.

Presentation of selected results for Scenario 1: Ceiling fan **NOT OPERATING** inside generic work space

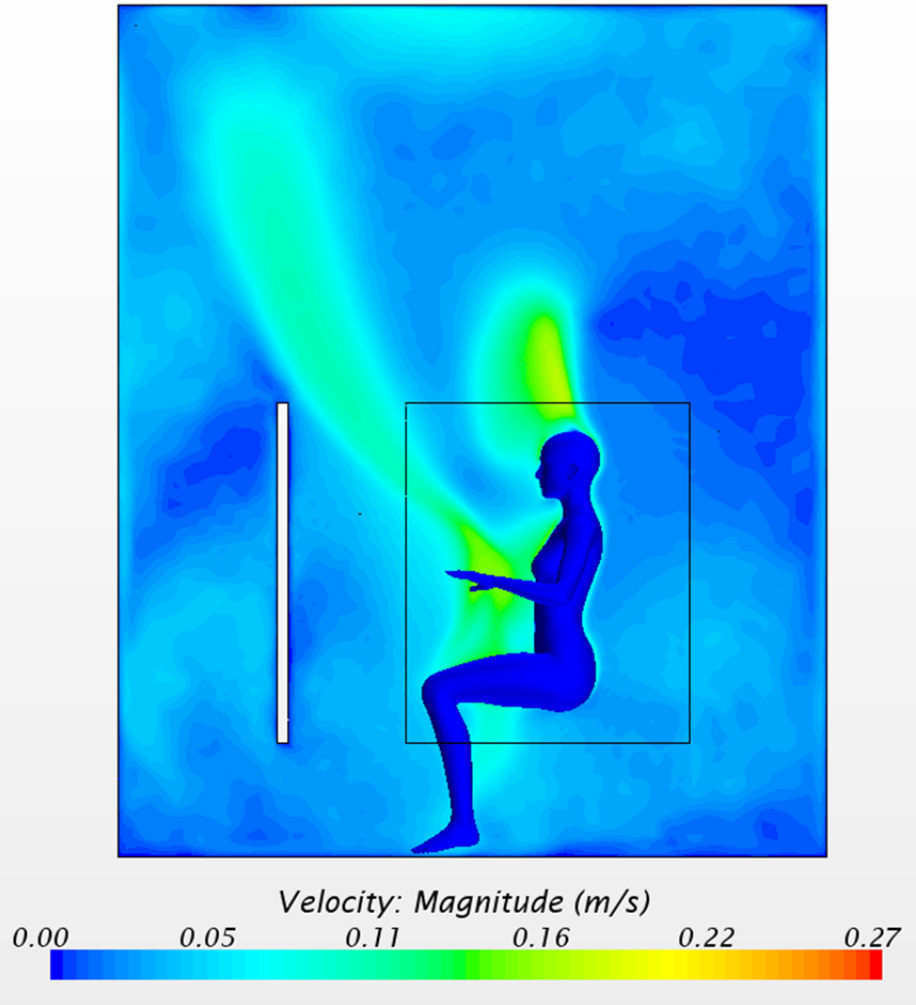

Figure B- 9: **Scenario 1 -** Velocity contour map on the longitudinal section plane

Presentation of selected results for Scenario 2: Ceiling fan **OPERATING** inside generic work space

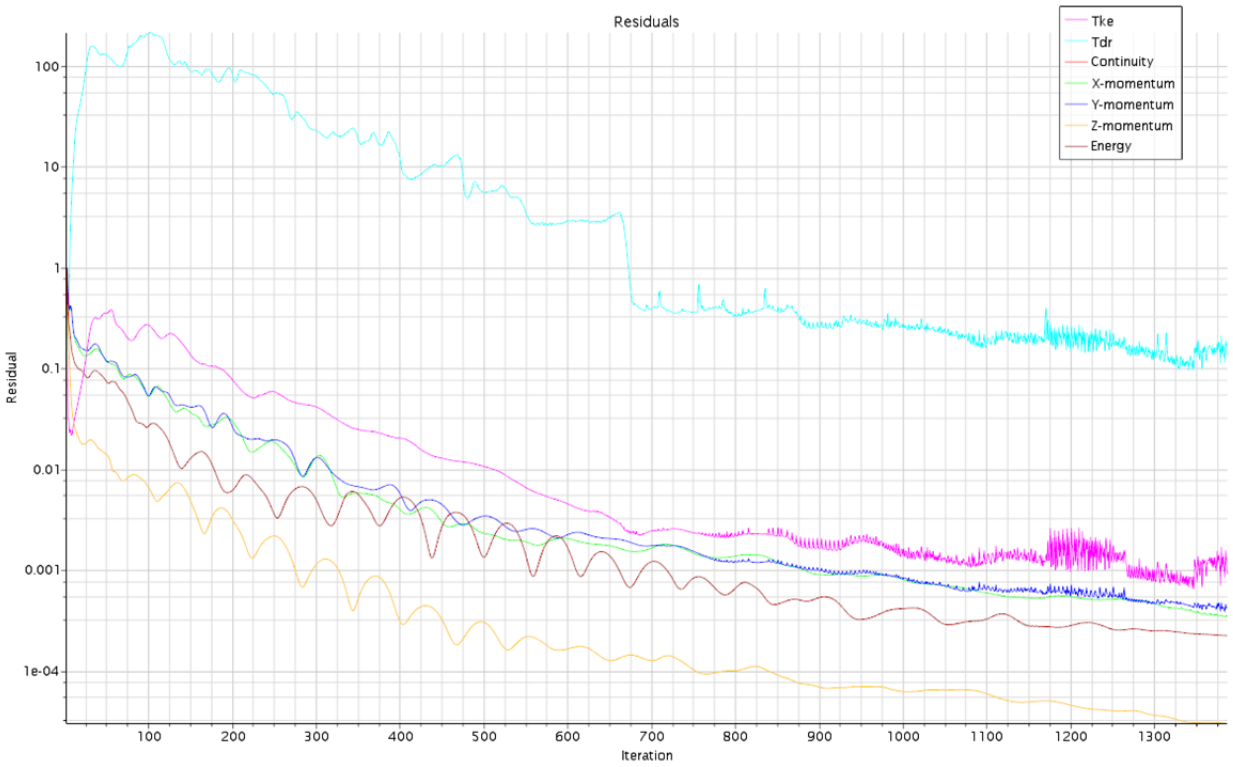

Figure B- 10: **Scenario 2 -** Solution convergence monitor of RMS residuals

Presentation of selected results for Scenario 2: Ceiling fan **OPERATING** inside generic work space

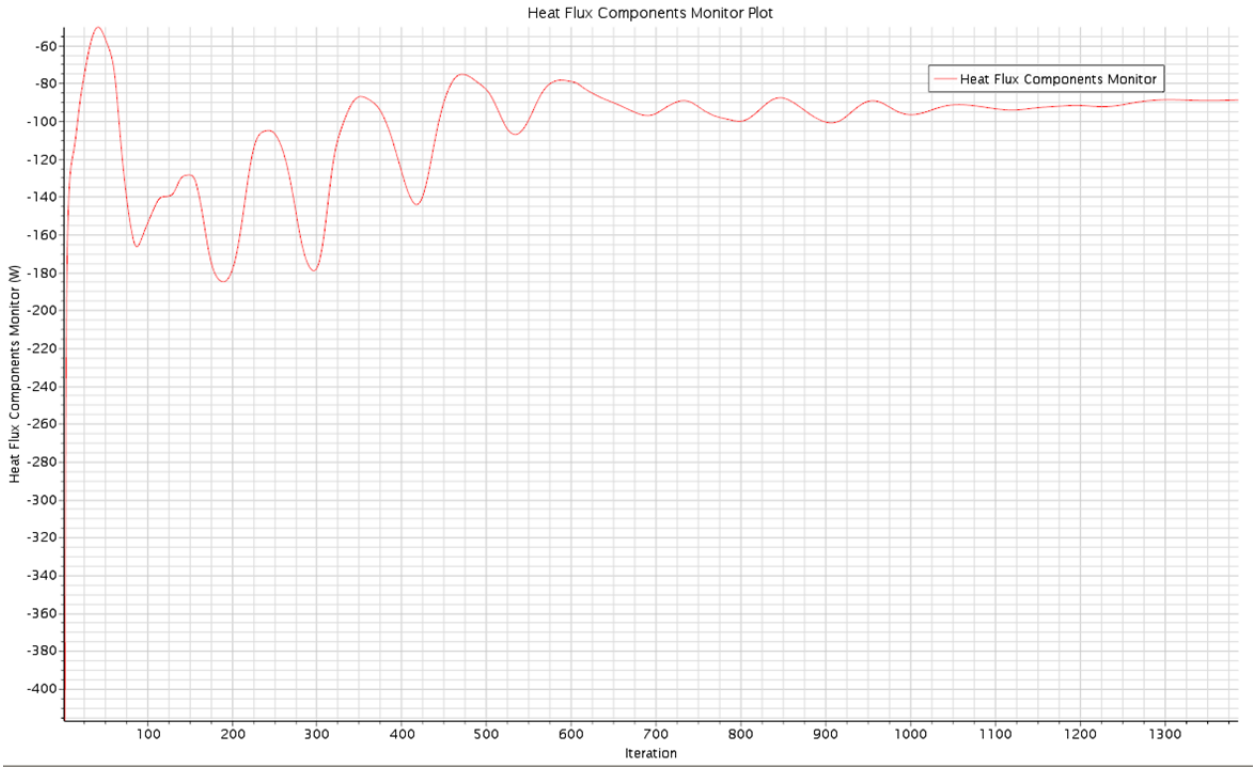

Figure B- 11: **Scenario 2 -** Solution convergence monitor of total heat flux (convective and radiative hat flux)

Presentation of selected results for Scenario 2: Ceiling fan **OPERATING** inside generic work space

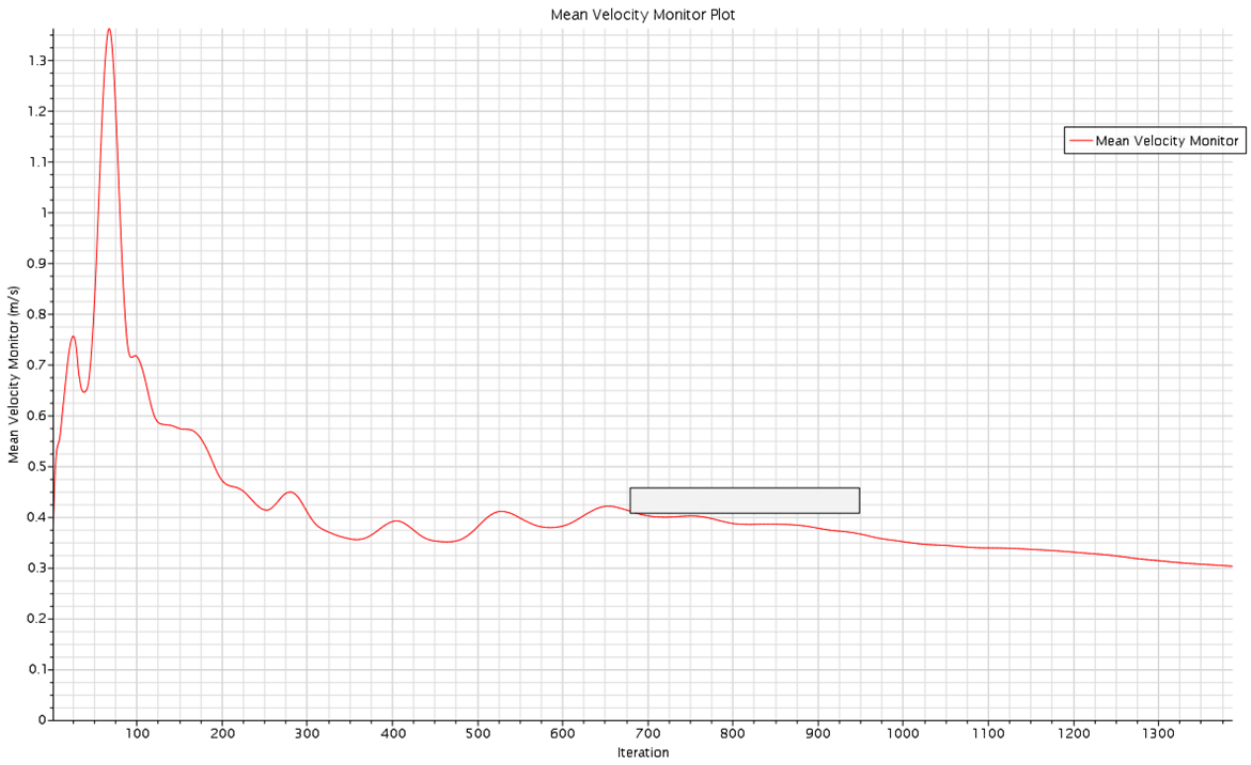

Figure B- 12: **Scenario 2 -** Solution convergence monitor of mean air velocity. Solution converged when mean air velocity reached 0.3m/s

Presentation of selected results for Scenario 2: Ceiling fan **OPERATING** inside generic work space

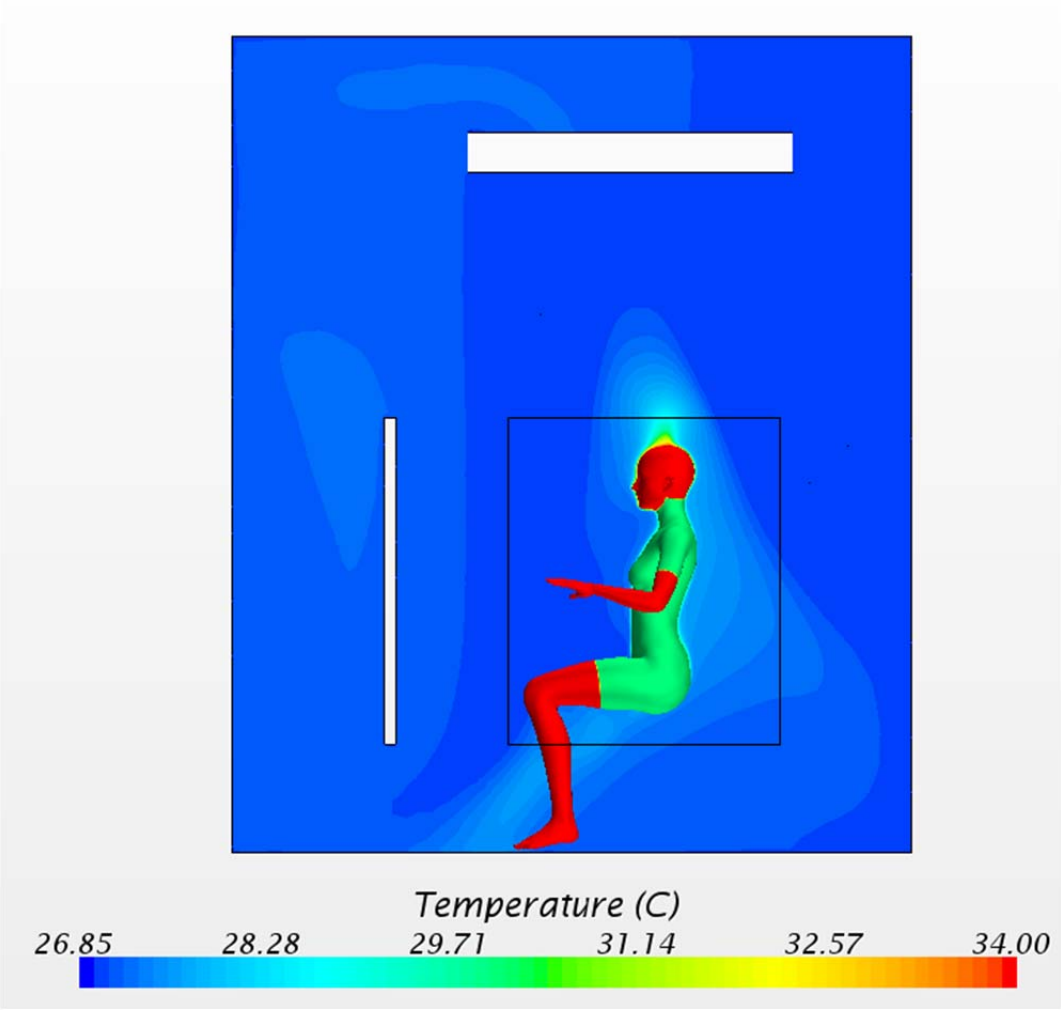

Figure B- 13: **Scenario 2 -** Temperature contour map on the longitudinal section plane

Presentation of selected results for Scenario 2: Ceiling fan **OPERATING** inside generic work space

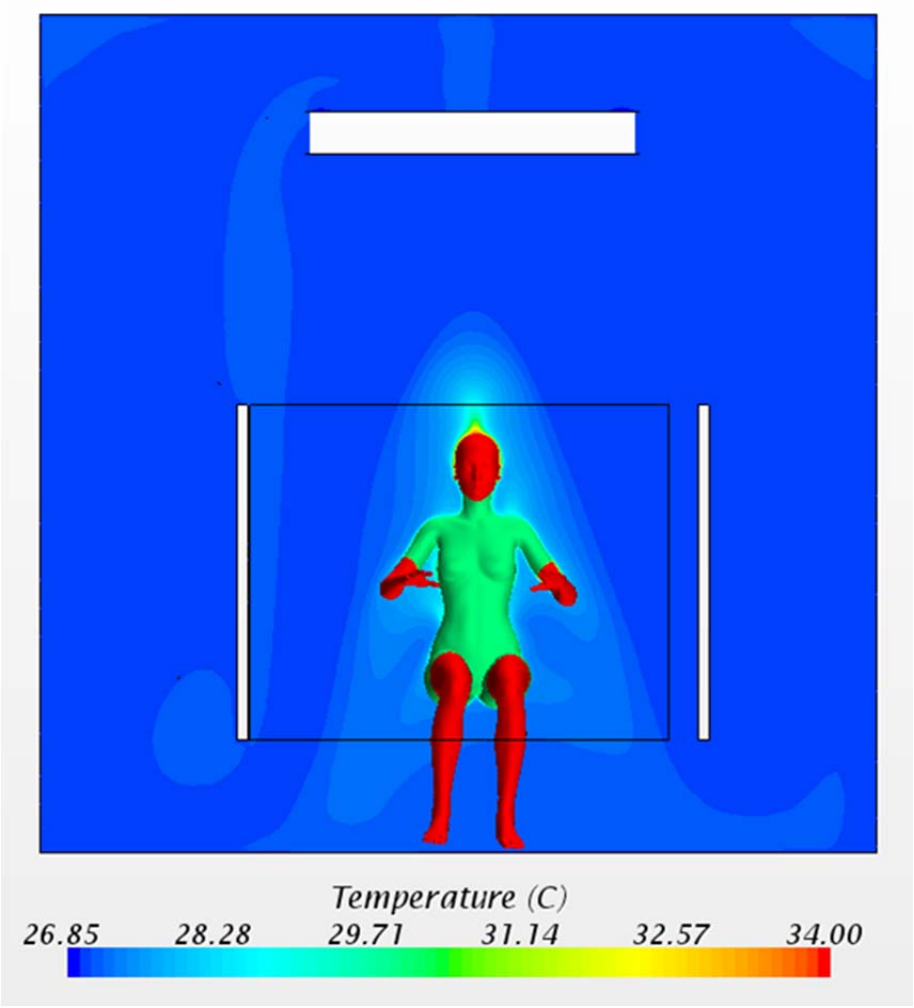

Figure B- 14: **Scenario 2 -** Temperature contour map on the horizontal section plane at 1.0m above the floor level.

Presentation of selected results for Scenario 2: Ceiling fan **OPERATING** inside generic work space

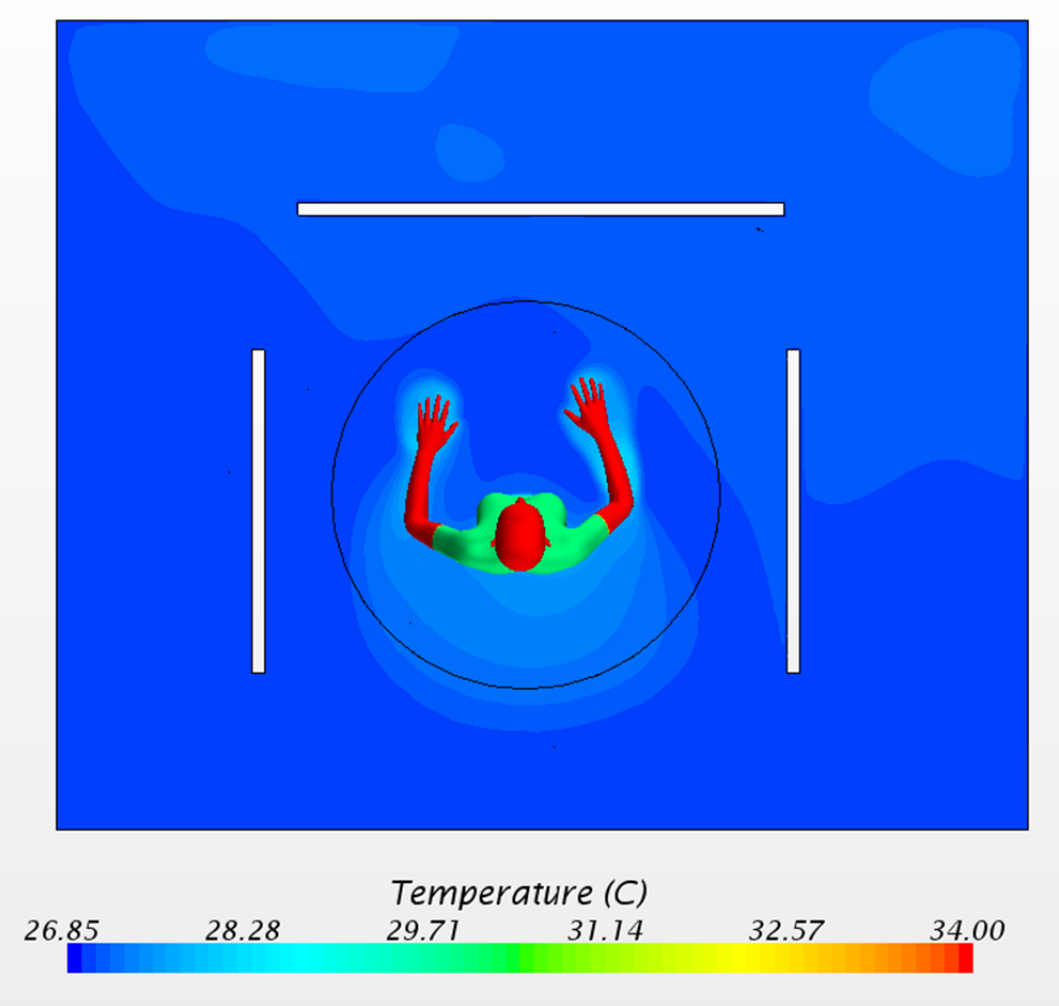

Figure B- 15: **Scenario 2 -** Temperature contour map on the transverse section plane

Presentation of selected results for Scenario 2: Ceiling fan **OPERATING** inside generic work space

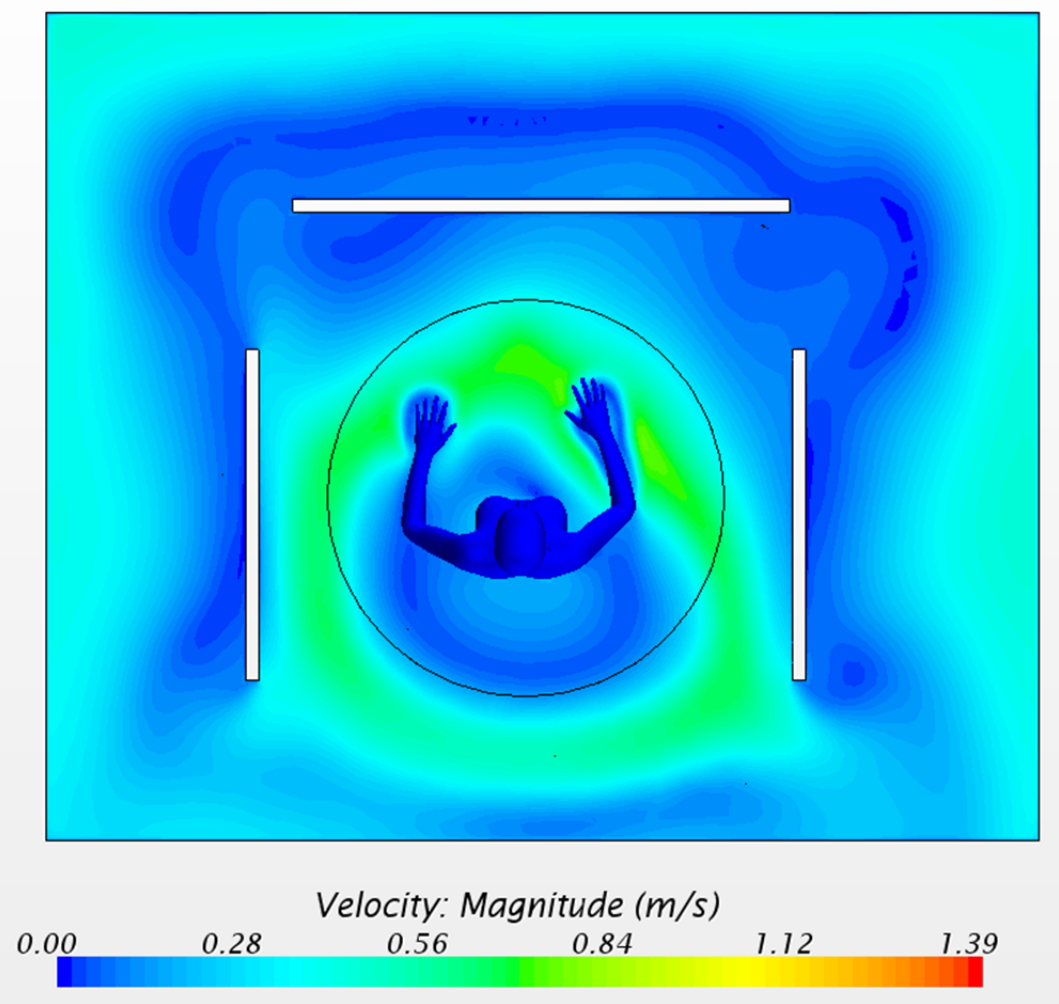

Figure B- 16: **Scenario 2 -** Velocity contour map on the horizontal section plane, at 1.0m above the floor level.

Presentation of selected results for Scenario 2: Ceiling fan **OPERATING** inside generic work space

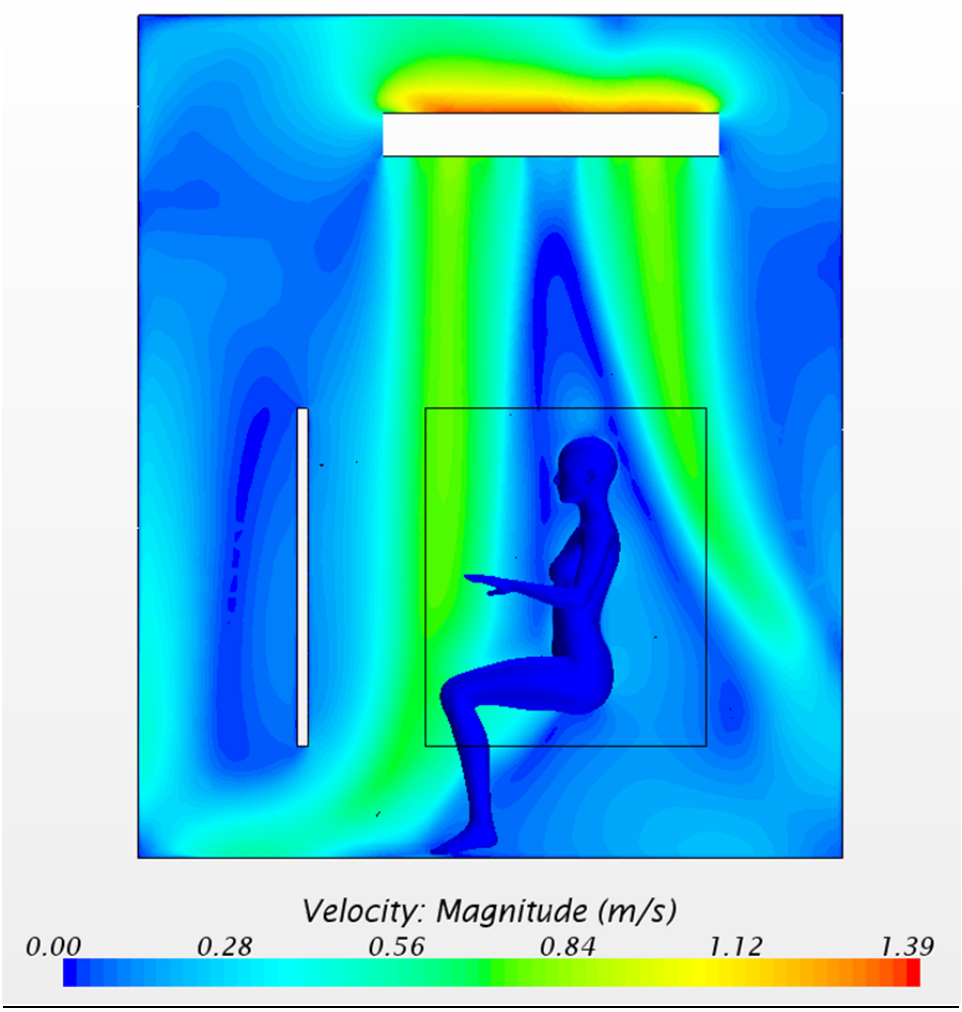

Figure B- 17: **Scenario 2 -** Velocity contour map on the longitudinal section plane

Presentation of selected results for Scenario 2: Ceiling fan **OPERATING** inside generic work space

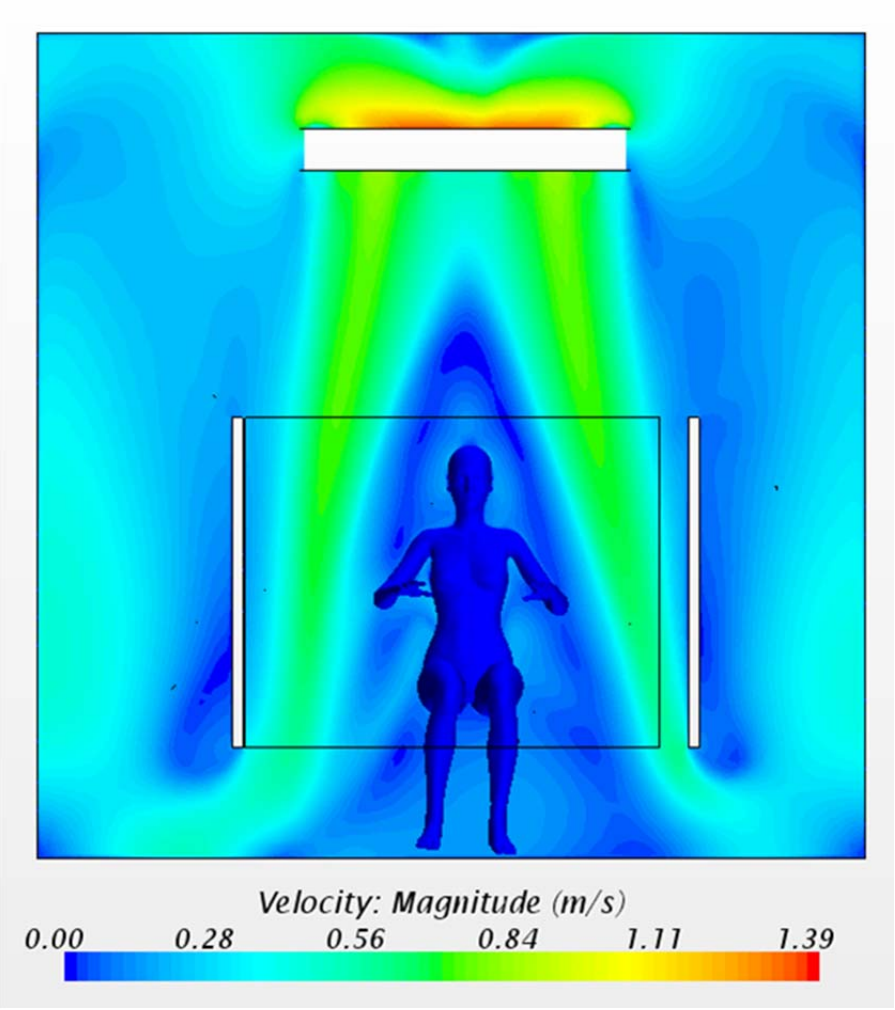

Figure B- 18: **Scenario 2 -** Velocity contour map on the transverse section plane

Presentation of selected results for Scenario 1 and 2:

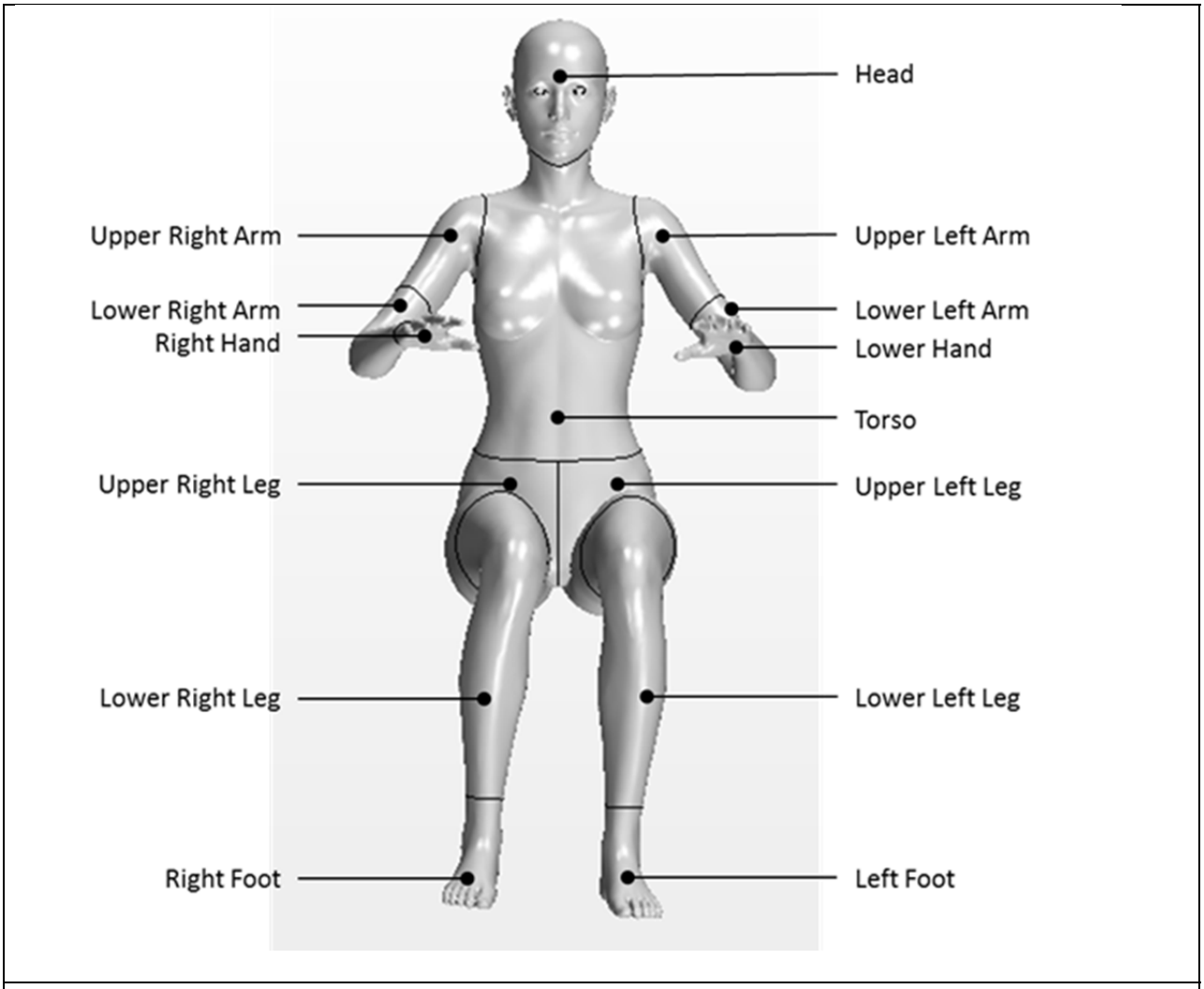

Figure B- 19: Body surface split into body regions

	Scenario 1		Scenario 2	
	Convective heat transfer C (w)	Radiative heat transfer R (w)	Convective heat transfer C (w)	Radiative heat transfer R (w)
Head	2.87	4.95	3.59	4.41
Torse	1.88	-	3.41	-
Upper Left Arm	0.21	-	0.48	-
Upper Right Arm	0.21	-	0.61	-
Lower Left Arm	1.95	2.78	3.03	2.47
Lower Right Arm	1.99	2.79	4.91	2.49
Left Hand	1.26	1.26	4.12	1.13
Right Hand	1.37	1.25	4.47	1.12
Upper Left Leg	1.26	-	2.49	-
Upper Right Leg	1.36	-	2.63	-
Lower Left Leg	4.09	7.17	7.93	6.45
Lower Right Leg	4.18	7.11	7.93	6.39
Left Foot	1.58	2.50	2.12	2.25
Right Foot	1.64	2.52	2.16	2.26
Total	**25.82**	**32.33**	**49.87**	**28.97**

Table B-1: The heat convective (C) and radiative (R) transfer of each body part per CFD run scenario. Note that body parts having cloth do not have radiative heat transfer.

APPENDIX C
RESULTS OF PMV ANALYTICAL CALCULATION OF TWO TEST SCENARIOS

The following spreadsheet shows calculations of PMV and PPD for two scenarios, **Scenario 1 (ceiling is off) and Scenario 2 (ceiling fan is on).** The mean air temperature, mean radiant temperature and average air velocity from initial CFD run were used as inputs for the PMV analytical calculation. The resulting skin and clothing temperatures were then used as inputs for the final CFD to predict the convective and radiative heat transfer of the model.

Input		
Clothing	{clo}	*0.57*
Skin area	{m2}	*1.8*
Metabolic rate	{met}	*1*
External work	{met}	*0*
Air temperature	{C}	*27*
Mean radiant temperature	{C}	*27*
Relative air velocity	{m/s}	*0.05*
Relative humidity	{%}	*60*

Clothing thermal resistance (Rcl)	{m2.K/W}	0.08835
Clothing area factor (fcl)	n/a	1.107
Convective heat transfer coefficient (hc)	{W/m2.K}	3.33
Radiative heat transfer coefficient (hr)	{W/m2.K}	4.37
Total heat transfer coefficient of skin	{W/m2.K}	7.71
Total heat transfer coefficient of clothing	{W/m2.K}	6.96
Skin temperature	{C}	34.1
Clothing temperature	{C}	31.2
Vapor pressure of air	{kPa}	2.177

Metabolism	{W/m2}	{W}
Metabolic heat generation	58.2	104.7
Total Heat Generation	**58.2**	**104.7**

Skin	{W/m2}	{W}
Heat loss by convection (C)	14.3	25.7
Heat loss by radiation (R)	18.7	33.7
Heat loss from vapor difussion through skin (Edif)	9.6	17.3
Heat loss from sweating (Ersw)	0.0	0.0
Respiration	{W/m2}	{W}
Evaporative heat loss from respiration (Eres)	3.7	6.7
Convective heat loss from respiration (Cres)	0.5	1.0
Total Heat Loss	**46.8**	**84.3**

Heat Load	**11.3**
PMV	**0.7**
PPD (%)	**17**

Figure C-1: The PMV analytical calculation for Scenario 1 (**ceiling fan is OFF**)

Input		
Clothing	{clo}	*0.57*
Skin area	{m2}	*1.8*
Metabolic rate	{met}	*1*
External work	{met}	*0*
Air temperature	{C}	*27*
Mean radiant temperature	{C}	*27*
Relative air velocity	{m/s}	*0.3*
Relative humidity	{%}	*60*

Clothing thermal resistance (Rcl)	{m2.K/W}	0.08835
Clothing area factor (fcl)	n/a	1.107
Convective heat transfer coefficient (hc)	{W/m2.K}	6.63
Radiative heat transfer coefficient (hr)	{W/m2.K}	4.36
Total heat transfer coefficient of skin	{W/m2.K}	10.99
Total heat transfer coefficient of clothing	{W/m2.K}	9.93
Skin temperature	{C}	34.1
Clothing temperature	{C}	30.6
Vapor pressure of air	{kPa}	2.177

Metabolism	{W/m2}	{W}
Metabolic heat generation	58.2	104.7
Total Heat Generation	**58.2**	**104.7**

Skin	{W/m2}	{W}
Heat loss by convection (C)	23.9	43.1
Heat loss by radiation (R)	15.7	28.3
Heat loss from vapor difussion through skin (Edif)	9.6	17.3
Heat loss from sweating (Ersw)	0.0	0.0
Respiration	{W/m2}	{W}
Evaporative heat loss from respiration (Eres)	3.7	6.7
Convective heat loss from respiration (Cres)	0.5	1.0
Total Heat Loss	**53.5**	**96.3**

Heat Load	**4.6**
PMV	**0.3**
PPD (%)	**7**

Figure C-2: The PMV analytical calculation for Scenario 1 (**ceiling fan is ON**)

-

APPENDIX D
SIMULATING THE CEILING FAN

The velocity profile of the ceiling fan at a point of below the fan plane was measured to obtain the boundary conditions for the CFD simulations. The field measurements were conducted to measure an array of air velocities in the plane parallel and 0.43m below the fan plane (Figure D-1). A handheld anemometer was used and placed at five points, one at a time, to measure the average air velocity of about 30-50 samples (one second interval), per fan speed. The velocity profiles of the ceiling fan at six speeds are shown in Figure D-2.

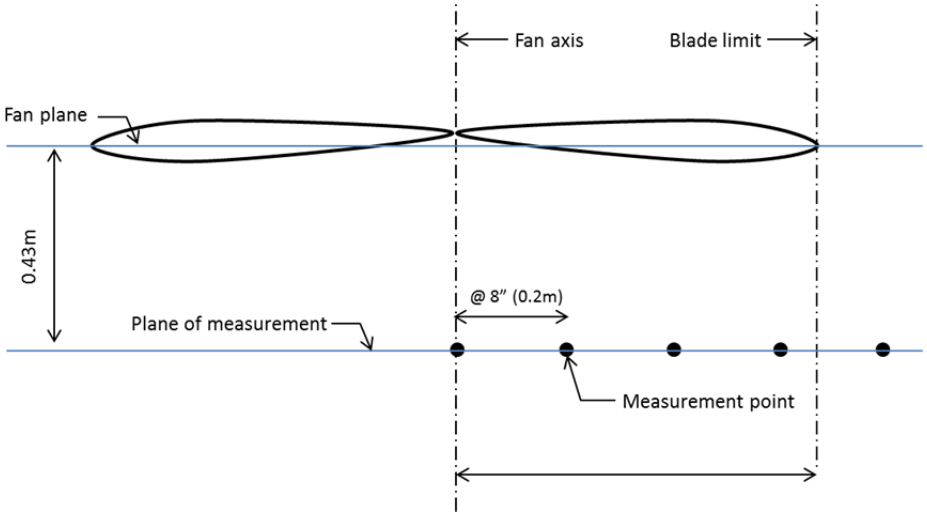

Figure D-1: Placement location of anemometers for measuring ceiling fans' air velocity profile.

-

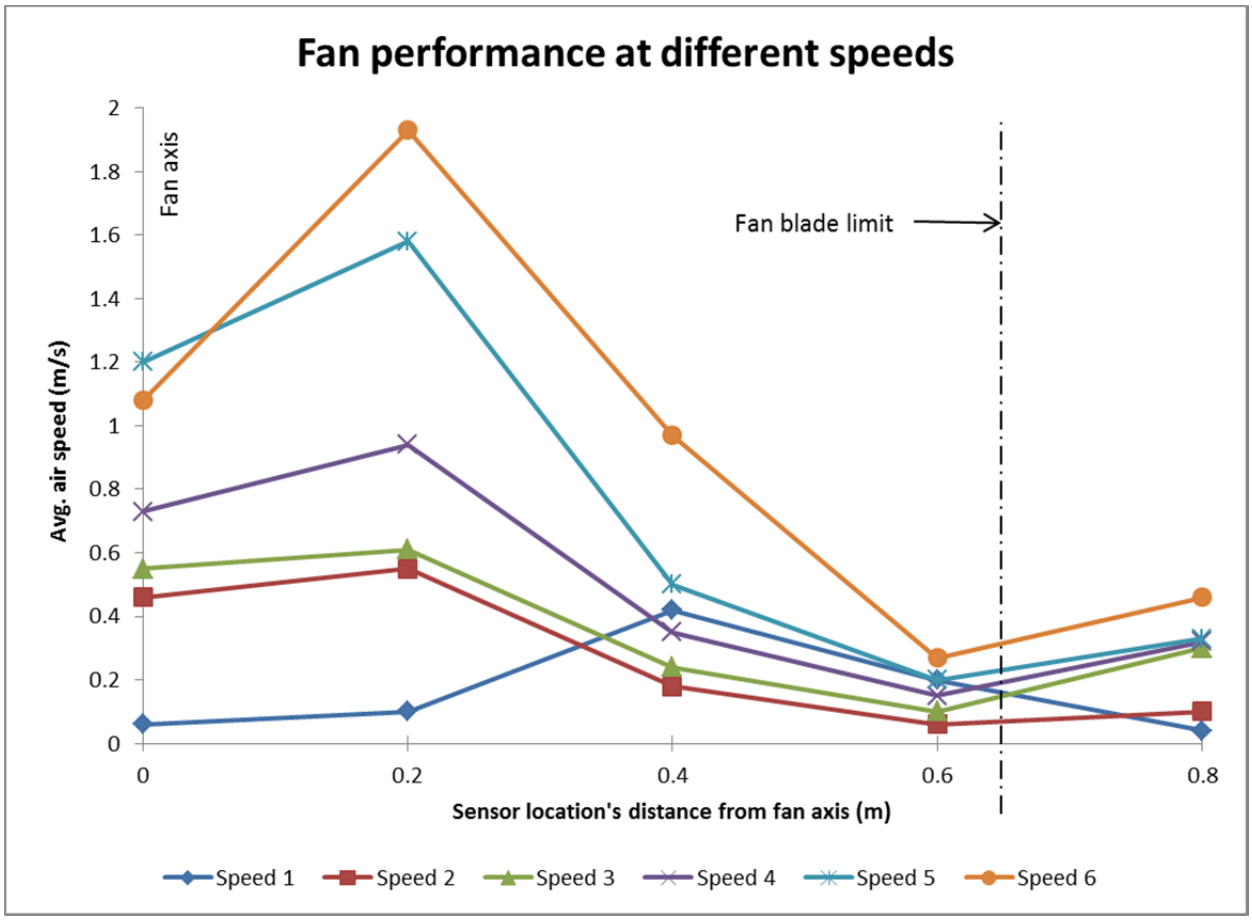

Figure D-2: Measured air velocity profiles of ceiling fan at different speeds

APPENDIX E
LINKING THE FAN VELOCITY PROFILE INTO CFD BOUNDARY CONDITION

In order to transfer the fan velocity profile into CFD boundary conditions for the ceiling fan in the CFD model, a user defined cylindrical coordinate system was created and named as "Cylindrical Ceiling Fan" with origin point, r axis, z axis and theta axis indicate in Figure 1.

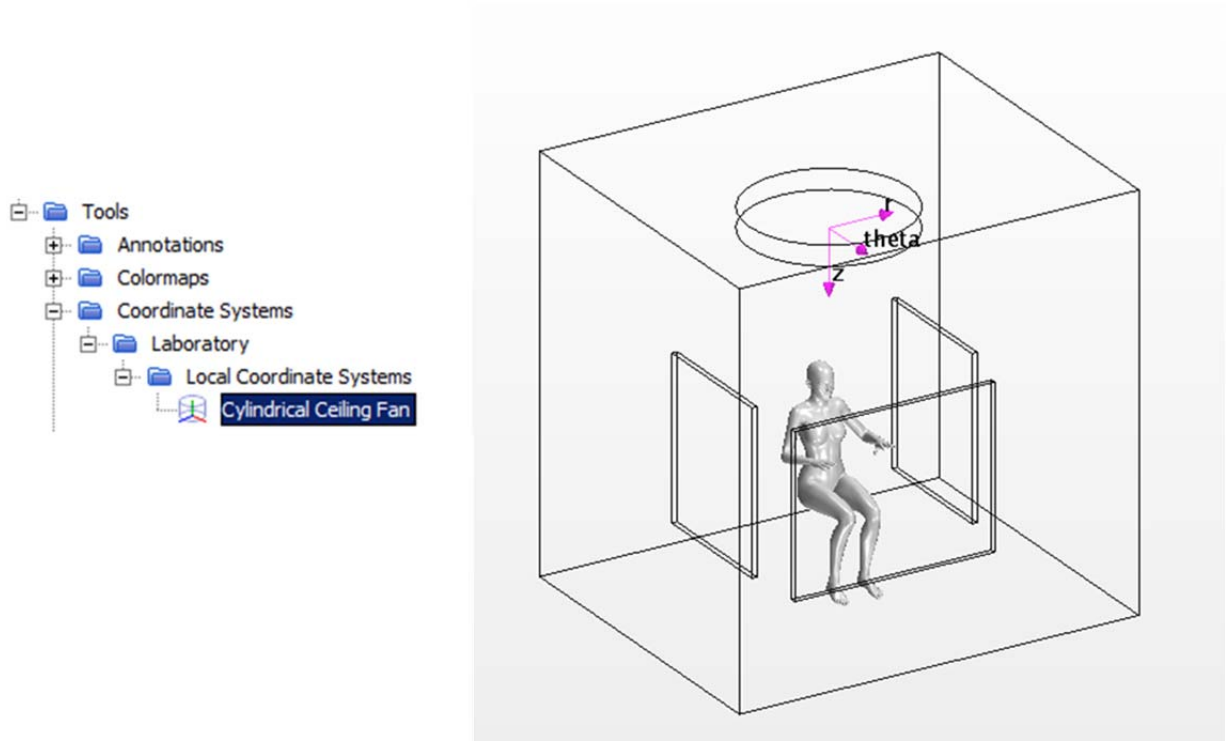

Figure E-1: User defined cylindrical coordinate system with indication of its origin point, r axis, z axis and theta axis.

The Cylindrical coordinates of all volume cells of the fan inlet was export to an external csv file (Figure E-2) which can be opened in Microsoft Excel where each coordinate will be assigned a given velocity vector based on the fan velocity profile. This external data set is then imported back into STAR-CCM+ where the velocity data is assigned as velocity component of the fan inlet (Figure E-3)

Figure E-22: Cylindrical coordinates of volume cells of the fan inlet were extracted and exported into an external csv file.

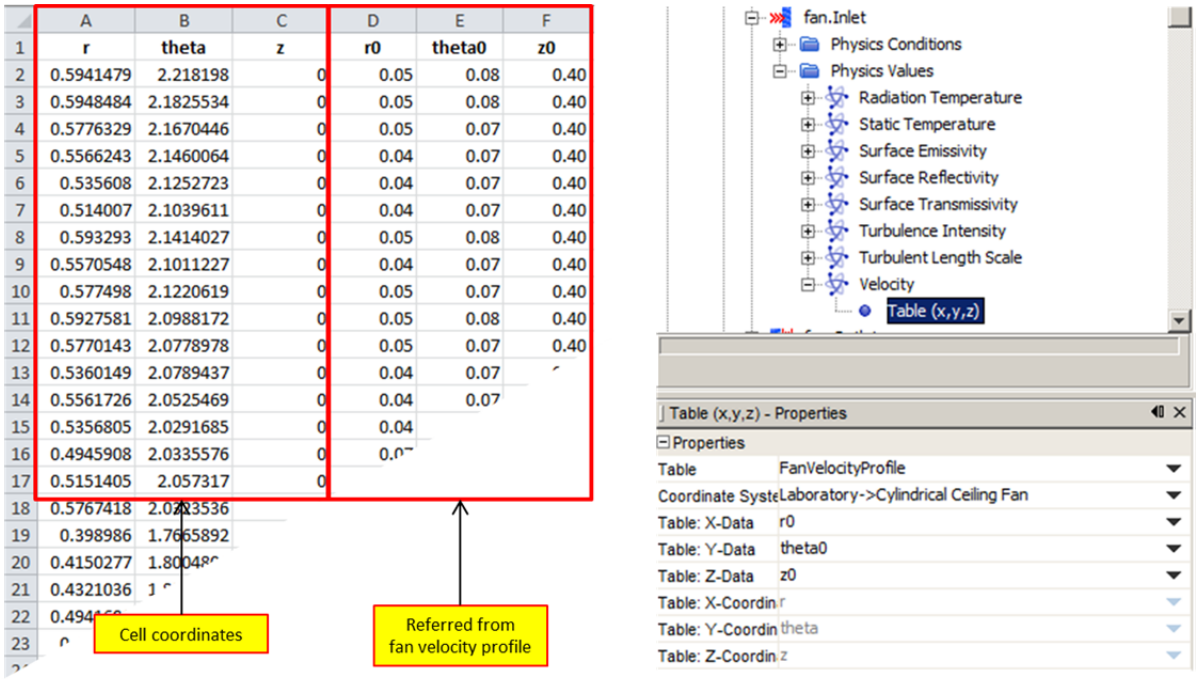

Figure E-3: A screen shot of the spreadsheet showing values of fan velocity profile which were used to calculate the velocity vector for each cell coordinate (left), the spreadsheet data was imported into STAR-CCM+ as a table and assigned as velocity profile for the ceiling fan inlet (right)

APPENDIX F
Metabolic rate

TYPICAL METABOLIC HEAT GENERATION FOR VARIOUS ACTIVITIES

(ASHRAE Fundamental 2009)

	W/m²	met*
Resting		
Sleeping	40	0.7
Reclining	45	0.8
Seated, quiet	60	1.0
Standing, relaxed	70	1.2
Walking (on level surface)		
3.2 km/h (0.9 m/s)	115	2.0
4.3 km/h (1.2 m/s)	150	2.6
6.4 km/h (1.8 m/s)	220	3.8
Office Activities		
Reading, seated	55	1.0
Writing	60	1.0
Typing	65	1.1
Filing, seated	70	1.2
Filing, standing	80	1.4
Walking about	100	1.7
Lifting/packing	120	2.1
Driving/Flying		
Car	60 to 115	1.0 to 2.0
Aircraft, routine	70	1.2
Aircraft, instrument landing	105	1.8
Aircraft, combat	140	2.4
Heavy vehicle	185	3.2
Miscellaneous Occupational Activities		
Cooking	95 to 115	1.6 to 2.0
Housecleaning	115 to 200	2.0 to 3.4
Seated, heavy limb movement	130	2.2
Machine work		
sawing (table saw)	105	1.8
light (electrical industry)	115 to 140	2.0 to 2.4
heavy	235	4.0
Handling 50 kg bags	235	4.0
Pick and shovel work	235 to 280	4.0 to 4.8
Miscellaneous Leisure Activities		
Dancing, social	140 to 255	2.4 to 4.4
Calisthenics/exercise	175 to 235	3.0 to 4.0
Tennis, singles	210 to 270	3.6 to 4.0
Basketball	290 to 440	5.0 to 7.6
Wrestling, competitive	410 to 505	7.0 to 8.7

Sources: Compiled from various sources. For additional information, see Buskirk (1960), Passmore and Durnin (1967), and Webb (1964).
*1 met = 58.1 W/m²

APPENDIX G
CLOTHING THERMAL INSULATION

Typical Insulation and Permeability Values for Clothing Ensembles
(2009 ASHRAE Handbook – Fundamentals)

Ensemble Description[a]	I_{cl}, clo	I_t,[b] clo	f_{cl}	i_{cl}	i_m[b]
Walking shorts, short-sleeved shirt	0.36	1.02	1.10	0.34	0.42
Trousers, short-sleeved shirt	0.57	1.20	1.15	0.36	0.43
Trousers, long-sleeved shirt	0.61	1.21	1.20	0.41	0.45
Same as above, plus suit jacket	0.96	1.54	1.23		
Same as above, plus vest and T-shirt	1.14	1.69	1.32	0.32	0.37
Trousers, long-sleeved shirt, long-sleeved sweater, T-shirt	1.01	1.56	1.28		
Same as above, plus suit jacket and long underwear bottoms	1.30	1.83	1.33		
Sweat pants, sweat shirt	0.74	1.35	1.19	0.41	0.45
Long-sleeved pajama top, long pajama trousers, short 3/4 sleeved robe, slippers (no socks)	0.96	1.50	1.32	0.37	0.41
Knee-length skirt, short-sleeved shirt, panty hose, sandals	0.54	1.10	1.26		
Knee-length skirt, long-sleeved shirt, full slip, panty hose	0.67	1.22	1.29		
Knee-length skirt, long-sleeved shirt, half slip, panty hose, long-sleeved sweater	1.10	1.59	1.46		
Same as above, replace sweater with suit jacket	1.04	1.60	1.30	0.35	0.40
Ankle-length skirt, long-sleeved shirt, suit jacket, panty hose	1.10	1.59	1.46		
Long-sleeved coveralls, T-shirt	0.72	1.30	1.23		
Overalls, long-sleeved shirt, T-shirt	0.89	1.46	1.27	0.35	0.40
Insulated coveralls, long-sleeved thermal underwear, long underwear bottoms	1.37	1.94	1.26	0.35	0.39

Source: From McCullough and Jones (1984) and McCullough et al. (1989).
[a]All ensembles include shoes and briefs or panties. All ensembles except those with panty hose include socks unless otherwise noted.
[b]For $t_r = t_a$ and air velocity less than 0.2 m/s (I_a = 0.72 clo and i_m = 0.48 when nude).
1 clo = 0.155 ($m^2 \cdot K/W$).